PB-227 579

SEDIMENT TRANSPORT IN SHALLOW SUB-CRITICAL FLOW DISTURBED BY SIMULATED RAINFALL

Jerry Lee Machemehl

Texas A and M University

Prepared for:

Federal Water Pollution Control Administration

September 1968

DISTRIBUTED BY:

NTIS
National Technical Information Service
U. S. DEPARTMENT OF COMMERCE
5285 Port Royal Road, Springfield Va. 22151

PB 227 579

SEDIMENT TRANSPORT IN SHALLOW SUBCRITICAL FLOW
DISTURBED BY SIMULATED RAINFALL

By

JERRY LEE MACHEMEHL

Technical Report No. 14
Water Resources Institute
Texas A&M University
September 1968

Reproduced by
NATIONAL TECHNICAL
INFORMATION SERVICE
U S Department of Commerce
Springfield VA 22151

The investigations leading to this report were a portion of the research under Research Grant Number WP-00757-03, Federal Water Pollution Control Administration, U.S. Department of the Interior, with Dr. Ernest T. Smerdon as principal investigator. The research was performed in the Agricultural Engineering Research Laboratory, Texas A&M University, College Station, Texas.

FOREWORD

This investigation was a part of a research project sponsored by the Federal Water Pollution Control Administration to study water pollution from eroded sediments.

The segment of the problem with which this research is concerned is the transport of sediment in a shallow stream from the point of detachment to a stream of appreciable size. This is the region of transport where the external effect of rainfall energy influences the sediment transport mechanics.

This investigation was designed to study the effects of rainfall on sediment transport in shallow subcritical flow.

ABSTRACT

Sediment Transport in Shallow Subcritical Flow Disturbed
by Simulated Rainfall. (August 1968)
Jerry L. Machemehl, B.S., Texas A&M University
Directed by: Dr. Ernest T. Smerdon

Studies were conducted in a closed system recirculating research flume to evaluate the relative effects of high intensity rainfall on von Karman's universal constant and the sediment transport capacity of shallow flow. The tests in this study were conducted at flow depths of 0.3 ft and less, with discharges less than 0.5 cfs. The point velocities in the flow were determined with a Pace CD-25 pressure transducer and an inclined manometer connected in parallel to a Pitot-static tube of the standard Prandtl design. Regression analyses were performed on the velocity data to determine the best fit dimensionless velocity curve on semilogarithmic paper. Von Karman's universal constant was then evaluated from the slope of the regression line.

Point sediment samples were siphoned from the flow with a stainless steel-pipette sediment sampler. Sediment concentrations were found with a filtering technique. Sediment samples were taken with and without rainfall to evaluate the relative effect of the rainfall on the transport capacity of shallow flow.

ACKNOWLEDGMENTS

The writer expresses his respect and gratitude to Dr. Ernest T. Smerdon for his guidance and assistance given throughout the course of this study. Sincere appreciation is expressed to Dr. William B. Davis, Dr. Otto R. Kunze, Professor Robert E. Schiller, and Mr. Larry J. Glass for their review and comments.

Acknowledgment is also extended to the Agricultural Engineering Department and the State Chemist Office for providing the facilities and equipment. The Federal Water Pollution Control Administration is sincerely thanked for the financial assistance provided throughout this study.

TABLE OF CONTENTS

CHAPTER Page

I INTRODUCTION 1

Review of Literature 3

Modes of transport 3
Bed-load Transport Theories and Equations . . 4
Suspended-load Transport Theories and Equations 11
Sediment Transport Disturbed by Rainfall . . 15

II RESEARCH APPARATUS AND PROCEDURES 17

Research Apparatus 17

Research flume 17
Rainfall simulator 20
Simulated sediment 21

Measurements 21

Depth measurements 21
Velocity measurements 27
Discharge measurements 27
Point sediment measurements 30
Total sediment measurements 30
Flow adjustment 30
Flow profile 32
Temperature measurements 32

Test Program 32

Procedure 32

Test conditions 33
Test series 34
Data reduction 37

III ANALYSIS OF DATA AND DISCUSSION OF RESULTS . . . 39

Von Karman's Universal Constant 39

Clear water flow without rainfall 39
Effect of simulated rainfall 40

CHAPTER Page

Effect of suspended sediment 47
Effect of simulated rainfall and suspended sediment 56

Effect of Rainfall on Sediment Transport Capacity of Shallow Flow 73

Variations Between Test Series 74

Infinitely Wide Channel 75

Rainfall Intensity 75

Flow Conditions 80

Uniform flow 80
Gradually varied flow 80
Spatially varied flow 81

Secondary Flow 82

Instrument Error 83

IV SUMMARY AND CONCLUSIONS 85

Summary 85

Conclusions 85

Future Studies 86

LIST OF REFERENCES 88

RELATED LITERATURE 91

APPENDIX A 93

APPENDIX B 97

APPENDIX C 133

LIST OF TABLES

Table Page

I PHYSICAL PROPERTIES OF THE GLASS BEADS 24

II PRELIMINARY TEST PROGRAM 33

III PITOT-STATIC TUBE AND POINT SEDIMENT LOCATIONS FOR TEST PROGRAM 35

IV REGRESSION ANALYSIS RESULTS OF VELOCITY DEFECT LAW FOR TESTS CONDUCTED WITHOUT SIMULATED RAINFALL. 46

V REGRESSION ANALYSIS RESULTS OF VELOCITY DEFECT LAW FOR TEST RUNS CONDUCTED WITH SEDIMENT AND WITHOUT AND WITH SIMULATED RAINFALL (Series 3 - Runs 7 through 33) 57

VI REGRESSION ANALYSIS RESULTS OF VELOCITY DEFECT LAW FOR TEST RUNS CONDUCTED WITH SEDIMENT AND WITHOUT AND WITH SIMULATED RAINFALL (Series 4 - Runs 7 through 33) 64

APPENDIX B

VII REGRESSION ANALYSIS RESULTS OF VELOCITY DEFECT LAW FOR TESTS CONDUCTED WITHOUT SIMULATED RAINFALL (Series A through 4 - Runs 1 through 6) . 98

VIII REGRESSION ANALYSIS RESULTS OF VELOCITY DEFECT LAW FOR TEST RUNS CONDUCTED WITHOUT AND WITH SIMULATED RAINFALL (Series 3 and 4 - Runs 7 through 33) 102

IX VELOCITY DATA FOR TEST RUNS WITHOUT SIMULATED RAINFALL (Series A through 4 - Runs 1 through 6) . 105

X VELOCITY DATA FOR TEST RUNS WITHOUT AND WITH SIMULATED RAINFALL (Series 3 and 4 - Runs 7 through 33) 111

XI SEDIMENT CONCENTRATION DATA FOR TEST RUNS WITHOUT SIMULATED RAINFALL (Series 3 and 4 - Runs 1 through 6) 115

Table | Page

XII SEDIMENT CONCENTRATION DATA FOR TEST RUNS WITHOUT AND WITH SIMULATED RAINFALL (Series 3 and 4 - Runs 7 through 33) 116

XIII RESEARCH FLUME DATA FOR TEST RUNS CONDUCTED WITHOUT SIMULATED RAINFALL (Series A through 4 - Runs 1 through 6) 120

XIV RESEARCH FLUME DATA FOR TEST RUNS CONDUCTED WITHOUT AND WITH SIMULATED RAINFALL (Series 3 and 4 - Runs 7 through 33) 123

XV VELOCITY DISTRIBUTION CALCULATIONS FOR TEST RUNS CONDUCTED WITHOUT SIMULATED RAINFALL (Series A through 4 - Runs 1 through 6) 126

XVI VELOCITY DISTRIBUTION CALCULATIONS FOR TEST RUNS CONDUCTED WITHOUT AND WITH SIMULATED RAINFALL (Series 3 and 4 - Runs 7 through 33) . . . 130

LIST OF FIGURES

Figure		Page
1	Schematic of Facilities Used for this Study	18
2	Partial View of Recirculating Research Flume and Rainfall Simulator	19
3	Partial View of Recirculating Research Flume	19
4	Flow in Research Flume without Simulated Rainfall	22
5	Flow in Research Flume with Simulated Rainfall	22
6	Grain Size Distribution Curve	23
7	Photomicrograph of Glass Beads (50µ squares)	25
8	Instrument Carriage with Prandtl Tube and Point Sediment Sampler Positioned in the Research Flume	26
9	Differential Inclined Manometer, Transducer Indicator, and Transducer Calibration Apparatus	28
10	Vertical Manometer Board and Dall Flow Tube	29
11	Variable Speed Motor and Centrifigual Pump	31
12	Bed Configuration	36
13	Velocity Distribution Regression Curve for Test Series A (0.30 ft Depth of Flow) Using Prandtl Tube and Manometer	41
14	Velocity Distribution Regression Curve for Test Series B (0.30 ft Depth of Flow) Using Prandtl Tube and Manometer	42
15	Velocity Distribution Regression Curve for Test Series B (0.30 ft Depth of Flow) Using Prandtl Tube and Transducer	43

Figure Page

16 Velocity Distribution Regression Curve for Test Series C (0.20 ft Depth of Flow) Using Prandtl Tube and Manometer 44

17 Velocity Distribution Regression Curve for Test Series C (0.20 ft Depth of Flow) Using Prandtl Tube and Transducer 45

18 Velocity Distribution Regression Curve for Test Series 1 (0.30 ft Depth of Flow) Using Prandtl Tube and Manometer 48

19 Velocity Distribution Regression Curve for Test Series 1 (0.30 ft Depth of Flow) Using Prandtl Tube and Transducer 49

20 Velocity Distribution Regression Curve for Test Series 2 (0.30 ft Depth of Flow) Using Prandtl Tube and Manometer 50

21 Velocity Distribution Regression Curve for Test Series 2 (0.30 ft Depth of Flow) Using Prandtl Tube and Transducer 51

22 Velocity Distribution Regression Curve for Test Series 3 (0.20 ft Depth of Flow) Using Prandtl Tube and Manometer 52

23 Velocity Distribution Regression Curve for Test Series 3 (0.20 ft Depth of Flow) Using Prandtl Tube and Transducer 53

24 Velocity Distribution Regression Curve for Test Series 4 (0.112 ft Depth of Flow) Using Prandtl Tube and Manometer 54

25 Velocity Distribution Regression Curve for Test Series 4 (0.112 ft Depth of Flow) Using Prandtl Tube and Transducer 55

26 Velocity Distribution Regression Curve for Test Series 3 (0.20 ft Depth of Flow) Using Prandtl Tube and Transducer (Runs 7 through 15 - With Sediment Without Rainfall) 58

Figure Page

27 Velocity Distribution Regression Curve for Test Series 3 (0.20 ft Depth of Flow) Using Prandtl Tube and Transducer (With Rainfall - 0:15 Min) . . . 59

28 Velocity Distribution Regression Curve for Test Series 3 (0.20 ft Depth of Flow) Using Prandtl Tube and Transducer (With Rainfall - 1:00 Min) . . . 60

29 Velocity Distribution Regression Curve for Test Series 3 (0.20 ft Depth of Flow) Using Prandtl Tube and Transducer (With Rainfall - 1:45 Min) . . . 61

30 Velocity Distribution Regression Curve for Test Series 3 (0.20 ft Depth of Flow) Using Prandtl Tube and Transducer (With Rainfall - 2:30 Min) . . . 62

31 Velocity Distribution Regression Curve for Test Series 3 (0.20 ft Depth of Flow) Using Prandtl Tube and Transducer (With Rainfall > 4:00 Min) . . . 63

32 Velocity Distribution Regression Curve for Test Series 4 (0.112 ft Depth of Flow) Using Prandtl Tube and Transducer (Runs 7 through 12 - With Sediment Without Rainfall) 65

33 Velocity Distribution Regression Curve for Test Series 4 (0.112 ft Depth of Flow) Using Prandtl Tube and Transducer (With Rainfall - 0:15 Min) . . . 66

34 Velocity Distribution Regression Curve for Test Series 4 (0.112 ft Depth of Flow) Using Prandtl Tube and Transducer (With Rainfall - 1:00 Min) . . . 67

35 Velocity Distribution Regression Curve for Test Series 4 (0.112 ft Depth of Flow) Using Prandtl Tube and Transducer (With Rainfall - 1:45 Min) . . . 68

36 Velocity Distribution Regression Curve for Test Series 4 (0.112 ft Depth of Flow) Using Prandtl Tube and Transducer (With Rainfall - 2:30 Min) . . . 69

37 Velocity Distribution Regression Curve for Test Series 4 (0.112 ft Depth of Flow) Using Prandtl Tube and Transducer (With Rainfall > 4:00 Min) . . . 70

Figure Page

38 Energy Grade Line Slope for Series 3 (0.200 ft Depth of Flow) Before and After Rainfall 71

39 Von Karman's Constant for Series 3 (0.200 ft Depth of Flow) Before and After Rainfall 71

40 Sediment Concentrations at y = 0.16 ft for Series 3 (0.20 ft Depth of Flow) Before and After Rainfall 71

41 Sediment Concentrations at y = 0.10 ft for Series 3 (0.20 ft Depth of Flow) Before and After Rainfall 71

42 Energy Grade Line Slope for Series 4 (0.112 ft Depth of Flow) Before and After Rainfall 72

43 Von Karman's Constant for Series 4 (0.112 ft Depth of Flow) Before and After Rainfall 72

44 Sediment Concentrations at y = 0.08 ft for Series 4 (0.112 ft Depth of Flow) Before and After Rainfall 72

45 Sediment Concentrations at y = 0.06 ft for Series 4 (0.112 ft Depth of Flow) Before and After Rainfall 72

46 Clear Water Isovels for Series B (0.30 ft Depth of Flow) with Simulated Rainfall Using Pressure Transducer 76

47 Clear Water Isovels for Series B (0.30 ft Depth of Flow) Without Simulated Rainfall Using Pressure Transducer 76

48 Clear Water Isovels for Series B (0.30 ft Depth of Flow) With Simulated Rainfall Using Inclined Manometer 77

49 Clear Water Isovels for Series B (0.30 ft Depth of Flow) Without Simulated Rainfall Using Inclined Manometer 77

Figure Page

50 Clear Water Isovels for Series C (0.20 ft Depth of Flow) Without Simulated Rainfall Using Inclined Manometer 78

51 Clear Water Isovels for Series C (0.20 ft Depth of Flow) Without Simulated Rainfall Using Pressure Transducer 78

52 Rainfall Intensity Distribution in Research Flume 79

APPENDIX C

53 Water Surface Slopes for Series 1 Without Rainfall 134

54 Water Surface Slopes for Series 2 Without Rainfall 135

55 Water Surface Slopes for Series 3 Without Rainfall 136

56 Water Surface Slopes for Series 3 With Rainfall 136

57 Water Surface Slopes for Series 4 Without Rainfall 137

58 Water Surface Slopes for Series 4 With Rainfall 137

CHAPTER I

INTRODUCTION

Many important pollution problems of today involve the movement of sediments by water. Although extensive research has been directed towards reducing or eliminating sediment at its source, less research has been directed towards understanding the mechanics of sediment transport between the origin and the point of deposition. Within the continental United States, an estimated one billion tons of sediment are transported to the sea each year (21). This sediment travels by various modes through a system of rivulets, channels, and gullies which enter major waterways. This sediment ultimately causes extensive damage by sedimentation of the streams and reservoirs and, in general, by polluting the water supplies. Much of this vast sediment load in the streams results from land erosion which occurs during the rain storms. Since the sediment is eroded during the high intensity rainfall period of the storm, the sediment is initially transported by shallow flowing water during the time rainfall is occurring.

This study involves transport of sediment, both as suspended load and bed-load in shallow subcritical flow when rainfall is occurring and thereby disturbing the physical processes in the sediment laden flow.

The citations on the following pages follow the style of the Journal of the Hydraulics Division, Proceedings of the American Society of Civil Engineers.

The primary objectives of this study were:

1. To determine the effect of simulated rainfall on sediment concentration, suspended load transport capacity, and bed-load transport capacity of shallow subcritical flow.
2. To determine the effect of suspended sediment and simulated rainfall on von Karman's universal constant, κ.

The problem was divided into the following four major categories:

1. Pollution of Water by Sedimentation: One billion tons of sediment per year constitutes a heavy load of pollutants. The resulting turbidity in streams used for water supplies increases the cost of purifying the water for domestic, public, and industrial use. High turbidity is also detrimental to fish and wildlife and decreases any potential recreational value.

2. Sedimentation in Reservoirs: Sediment deposits reduce reservoir capacity while increasing the exposed water surface area for a given quantity in storage. Increased evaporation losses per unit volume of storage result and transpiration losses are increased by vegetation growing at the head of the reservoir. Sediment deposits decrease the life of the reservoir project thus depreciating the value of the storage development.

3. Sedimentation in Improved Waterways: Sediment deposits reduce the capacity and efficiency of waterways resulting in higher flood stages. Canals and pools in improved waterways must continually be dredged to maintain navigation depths. Increased maintenance costs are experienced in irrigation canals and ditches.

4. Sediment Deposits on Land Improvements and Habitats: Agricultural crops and lands are severely damaged by layers of infertile deposits. Homes, industries, and transportation facilities in urban areas experience water and sedimentation damage during flooding. Drainage of agricultural and urban land areas is impaired.

Review of Literature

The sediment transport theories reviewed herein were developed primarily for the major water courses throughout the world. These theories are also applicable to sediment transport in shallow subcritical flow without rainfall.

Modes of transport

Sediment transport is accomplished by three methods. These are generally classified as suspended, bed, and saltation. These processes of transport may occur singly or in combination. The transported material is normally transported intermittently by all three methods.

The bed-load transported by flowing water is composed of the larger particles which move on or near the bed. This load travels along the bed by rolling or sliding and is in substantially continuous contact with the bed.

The saltation load transported by flowing water is composed of the material which bounces along the bed. It is moved directly or indirectly by the impact of the bouncing particles. It is extremely difficult to distinguish the saltation load from the suspended load since even suspended particles bounce against the bottom with a frequency proportional to their mass.

The suspended load transported by flowing water is composed of the smaller particles which are kept in suspension by the upward components of the turbulent currents. With erosion of clays the suspended load generally comprises the greatest part of the total sediment load and thereby is the greatest sediment problem.

Bed-load Transport Theories and Equations

Although attempts toward a rational approach have been made through the years, the equations to determine bed-load transportation are essentially empirical in nature. Since the turn of the century bed-load has received much attention; yet, bed-load movement still cannot be accurately predicted.

The basic concept in the early equations was that the loose bed material is sliding in layers under the action of flow. Early investigators reasoned that the top layer of the bed is set into motion by the shear of the water with the bed. In flows where energy is dissipated primarily to overcome friction this shear force, τ_o, is called tractive force and is equal to:

$$\tau_o = \gamma d S_e \quad . \; . \; . \; . \; . \; . \; . \; . \; . \; . \; . \; . \quad (1)$$

in which, γ is the unit weight of the water, d is the depth of flow, and S_e is the slope of the energy gradient. If this shear force, referred to as friction force, becomes larger than the force resisting motion of bed particles the bed will move. Rate of transport is therefore a function of the difference between these two forces.

This theory was first introduced by du Boys, according to Brown (1), in 1879 and is the basis for many bed-load equations. The du Boys equation for bed-load transportation is the first theoretical approach in which rate of transport is related to the flow conditions. Based on the assumption that a certain quantity of sediment is set into motion by excessive tractive force, du Boys concluded that the rate of bed-load transport is proportional to the excess of prevailing tractive force over the critical value required to initiate movement. Thus, du Boys proposed the classical bed-load formula:

$$q_s = C_s \tau (\tau - \tau_c) \quad . \; . \; . \; . \; . \; . \; . \; . \; . \; . \; . \qquad (2)$$

in which, q_s is the rate of transportation, C_s is a sediment coefficient which depends on the character of the sediment, τ and τ_c are the prevailing and critical tractive forces, respectively.

The du Boys equation is widely used because of its simplicity. It has been found to be very useful in discovering general trends in sediment movement. One of the inherent weaknesses in this approach is that it applies only an average value of the shear. This average value of the shear is assumed to be constant in time and space. The assumption is also made that all the particles will start moving simultaneously over the entire bed whenever the average value of the shear, τ, is larger than the critical value, τ_c. Although du Boys equation is based on questionable assumptions regarding the characteristics of sediment movement, it is still being used by many investigators to determine bed-load movement.

In 1926, Schoklitsch, as reported by Shulits (18), developed a bed-load discharge equation from experimental flume data and Forchheimer's exponential velocity equation. The Schoklitsch equation for bed-load transport may be written:

$$q_s = \frac{4.365}{\sqrt{D}} S^{1.5} (q - q_c) \quad \ldots\ldots\ldots\ldots \quad (3)$$

in which, q_s is the rate of bed-load transport, S is the slope of the bed, D is the particle diameter, q and q_c are the observed and critical discharges, respectively.

In 1933, MacDougall (11) concluded that the bed-load is strictly a function of the tractive force which can be expressed as the product of the slope times the depth, or of the slope times the discharge. From a best curve fit analysis of experimental flume data he developed an equation of the form:

$$q_s = C_s S^m (q - q_c) \quad \ldots\ldots\ldots\ldots \quad (4)$$

for sand mixtures in which m is an empirical exponent and C_s is a sediment coefficient.

Evidence that the purely empirical approach was not completely satisfactory came with the introduction of the similarity and dimensional analysis approach. Chien (2) reported the following equation developed in 1934 by Meyer-Peter:

$$\frac{q^{2/3} S_e}{D} = A' + B' \frac{q_s^{2/3}}{D} \quad \ldots\ldots\ldots \quad (5)$$

in which, D is the sediment diameter, S_e is the slope of the energy gradient expressed as a fraction, A' and B' are constants, and q and q_s are flow discharge and flow rate of sediment, respectively.

Shields, according to Brown (1), developed an equation for bed-load transport in 1936. His bed-load equation is dimensionally homogeneous and can be used with any consistent set of units. Shields postulated that the ratio $\frac{\tau_c}{(\gamma_s - \gamma) D}$ is a function of the ratio $\frac{D}{\delta}$ in which, τ_c is the critical tractive force at the channel bed, D is the grain size, δ is the thickness of the laminar sublayer, and γ and γ_s are the unit weight of water and sediment, respectively.

From experimental data Shields developed a diagram showing the dependency of the critical tractive force upon the ratio of the particle size to the thickness of the laminar sublayer.

Kalinske (9) applied fluid turbulence concepts to the critical tractive force theory in 1947. He developed a bed-load transport equation of the form:

$$\frac{q_s}{V_* \gamma_s D} = f\left(\frac{\tau_c}{\tau}\right) \quad \ldots\ldots\ldots\ldots\ldots \quad (6)$$

in which, V_* is the shear velocity, f is a function involving the characteristics of the fluid turbulence and other notations are the same as those previously defined.

In 1948, Meyer-Peter and Muller, as reported by Chien (2), modified Equation 5 in an attempt to develop an empirical equation with all the essential variables. In Modifying Equation 5, Meyer-Peter and Muller separated bar resistance from the total bed resistance. They also introduced the effects of sediment density into their equation:

$$\left(\frac{\eta_b'}{\eta_b}\right)^{3/2} \gamma R_b S_e = A' (\gamma_s - \gamma)D + B' \left(\frac{\gamma}{g}\right)^{1/3} \left(\frac{\gamma_s - \gamma}{\gamma}\right)^{2/3} q_s^{2/3} . \quad (7)$$

in which, η_b and η_b' are roughness coefficients due to the bed and and particles, respectively, A' and B' are empirical coefficients, and R_b is the hydraulic radius of the bed.

Einstein (6) departed from the previous bed-load formulae and developed a new bed-load equation based on probability considerations. Einstein concluded that a given particle size moves in a series of steps of a constant average length and that the particles are periodically deposited in the bed after performing a step.

He assumed that the number of particles deposited per unit of time in a unit bed area can be expressed in terms of the rate of transport and the size and weight of the particles. The rate at which these sediment particles will be eroded from the bed is proportional to the number of particles in the surface of the channel bed, and the probability that such a particle will be eroded. This probability was then expressed as a function of the ratio of dynamic lift on the particle to the weight of the particle under water. The equilibrium rate of bed-load transportation is then determined by equating the number of particles eroded from a unit bed area per unit time. Equating the two forms of probability provided the general function:

$$\phi = f'(\psi) \quad . \; . \; . \; . \; . \; . \; . \; . \; . \; . \; . \; . \quad (8)$$

in which ψ involves the particle characteristics and the bed shear and ϕ involves the rate of movement, the particle size and weight in water, and a dimensionless function of the fall velocity.

In 1950, Einstein (7) replaced his general function with the function:

$$1 - \frac{1}{\sqrt{\pi}} \int_{-B_*\psi - \left(\frac{1}{\eta_o}\right)}^{B_*\psi - \left(\frac{1}{\eta_o}\right)} e^{-t^2} dt \quad . \; . \; . \; . \; . \quad (9)$$

which is equal to:

$$\frac{A_* \phi}{1 + A_* \phi} \quad . \; . \; . \; . \; . \; . \; . \; . \; . \; . \; . \; . \; . \quad (10)$$

in which

$$\phi = \frac{q_s}{\rho_s g} \left(\frac{\rho}{\rho_s - \rho} \right)^{1/2} \left(\frac{1}{qD^3} \right)^{1/2} \quad . \; . \; . \quad (11)$$

$$\psi = \frac{\rho_s - \rho}{\rho} \quad \frac{D}{R'_b S_e} \quad \ldots\ldots \quad (12)$$

A_*, B_* and η_o are universal constants, R'_b is the hydraulic radius of the sediment particles, and ρ_s and ρ are density of sediment particles and fluid, respectively.

Using the Einstein equation to determine bed-load transport in the Niabrara River, Colby and Hembree (4) found that the Einstein equation was not applicable to a single cross section of a reach and was in considerable error. They found that it gave an incorrect distribution of sizes. On the basis of actual measurements, Colby and Hembree developed a modified Einstein procedure for determining total sediment transport.

As reported by Culbertson and Dawdy (5),Bagnold in 1956 developed a theory that predicts the relationship between transport function and shear function for materials of uniform grain size. This transport function is composed of (1) a bed-load transport function, ϕ_b, and (2) a suspended-load transport function, ϕ_s. Assuming the energy distribution is such that the work rate represented by ϕ_s is equal to that represented by ϕ_b, Bagnold derived the functions:

$$\phi_s = \phi_b \left(\frac{B_s}{B_b}\right) \quad \ldots\ldots\ldots \quad (13)$$

and

$$\phi_t = \phi_b \left(\frac{1 + B_s}{B_b}\right) \quad \ldots\ldots \quad (14)$$

in which ϕ_b, ϕ_s, ϕ_t, are the bed-load, suspended-load and total-load transport functions, respectively, and B_s is the dimensionless part of ϕ_s, and B_b is the dimensionless part of ϕ_b.

Bed-load equations are summarized in Reference 17.

Suspended-load Transport Theories and Equations

Prior investigators (15) have established that sediment is kept in suspension by the diffusive power of turbulence. In fluid flow this turbulence can be defined as the irregular motion of eddies of various sizes which are carried along by the flow. Reynolds, as given by Pien (15), first proposed the theory of turbulent flow in 1895. In his analysis of two-dimensional flow he considered the instantaneous rate of transfer of the x-component of momentum per unit area at any point in the y-direction to be:

$$- \rho \, v \, (\bar{u} + u) \quad . \; . \; . \; . \; . \; . \; . \; . \; . \; . \; . \; . \qquad (15)$$

in which, ρ is the mass density of the fluid, and u and v are the turbulent velocity fluctuations in the x and y directions, respectively, and the bar denotes mean value.

Taking the time average of this momentum transfer and integrating, Reynolds determined the shear parallel to x on a plane normal to y. This shear is expressed in the form:

$$\tau = - \rho \, \overline{uv} \quad . \; . \; . \; . \; . \; . \; . \; . \; . \; . \; . \; . \qquad (16)$$

Prandtl, according to Rouse (17), introduced the "mixing length concept" in an attempt to describe the scale of turbulence. The mixing length as proposed by Prandtl is the average distance a small fluid mass will travel before it losses its identity. Prandtl assumed that the mean absolute values of the velocities in the x and y directions are proportional. He also assumed that these velocities are proportional to the mixing length times the mean velocity gradient if the fluid mass travels the mixing length distance in the y-direction before losing its identity. These two proportionalities may be written as follows:

$$/\overline{u}/ \propto /\overline{v}/ \quad . . . . \quad (17)$$

$$/\ \overline{u}\ / \propto 1' \frac{du}{dy} \quad . . . . \quad (18)$$

and

$$/\ \overline{v}\ / \propto 1' \frac{du}{dy} \quad . . . . \quad (19)$$

in which, 1' is length. Prandtl then considered the mean velocity fluctuations in Equation 16 equal to the absolute mean velocity fluctuations in Equation 17 times a proportionality constant. He then expressed the shear intensity as

$$\tau = -\rho\ \overline{uv} = \rho\ K\ /\overline{u}//\ \overline{v}/ = \rho 1^2 \Bigg/\frac{d\overline{u}}{dy}\Bigg/ \Bigg/\frac{d\overline{u}}{dy}\Bigg/ \quad . . . . \quad (20)$$

in which 1 is the mixing length which absorbs the proportionality constant, K.

Introducing Boussinesq kinematic viscosity term:

$$\eta = \rho\varepsilon_m = \rho 1^2 \Bigg/\frac{d\overline{u}}{dy}\Bigg/ \quad . . . . \quad (21)$$

gives the shear intensity in terms of the momentum transfer coefficient, ε_m, representing the exchange of momentum between neighboring filaments. The shear intensity equation can be written:

$$\tau = \rho\tau_m \frac{du}{dy} \quad \ldots\ldots\ldots\ldots\ldots \quad (22)$$

In 1933, O'Brien (14) introduced the basic equation for the distribution of suspended material. Assuming the sediment transfer coefficient, ε_s, is approximately equal to the momentum diffusion coefficient, ε_m, he derived the equilibrium equation:

$$v_f\ c + \varepsilon_s \frac{dc}{dy} = 0 \quad \ldots\ldots\ldots\ldots \quad (23)$$

in which v_f is the fall velocity of the particle in still water, c is the sediment concentration at a distance y above the bed, and ε_s is the sediment transfer coefficient. Integrating Equation 23 leads to the equation:

$$\mathrm{Ln}\ \frac{c}{c_a} = -\ v_f \int_a^y \frac{dy}{\varepsilon_s} \quad \ldots\ldots\ldots\ldots\ldots \quad (24)$$

in which c_a is the concentration at an arbitrary reference level $y = a$.

According to Vanoni (20), von Karman in 1934 introduced Equation 24 to yield the relation:

$$\mathrm{Ln}\,\frac{c}{c_a} = -\rho\, v_f \int_a^y \frac{1}{\tau}\left(\frac{d\bar{u}}{dy}\right) dy \quad \ldots\ldots \quad (25)$$

in which, τ is shear stress. In uniform open-channel flow with a large width to depth ratio the expression for shear at any depth is:

$$\tau = \tau_o\,\frac{d-y}{d} \quad \ldots\ldots\ldots\ldots \quad (26)$$

in which τ_o is the shear at the channel bottom and d is the depth of flow as defined in Equation 1.

Introducing Equation 26 into Equation 25 yields the relation:

$$\mathrm{Ln}\,\frac{c}{c_a} = -\frac{v_f}{\frac{\tau_o}{\rho}} \int_a^y \frac{\frac{d\bar{u}}{dy}}{\frac{d-y}{d}}\, dy \quad \ldots\ldots \quad (27)$$

Introducing von Karman's universal velocity defect law:

$$\frac{d\bar{u}}{dy} = \frac{1}{\kappa}\sqrt{\frac{\tau_o}{\rho}}\;\frac{1}{y} \quad \ldots\ldots\ldots\ldots \quad (28)$$

into Equation 27 yields the relation:

$$\mathrm{Ln}\,\frac{c}{c_a} = -\frac{v_f}{\kappa\sqrt{\tau_o/\rho}} \int_a^y y\,\frac{dy}{\frac{d-y}{d}} \quad \ldots \quad (29)$$

in which κ is von Karman's constant.

Integrating Equation 29 gives the following expression:

$$\frac{c}{c_a} = \left(\frac{d - y}{y} \; \frac{a}{d - a}\right)^z \quad \ldots\ldots\ldots \quad (30)$$

$$z = \frac{v_f}{\kappa\sqrt{\tau_o/\rho}}$$

and permits sediment concentrations at various depths in the flow to be determined if the concentration at depth a is known.

Sediment Transport Disturbed by Rainfall

Smerdon (19) was among the first investigators to recognize and study the problem of sediment transportation in shallow channels disturbed by rainfall. His research showed that the rainfall on a shallow channel will retard the surface velocity of the flowing water and decrease the sediment transport capacity of the flow. Smerdon also found that the mean velocity of the flow was reduced with rainfall. He developed the following empirical logarithmic regression equation from flume data:

$$\frac{V}{V_r} = 0.958d^{-0.046} \quad \ldots\ldots\ldots \quad (31)$$

where V is the mean velocity of low without rainfall in feet per second, V_r is the mean velocity of flow with rainfall in feet per second, and d is the depth of flow without rainfall in feet. His data indicated that the logarithmic velocity defect law was satisfied, but the rainfall slightly retarded the surface velocity thus reducing the velocity gradient. Smerdon's investigation also indicated that the critical tractive force was slightly increased by rainfall due to the reduction of shear at the bottom of the channel.

Glass (8) studying the effects of rainfall on velocity distribution in shallow channel flow substantiated Smerdon's findings. His data also indicated that simulated rainfall retards the velocity near the surface and reduces the velocity gradient of the flow and that the flow velocity with rainfall follows the logarithmic velocity distribution:

$$\frac{v - V}{\sqrt{gdS_e}} = A \log_{10} \frac{y}{d} + E \quad . \; . \; . \; . \; . \qquad (32)$$

where A and E are regression constants and other notations are the same as those previously defined.

Nail (13) studying the effect of two levels of rainfall intensities and velocity rates on the suspension of glass beads in shallow flow found no change in the variance of concentrations resulting from the addition of rainfall. Nail's findings indicated that changes resulting from rainfall are small and accurate instrumentation and measuring techniques are needed for studies of rainfall-sediment transport relations.

CHAPTER II

RESEARCH APPARATUS AND PROCEDURES

This study was conducted in the Soil and Water Research Laboratory of the Agricultural Engineering Department.

Research Apparatus

Research flume. The experiments were performed in a closed-system recirculating research flume (Figure 1). The flume was 12.0 in. wide, 12.0 in. deep, and 39.0 ft long and arranged so that the slope and discharge could be varied. The exit end was supported by a pair of screw jacks. This arrangement allowed any desired slope up to a maximum of 3 per cent. The discharge was varied in the closed system by changing the speed of the pump in the system through a variable-ratio transmission in the electric motor.

The flume sides were constructed of 1/2 in. plexiglass allowing an unobstructed view of the flume bed as shown in Figure 2. The flume bottom was a 12 in. aluminum structural channel covered carefully with two coats of epoxy paint to give a reasonably smooth bed.

The flow entered the flume through a 12.0 in. by 12.0 in. vertical entrance header box with entrance section as shown in Figure 2. The header box was designed with a transition section from the 4. in. return pipe to the flume bed to eliminate any possibility of flow separation.

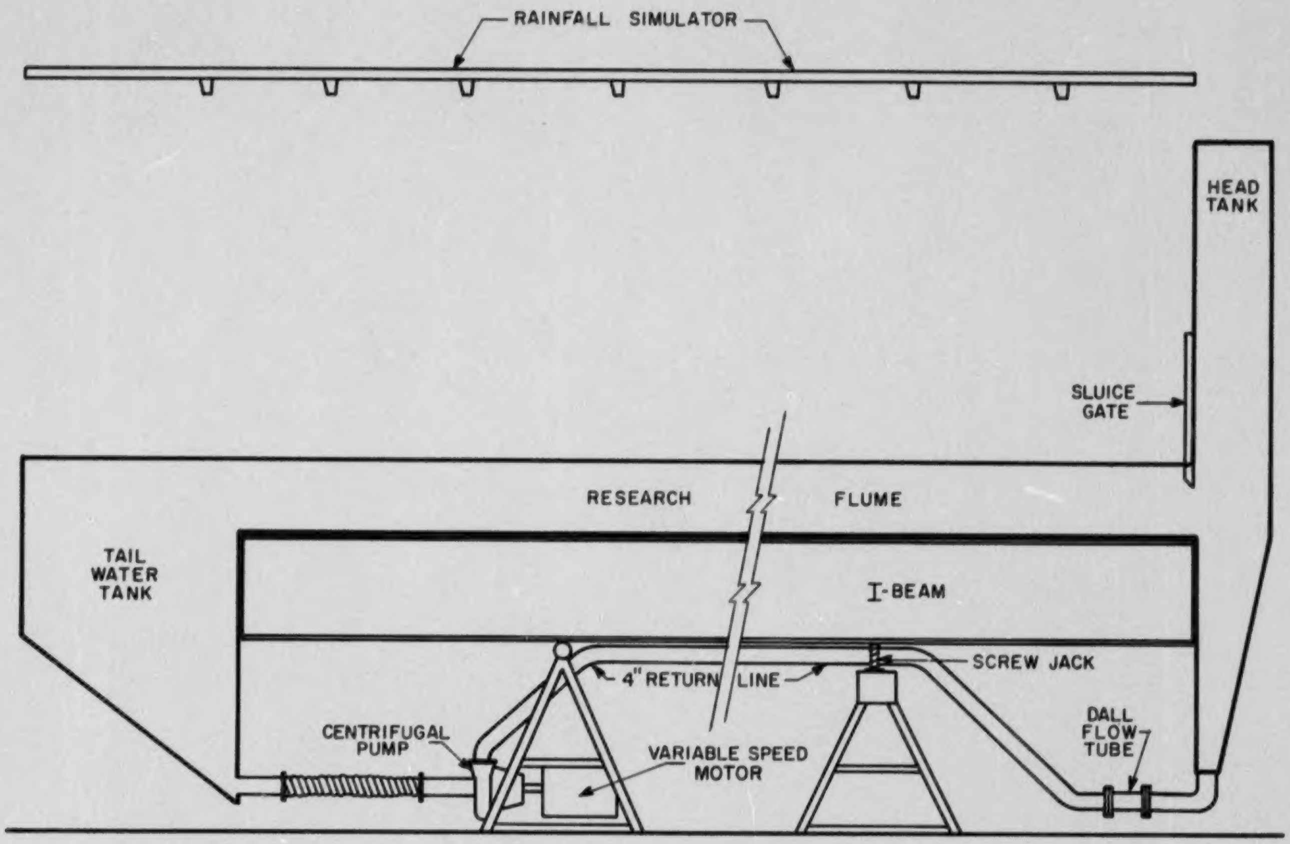
RAINFALL SIMULATOR
HEAD TANK
SLUICE GATE
RESEARCH FLUME
TAIL WATER TANK
I-BEAM
4" RETURN LINE
SCREW JACK
DALL FLOW TUBE
CENTRIFUGAL PUMP
VARIABLE SPEED MOTOR

FIGURE I SCHEMATIC OF FACILITIES USED FOR THIS STUDY

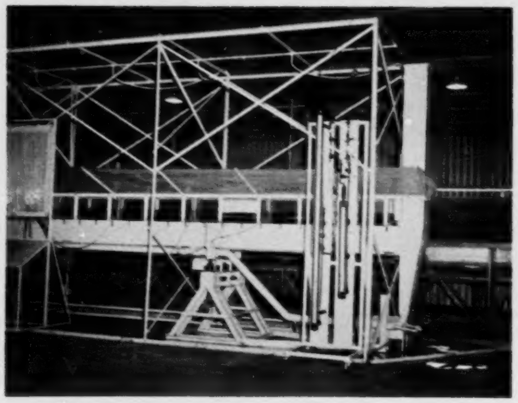

FIGURE 2 PARTIAL VIEW OF RECIRCULATING RESEARCH FLUME AND RAINFALL SIMULATOR

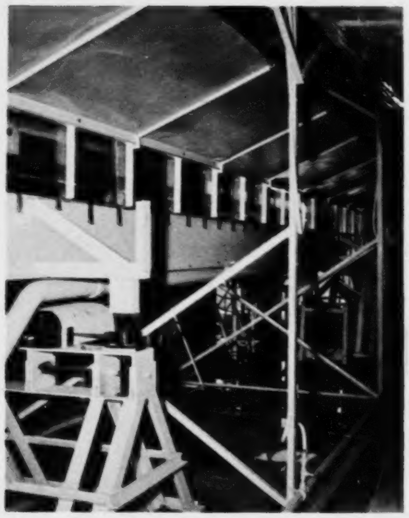

FIGURE 3 PARTIAL VIEW OF RECIRCULATING RESEARCH FLUME

The flow from the flume discharged into a 1 ft wide, 5 ft long, and 6 ft deep steel tailwater tank. The tank tapered downward towards a 4 in. return pipe. The sediment-laden flow was recirculated through the system by a centrifugal pump unit in the return line. By making the circulation system a closed system with the minimum velocity in the flume, the suspended sediment could be recirculated with the water without depositing sediment in the return system.

Rainfall simulator. The research flume was equipped with a rainfall simulator. The simulator design was based on research conducted by Meyer and McCune (12). Spraying Systems Company 80100 Veejet Nozzles were selected to simulate rainfall. Operated under a pressure of 6 psi at a height of 8 ft, the simulator produced rainfall with the following characteristics:

1. A drop size distribution similar to that of natural rainfall.
2. A drop fall velocity near the terminal velocity of raindrops (16 to 30 fps for drop diameters of 1.25 to 6.00 mm).
3. Random drop size distribution over the bed.
4. Reliable rainfall intensity during the study.

The simulated rainfall was produced from seven nozzles spaced at 5 ft intervals along a 1 in. overhead supply line. The water supply for the simulator was siphoned from the flume tailwater tank through a 1-1/2 in. perforated pipe intake. A separate 3/4 hp centrifugal pump unit was used to maintain pressure in the simulator supply lines. Four 5/8 in. rubber hose lines with control valves were spaced evenly along the overhead line to maintain uniform pressure at the nozzles. Three 5/8 in. rubber hoses with pressure gauges were spaced evenly along the overhead supply line for establishing and monitoring the pressure at the nozzles. Figures 4 and 5 show the rainfall simulator with and without simulated rainfall.

Simulated sediment. Spherical glass beads in the very fine sand and silt size ranges were chosen to simulate sediment. A hydrometer analysis indicated a distribution of 30 per cent very fine sand and 70 per cent silt (Figure 6). Very fine sand was defined as sediment particles having diameters from 50μ to 100μ. Silt was defined as sediment particles having diameters of 5μ to 50μ. Simulated sediment specifications are shown in Table I. The glass beads are shown in a photomicrograph (Figure 7).

Measurements

Depth measurements. Water depths were measured with a hook gauge mounted on the instrument carriage parallel to the Pitot-static tube as shown in Figure 8. The depth measurements were made by first verifying the elevation of the hook gauge and then lifting the hook to the water surface. Due to minor water surface fluctuations at very shallow depths the hook gauge was read to 0.01 ft by means of the vernier scale. During each test run the depth was

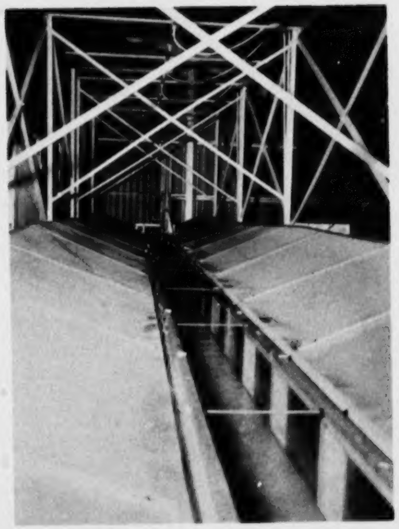

FIGURE 4 FLOW IN RESEARCH FLUME WITHOUT SIMULATED RAINFALL

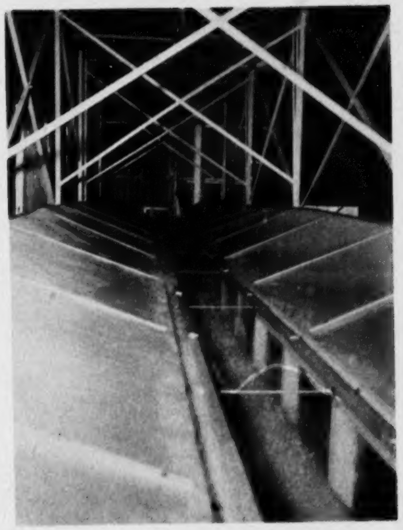

FIGURE 5 FLOW IN RESEARCH FLUME WITH SIMULATED RAINFALL

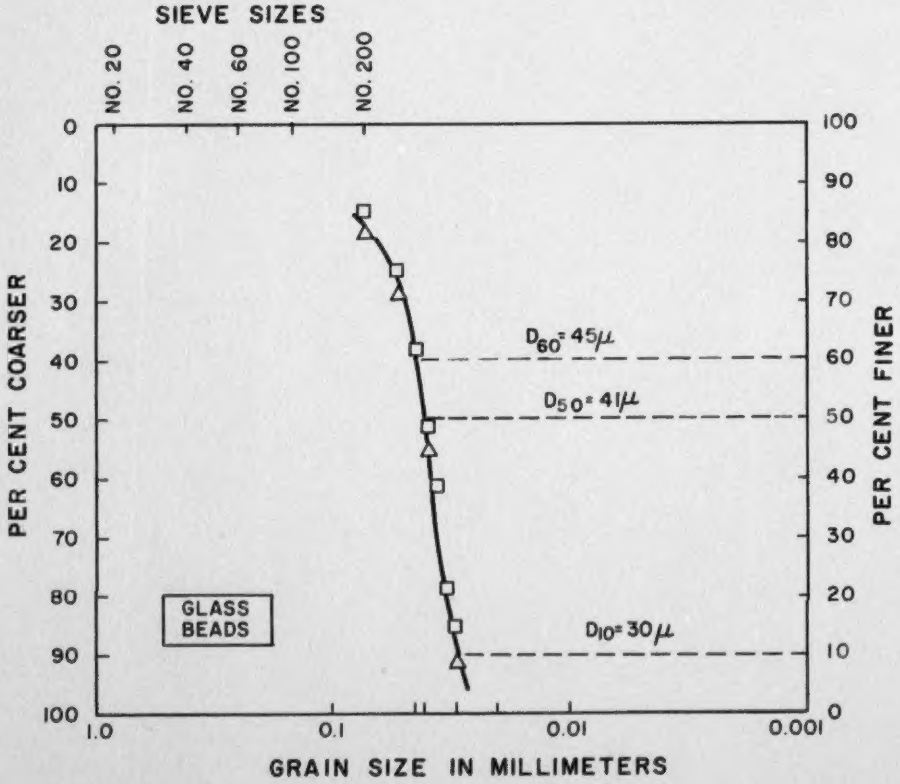

FIGURE 6 GRAIN SIZE DISTRIBUTION CURVE

TABLE I

PHYSICAL PROPERTIES OF THE GLASS BEADS

Physical Properties		
Mean Diameter	(D_{50})	41µ
	(D_{60})	45µ
	(D_{10})	30µ
Specific Gravity		2.50
Shape		3 to 10 per cent were not accurate spheres.
Size Range		31µ to 69µ (approximately 90 per cent by weight fell within the specified size range).
Fall Velocities (in water at 30°C)	(D_{50})	0.0042 ft/sec
	(D_{60})	0.0055 ft/sec
	(D_{10})	0.00225 ft/sec

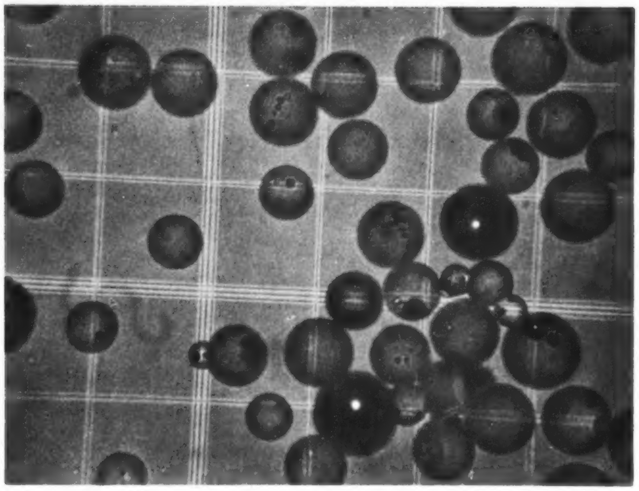

FIGURE 7 PHOTOMICROGRAPH OF GLASS BEADS (50μ SQUARES)

Reproduced from best available copy.

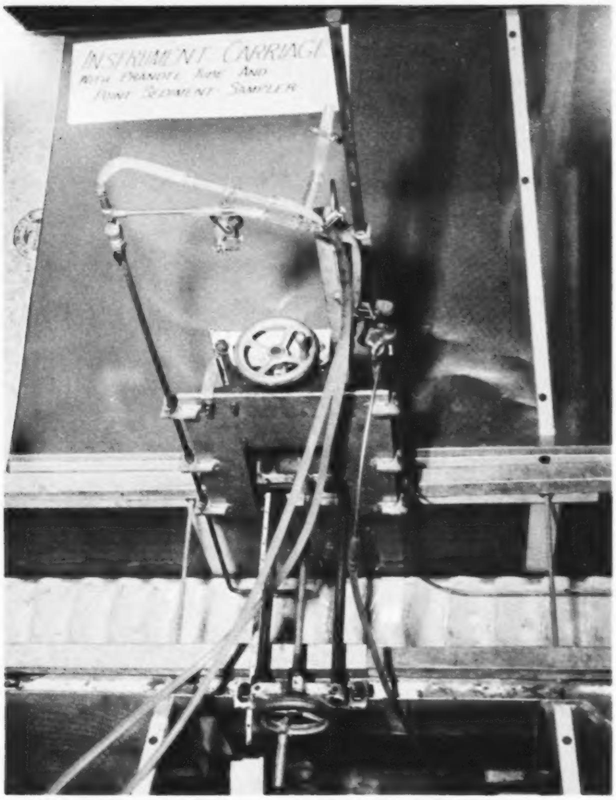

FIGURE 8 INSTRUMENT CARRIAGE WITH PRANDTL TUBE AND POINT SEDIMENT SAMPLER POSITIONED IN THE RESEARCH FLUME

continually verified by checking the water depth in stilling well number 8 which was immediately upstream from the test section in the flume. The average water depth for the flume was obtained from stilling well measurements.

Velocity measurements. Velocities were measured with a Pitot-static tube (O.D. 5/32 in. - I.D. 1/16 in.) of the standard Prandtl design as shown in Figure 8. The differential pressure on the Pitot-static tube was read to 0.005 ft on a differential inclined manometer containing an indicating fluid with a specific gravity of 1.75, and to 0.004 ft on a Pace CD-25 commercial pressure transducer indicator shown in Figure 9.

The readings were converted to velocities by assuming a coefficient of unity for the Pitot-static tube (assumption was verified by comparing the Pitot-static tube with a calibrated Prandtl tube). The pressure transducer indicator was calibrated by comparing the indicator reading with a static head of water as shown in Figure 9. The Pitot-static tube was mounted on an instrument carriage placed perpendicular to the flow in the flume. The instrument carriage was designed so that point velocities could be taken at any point in the flow cross section.

Discharge measurements. The flume discharge was measured with a Dall flow tube (Figure 10). The flow tube was connected to two well-type manometers, one containing an indicator fluid with a specific gravity of 1.75 and the other with mercury (specific

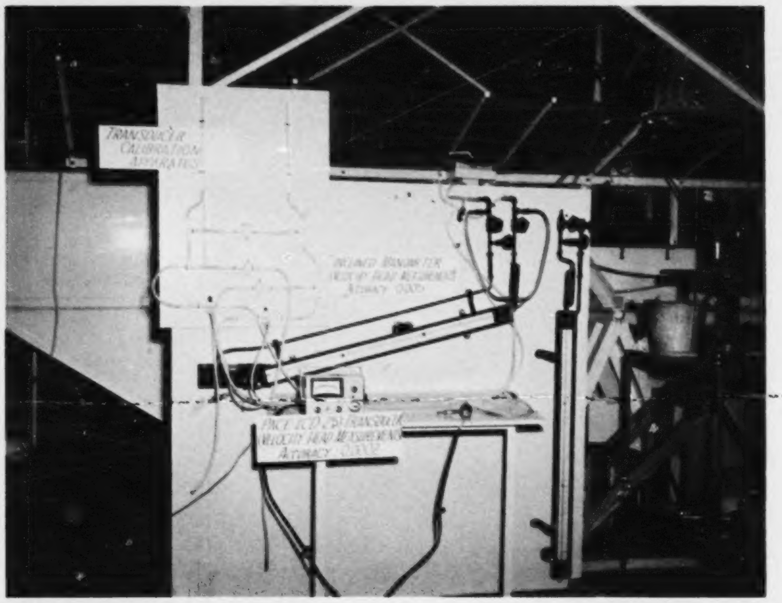
TRANSDUCER CALIBRATION APPARATUS
INCLINED MANOMETER
VELOCITY HEAD MEASUREMENTS
TRANSDUCER
VELOCITY HEAD MEASUREMENTS

FIGURE 9 DIFFERENTIAL INCLINED MANOMETER, TRANSDUCER INDICATOR, AND TRANSDUCER CALIBRATION APPARATUS

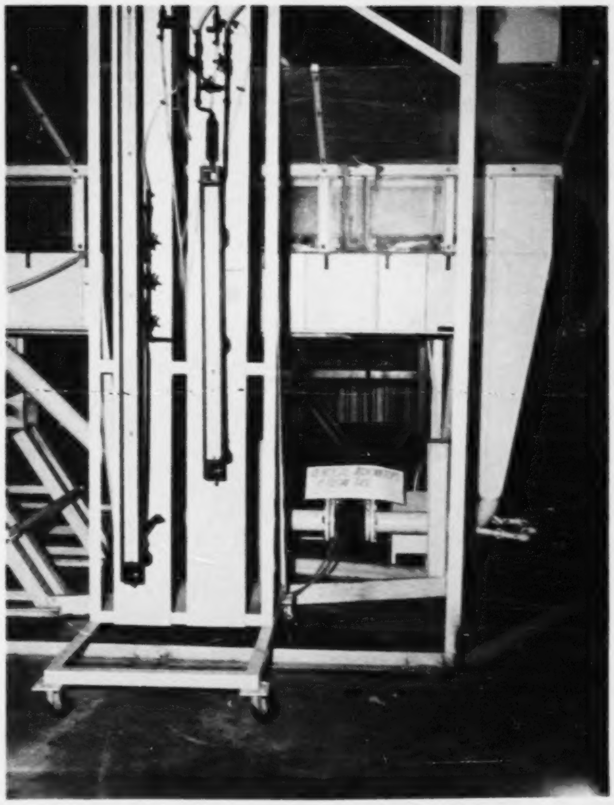

FIGURE 10 VERTICAL MANOMETER BOARD AND DALL FLOW TUBE.

gravity 13.55). The flume discharge was determined from rating curves furnished by the manufacturer.

Point sediment measurements. Sediment concentrations were determined from point sediment-water samples siphoned from the flow through a stainless steel pipette (O.D. 5/64 in. - I.D. 3/64 in.) as shown in Figure 8. The average velocity at which the sediment-water mixture entered the point sampler was made equal to the stream velocity at the sampling point by adjusting the siphoning head on the sampler. The point sediment sampler was mounted on an instrument carriage placed perpendicular to the flow in the flume. The instrument carriage was designed so that the point sediment samples could be taken at any point in the flow.

Total sediment measurements. Total load sediment concentrations were siphoned from the return system where all the material was transported in suspension. Samples taken from four point sediment samplers in the vertical section of the header box were averaged to obtain the total load sample.

Flow adjustment. Discharge in the flume was set and adjusted by changing the variable speed pump setting prior to the test (Figure 11). The discharge was varied until the predetermined depth was established in the test section. Uniform flow for test series A and 2 with 0.3 ft depth of flow was easily attained in the flume. In test series 1, 3 and 4 with depths of 0.3, 0.2 and 0.1 ft, respectively, nonuniform flow conditions were experienced.

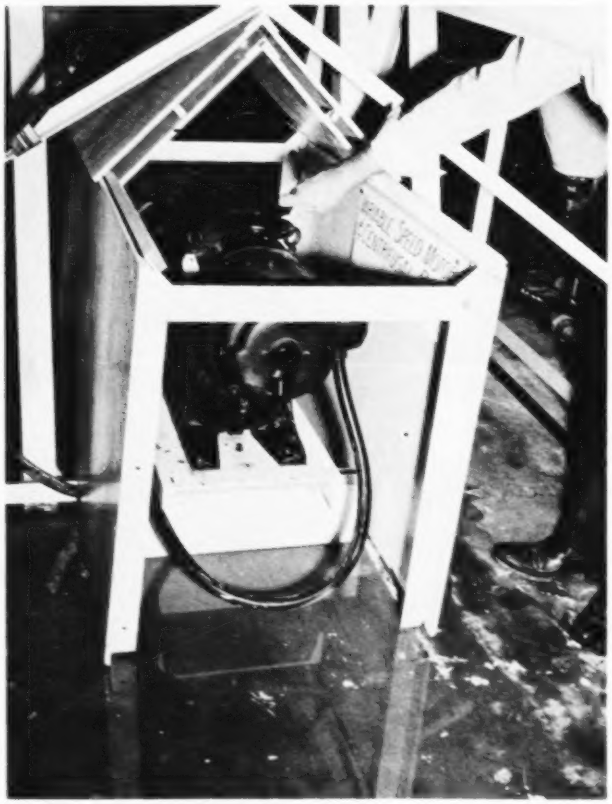

FIGURE II VARIABLE SPEED MOTOR AND CENTRIFUGAL PUMP

Uniform flow conditions were not attainable with an adjustment of the flow. Once the flow was set and adjusted it remained steady throughout the test. No difficulty was experienced in the closed system due to pendulations or any other instability.

Flow profile. The water surface profile was obtained from nine stilling wells spaced at 4 ft intervals along the flume. Depth measurements for the flow profile were read directly from the staff gauges mounted in the stilling wells. The change in depth per unit distance, $\frac{\Delta y}{\Delta x}$, was computed from the water surface profile for use in the gradually varied flow and spatially varied flow equations.

Temperature measurements. The water temperature was taken at the beginning of each test series and then monitored throughout the test. Temperature measurements were made with a standard Centigrade thermometer.

Test Program

Preliminary tests were run in the research flume to establish flow conditions for the test program which is shown in Table II.

Procedure

The testing program outlined in Table II was conducted during this study. Tests were run at flow depths of 0.1, 0.2 and 0.3 ft. A flume slope of 0.0008 ft/ft was maintained throughout the study.

TABLE II

PRELIMINARY TEST PROGRAM

Test Series	Rainfall Condition	Sediment Condition	Depth of Flow ft	Discharge cfs
A	W/O[1]	W/O	0.3	0.5
B	W/O	W/O	0.3	0.3
	W[2]	W/O	0.3	
C	W/O	W/O	0.2	0.3
	W	W/O	0.2	
1	W/O	W	0.3	0.5
2	W/O	W	0.3	0.3
3	W/O	W	0.2	0.3
	W	W	0.2	
4	W/O	W	0.1	0.15
	W	W	0.1	

[1] Without

[2] With

Test conditions. With the initiation of a test series the flume was filled to the desired depth of flow with the variable speed pump set and running for the desired discharge. Minor adjustments were then made in the flow conditions until the depth and discharge shown in Table II were obtained in the flume. With the flow at an equilibrium condition the system was checked. Both manometers were primed to remove entrapped air from the lines. All stilling wells were read to establish the slope of the water surface in each test.

Test series. Test series A (Runs 1 through 5) was conducted to determine von Karman's constant for clear water flow. The point velocity readings were taken at the centerline of the flow. Depth readings for test series A are shown in Table III.

Test series B and C were run with clear water to test the assumption of two-dimensional flow. The point velocity readings were taken at distances of 0.125 ft and 0.25 ft from each side and at the centerline. Depth readings for test series B and C are shown in Table III. Both test series were conducted with and without rainfall. An analysis of the data indicates that two-dimensional flow can be assumed for all test runs.

Test series 1 through 4 (Runs 1 through 6) were conducted to determine von Karman's constant for sediment-laden flow. At the initiation of a test series the simulated sediment was introduced into the flow in ten-pound increments until the simulated sediment covered the bed of the flume as shown in Figure 12. Approximately 90 pounds of simulated sediment were circulated in the closed system flume during the study. Upon establishing the flow condition for the test the point velocity data were obtained with the Pitot-static tube set at the depths shown in Table III. Point sediment data were taken simultaneously from the point sediment sampler set at the same

TABLE III

PITOT-STATIC TUBE AND POINT SEDIMENT LOCATIONS FOR TEST PROGRAM

Test Series	Total Depth of Flow ft	Depth of Pitot-static Tube above Bed ft	Depth of Point Sediment Sampler above Bed ft
A	0.3	0.933d, 0.800d, 0.667d,† 0.533d, 0.333d, 0.200d, 0.067d	
B	0.3	0.917d, 0.833d, 0.667d, 0.500d, 0.333d, 0.167d, 0.083d	
C	0.2	0.900d, 0.800d, 0.700d, 0.500d, 0.300d, 0.200d, 0.100d, 0.050d	
1	0.3	0.933d, 0.800d, 0.667d, 0.533d, 0.333d, 0.200d, 0.133d, 0.067d, 0.033d	0.933d, 0.800d, 0.677d,† 0.533d, 0.333d, 0.200d, 0.133d, 0.067d, 0.033d
2	0.3	0.933d, 0.800d, 0.667d 0.533d, 0.333d, 0.200d, 0.133d, 0.067d	0.933d, 0.800d, 0.667d, 0.533d, 0.333d, 0.200d, 0.133d, 0.067d
3	0.2	0.900d, 0.800d, 0.700d, 0.500d, 0.300d, 0.200d, 0.100d, 0.050d	0.900d, 0.800d, 0.700d, 0.500d, 0.300d, 0.200d, 0.100d, 0.050d
4	0.11	0.715d, 0.535d, 0.355d, 0.179d, 0.089d	0.715d, 0.535d, 0.355d, 0.179d, 0.089d

† d = total depth.

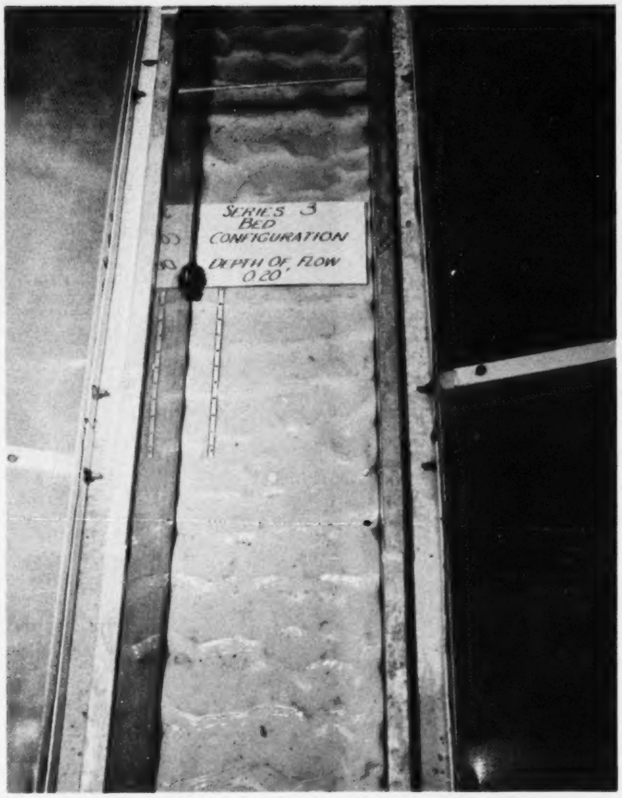
SERIES 3
BED
CONFIGURATION
DEPTH OF FLOW
0.20'

FIGURE 12 BED CONFIGURATION
SERIES 3
d = 0.20 FT.
q = 0.30 CFS.

depths. Three replications of the velocity and sediment data were obtained for each depth.

Test series 3 and 4 (Runs 7 through 33) were designed to determine the effects of simulated rainfall on both von Karman's universal constant and sediment transport. Upon establishing the flow condition for the test the velocity data were obtained with the Pitot-static tube set at the depths shown in Table III. Point sediment data were taken simultaneously from the point sediment sampler set at the same depths. Runs 7 through 15 were taken before simulated rainfall was imposed on the flow. Runs 16 through 18 were taken 15 seconds after the initiation of rainfall. Runs 19 through 27 were taken on 45-second intervals. Tests were concluded with runs 28 through 30 and 31 through 33 which were taken 4 minutes and 6 minutes, respectively, after the initiation of rainfall. Three replications of the velocity and sediment data were taken for each depth.

Data reduction. Upon completion of a series of test runs the pre-weighed collection bottles containing the simulated sediment and water samples were transported to the Soil and Water Analytical Laboratory for weighing on a Mettler balance (accuracy ± 0.01 grams). After weighing the simulated sediment and water samples a filtering technique was used to remove the simulated sediment from the samples. Whatman No. 41 (low ash) filter paper was used to remove the simulated sediment.

Upon completion of the filtering operation the filter papers with simulated sediment samples were placed in pre-weighed crucibles and transported to the State Chemist Analytical Laboratory for ashing in a high temperature oven (550 °C). The crucibles containing the filter paper and simulated sediment samples remained in the high temperature oven for two hours to assure complete ashing of the filter paper. Upon removal from the high temperature oven the crucibles with simulated sediment sample and filter paper ash (average ash weight 0.0003 grams) were placed in a dessicator for cooling and transportation to the Soil and Water Analytical Laboratory.

Upon reaching room temperature the crucibles with contents were weighed on an Ainsworth balance (accuracy ± 0.0001 grams). At the completion of this series of operations the crucibles were washed, dried, and stored in the dessicators for cooling and pre-weighing prior to the next test run.

CHAPTER III

ANALYSIS OF DATA AND DISCUSSION OF RESULTS

One of the primary objectives of this study was to determine the effect of suspended sediment and simulated rainfall on von Karman's universal constant.

Von Karman's Universal Constant

Test series A, B and C in this study were conducted to determine von Karman's universal constant for clear water flow without simulated rainfall. Test series 1 through 4 (Runs 1 through 6), without simulated rainfall, were run during this study to determine the effect of sediment on von Karman's universal constant while test series 3 and 4 (Runs 7 through 33), without and with simulated rainfall, were run to determine the combined effects of suspended sediment and simulated rainfall on von Karman's universal constant. All the data in this study were analyzed using the IBM 7094 computer.

Clear water flow without rainfall. Test series A, B and C were conducted to determine von Karman's universal constant, κ, for clear water flow without simulated rainfall. A regression analysis technique was used to determine the best fit dimensionless velocity profiles. The velocity profile was of the form:

$$\frac{v - V}{\sqrt{gdS_e}} = A \log_{10} \frac{y}{d} + E \quad . . . . . . \quad (32)$$

in which, A is the slope of the curve of the semilogarithmic graph and E is the intercept at $\log_{10} \frac{y}{d} = 0$. All the terms in Equation 32 were measured except A, E, and V. The constants A and E were determined from the regression analysis, while the mean velocity, V, was determined by dividing the integrated dimensionless velocity profile by the total depth of flow. Von Karman's university constant was evaluated from the slope A ($\kappa = \frac{2.3}{A}$) of the curve on the semilogarithmic graph. The computed values for von Karman's universal constant range from 0.562 to 0.699 for test series A, B and C and are shown in Figures 13 through 17. The average von Karman's constant for these tests in clear water is 0.617. Regression coefficients, von Karman's universal constant and goodness of fit for test series A, B and C are summarized in Table IV (Individual test runs are given in Table VIII in the Appendix). Glass (8) found values ranging from 0.487 to 0.602 in his studies of clear water flow. Smerdon (19) and Glass (8) computed average values of 0.552 and 0.553, respectively, in their studies of clear water flow using a different flume and related apparatus. The value of 0.40 (accepted value for von Karman's universal constant for clear flow in pipes) was greatly exceeded in all clear water studies. A satisfactory explanation for this increase above the accepted value of 0.40 requires a complete understanding of the turbulent mixing in the flow.

Effect of simulated rainfall. Glass (8) studied the effect of

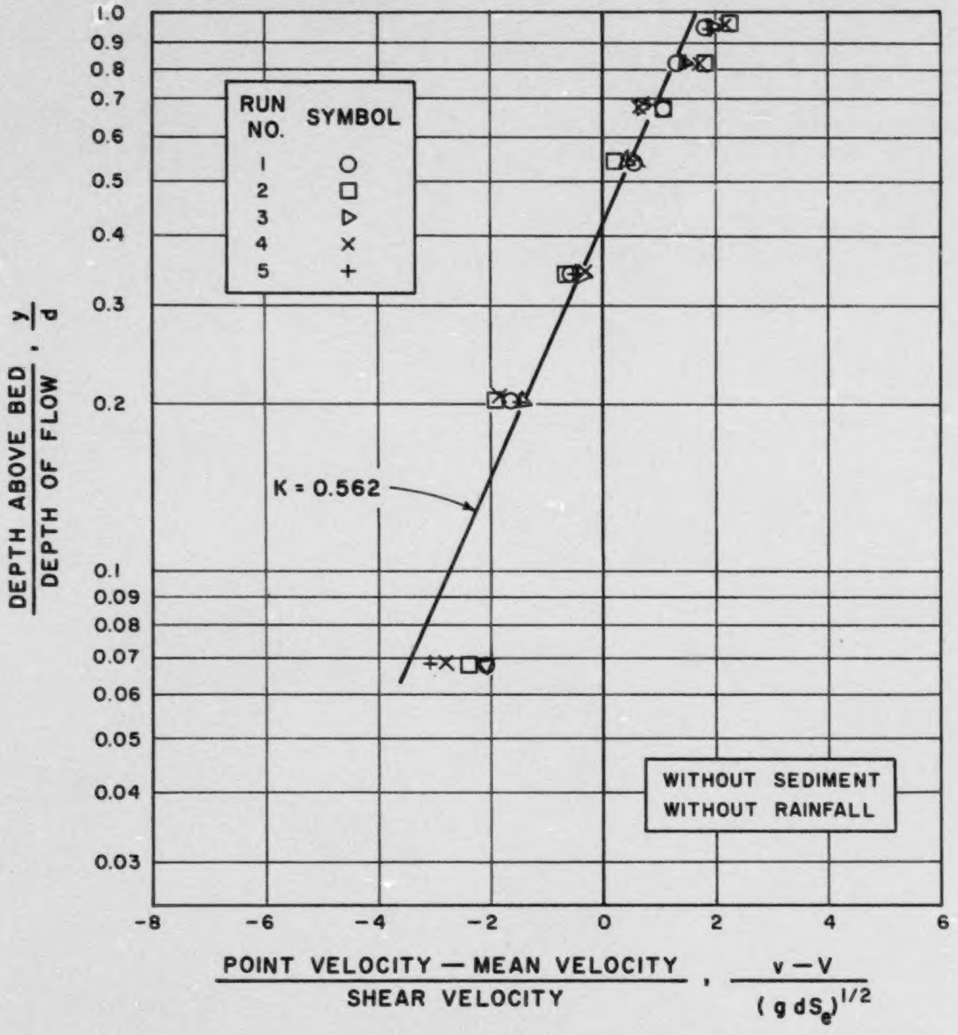

FIGURE 13. VELOCITY DISTRIBUTION REGRESSION CURVE FOR TEST SERIES A (0.30 FT. DEPTH OF FLOW) USING PRANDTL TUBE AND MANOMETER.

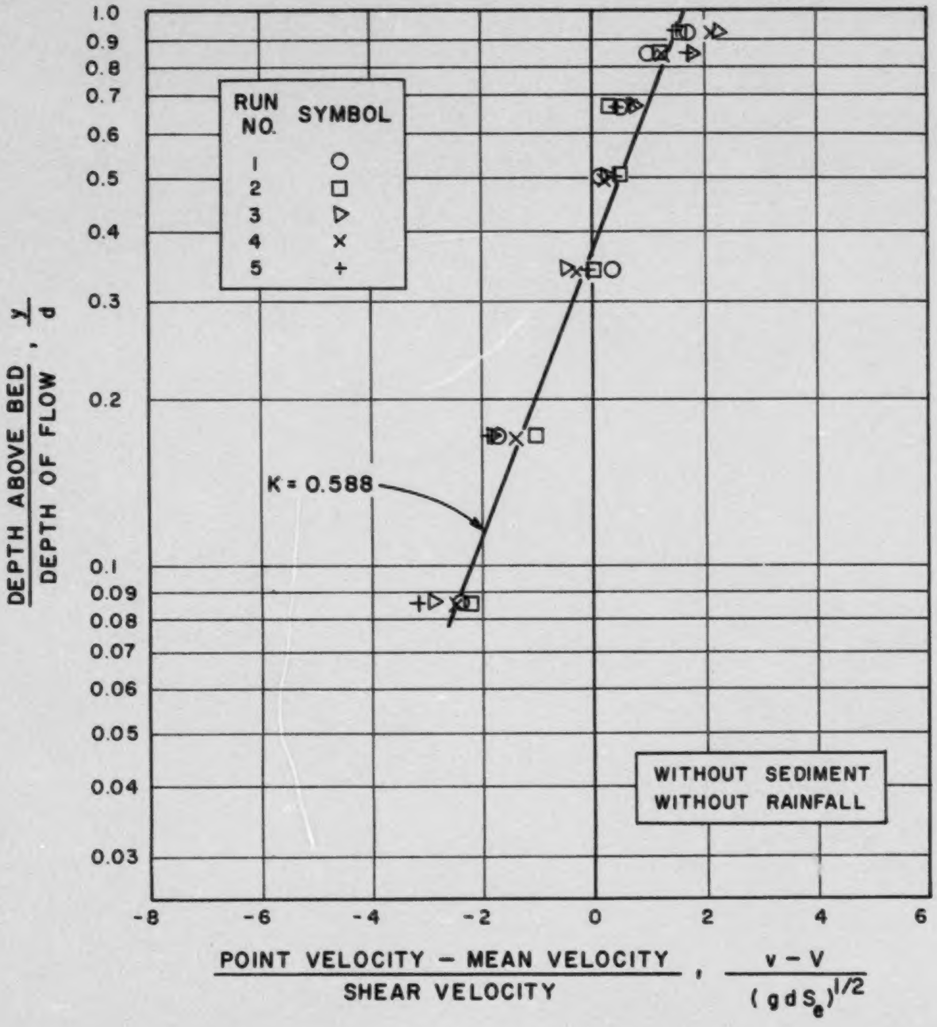

FIGURE 14 VELOCITY DISTRIBUTION REGRESSION CURVE FOR TEST SERIES B (0.30 FT. DEPTH OF FLOW) USING PRANDTL TUBE AND MANOMETER.

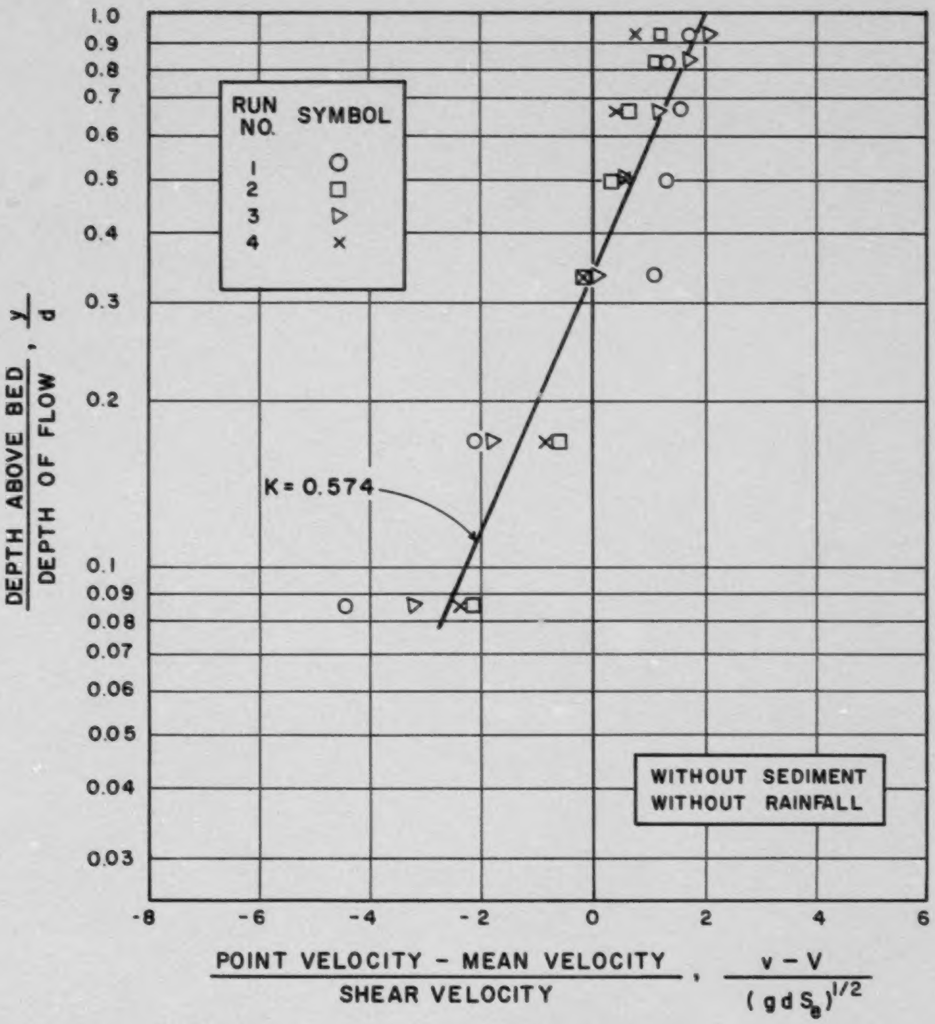

FIGURE 15 VELOCITY DISTRIBUTION REGRESSION CURVE FOR TEST SERIES B (0.30 FT. DEPTH OF FLOW) USING PRANDTL TUBE AND TRANSDUCER.

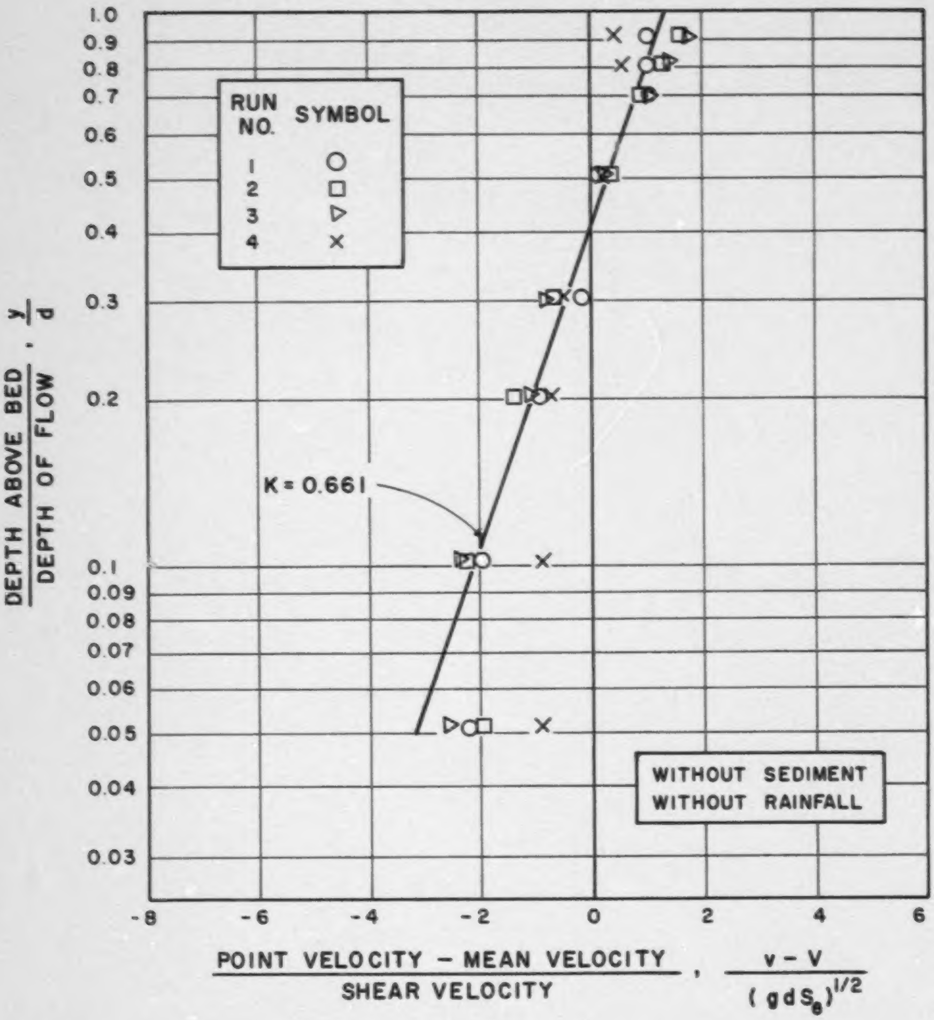

FIGURE 16 VELOCITY DISTRIBUTION REGRESSION CURVE FOR TEST SERIES C (0.20 FT. DEPTH OF FLOW) USING PRANDTL TUBE AND MANOMETER.
]

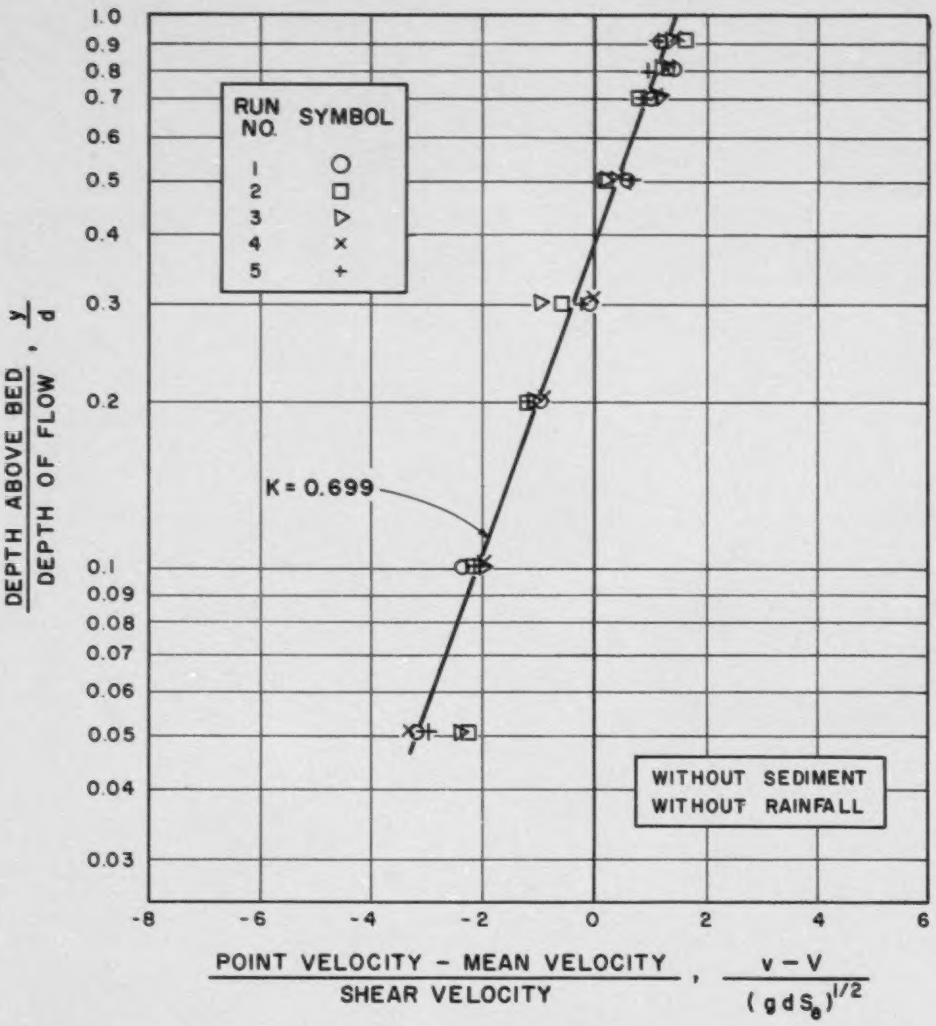

FIGURE 17 VELOCITY DISTRIBUTION REGRESSION CURVE FOR TEST SERIES C (0.20 FT. DEPTH OF FLOW) USING PRANDTL TUBE AND TRANSDUCER.

TABLE IV

REGRESSION ANALYSIS RESULTS OF VELOCITY DEFECT LAW FOR TESTS CONDUCTED WITHOUT SIMULATED RAINFALL

Series No.	Velocity Head Indicator[1]	Regression Coefficients A^2	Regression Coefficients E^2	κ^3	N^4	F^5	Significance Level	Velocity Distribution Regression Curve Figure No.
A	M	4.096	1.779	0.562	35	416.13	0.001	17
B*	M	-	-	0.588	35	-	-	18
	T	-	-	0.574	28	-	-	19
C*	M	-	-	0.661	28	-	-	20
	T	-	-	0.699	35	-	-	21
1	M	6.142	2.667	0.375	54	546.87	0.001	22
	T	6.129	2.661	0.375	54	627.96	0.001	23
2	M	5.893	2.559	0.391	48	-	-	24
	T	6.129	2.662	0.376	48	-	-	25
3	M	5.574	2.421	0.413	48	-	-	26
	T	5.380	2.336	0.428	48	-	-	27
4	M	7.585	3.924	0.303	30	403.35	0.001	28
	T	6.698	2.909	0.344	30	610.50	0.001	29

[1] M = Manometer; T = Transducer.

[2] A = Slope of the regression line; E = Intercept of the regression line at $\log_{10}\frac{y}{d} = 0$.

[3] κ = von Karman's universal constant.

[4] N = Number of readings included in the regression.

[5] F = Statistical test for goodness of fit.

* Test series data averaged from individual runs.

rainfall on the velocity distribution in clear water flow. Assuming a logarithmic distribution existed with simulated rainfall, Glass used a regression analysis technique to determine the constants for the dimensionless velocity profile. Glass (8) computed values of von Karman's constant ranging from 0.495 to 0.805 in his studies. The average for his tests with simulated rainfall was 0.633. Values of 0.479 to 0.602 for von Karman's constant were found during preliminary test runs. The average for these tests in clear water flow with rainfall was 0.540.

Effect of suspended sediment. Test series 1 through 4 (Runs 1 through 6), without simulated rainfall, were run to determine the effect of suspended sediment on von Karman's universal constant. Regression analysis was used to determine the best fit dimensionless velocity profiles (Figures 18 through 25). The velocity profile was of the form given in Equation 32. All the terms for each test run except A, E and V were measured. The constants A and E were evaluated from the regression analysis while the mean velocity was determined by the method previously discussed. Regression constants, von Karman's universal constant and goodness of fit for test series 1 through 4 (Runs 1 through 6) are given in Table IV (individual test runs are given in Table VII in the Appendix). The computed values for von Karman's universal constant range from 0.303 to 0.428 for test series 1 through 4. The average universal constant for these tests with sediment was 0.376.

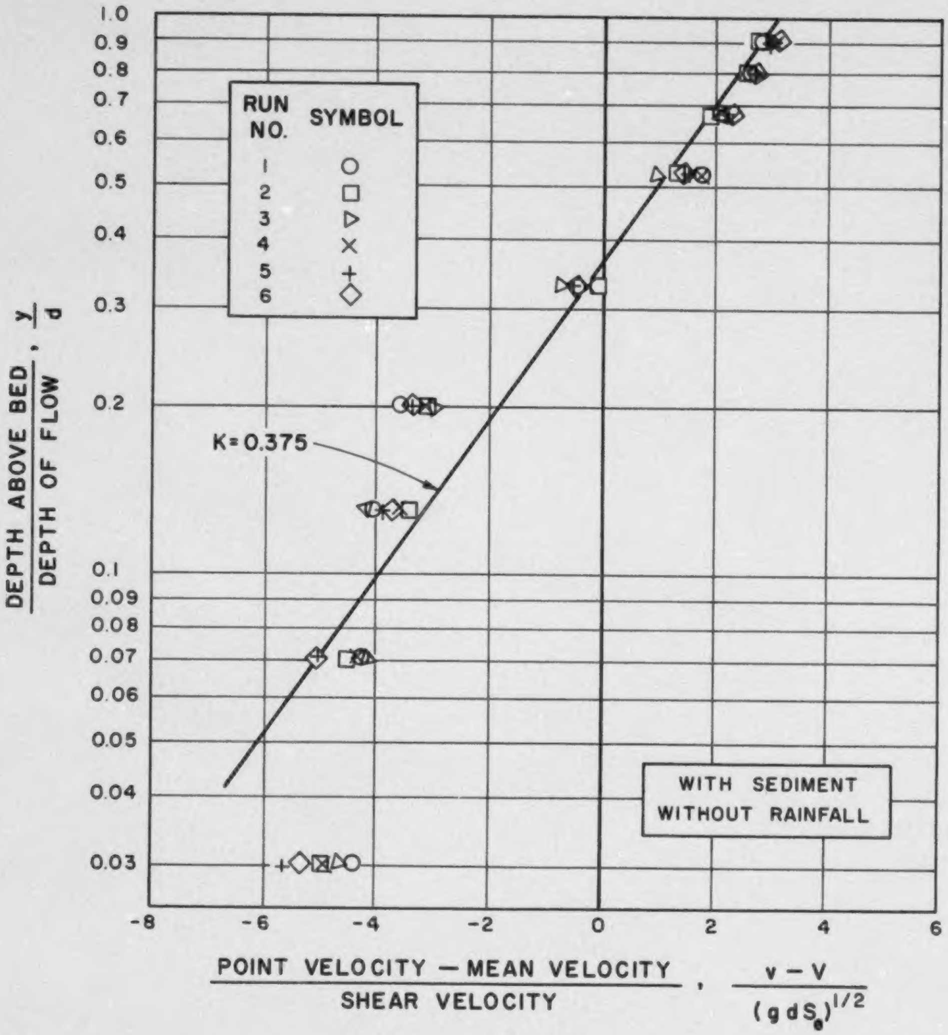

FIGURE 18 VELOCITY DISTRIBUTION REGRESSION CURVE FOR TEST SERIES I (0.30 FT. DEPTH OF FLOW) USING PRANDTL TUBE AND MANOMETER.

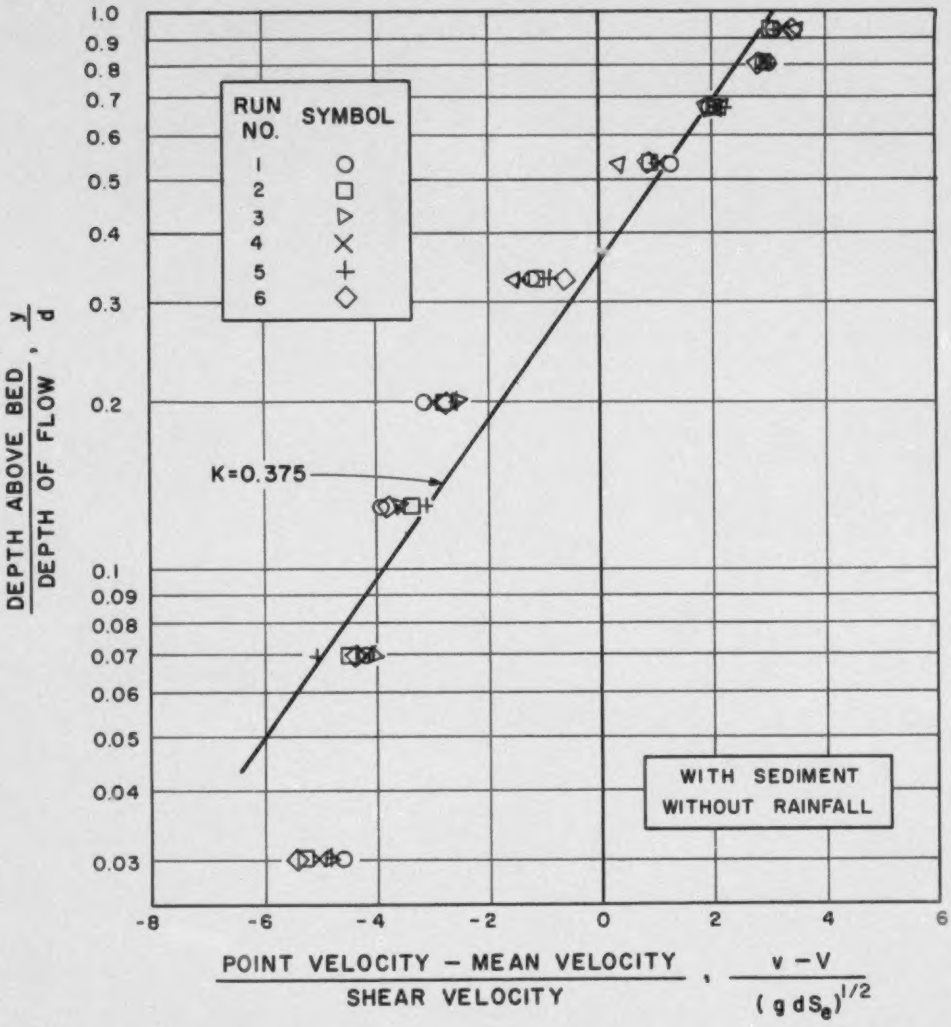

FIGURE 19 VELOCITY DISTRIBUTION REGRESSION CURVE FOR TEST SERIES I (0.30 FT. DEPTH OF FLOW) USING PRANDTL TUBE AND TRANSDUCER.

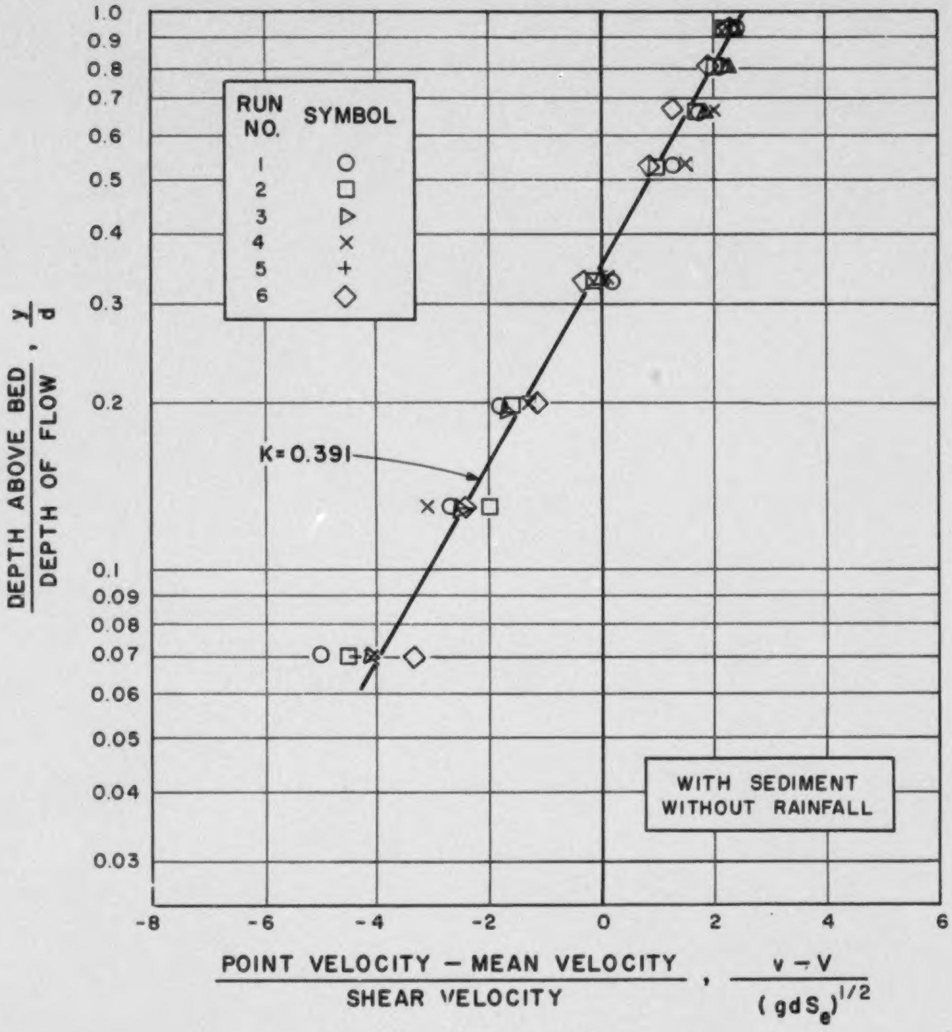

FIGURE 20 VELOCITY DISTRIBUTION REGRESSION CURVE FOR TEST SERIES 2 (0.30 FT. DEPTH OF FLOW) USING PRANDTL TUBE AND MANOMETER.

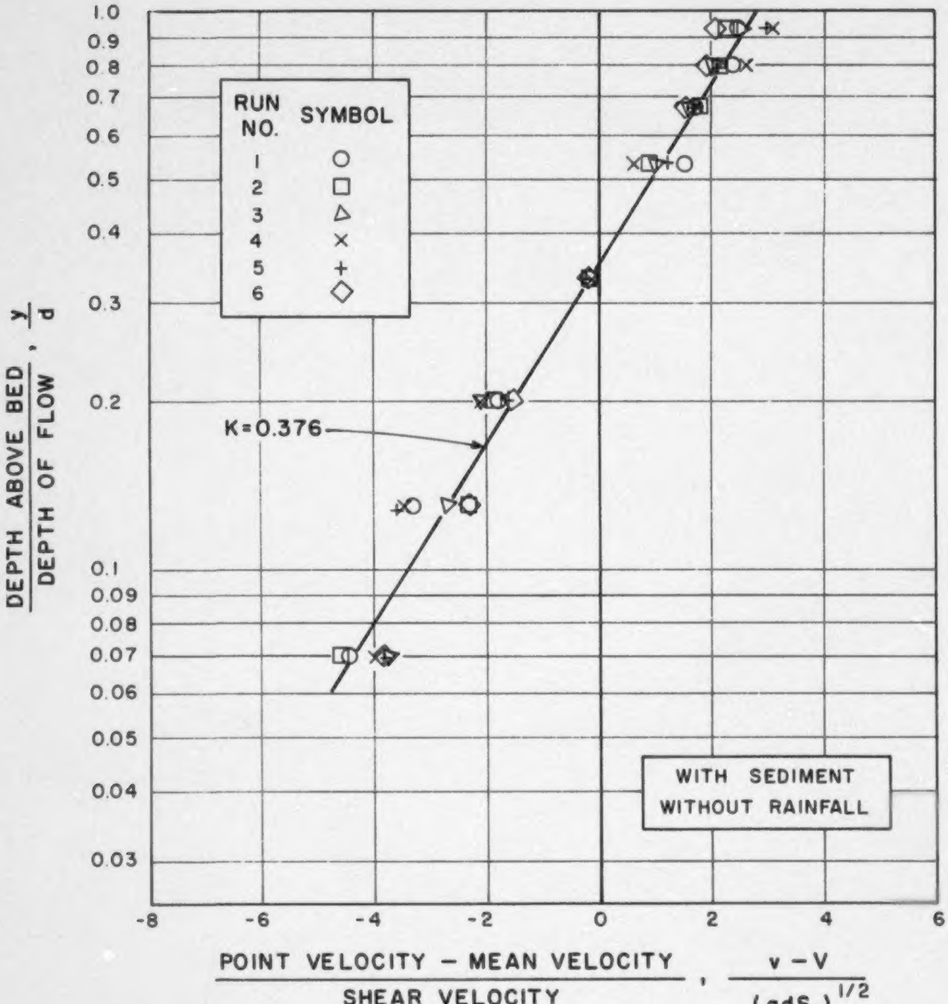

FIGURE 21 VELOCITY DISTRIBUTION REGRESSION CURVE FOR TEST SERIES 2 (0.30 FT. DEPTH OF FLOW) USING PRANDTL TUBE AND TRANSDUCER.

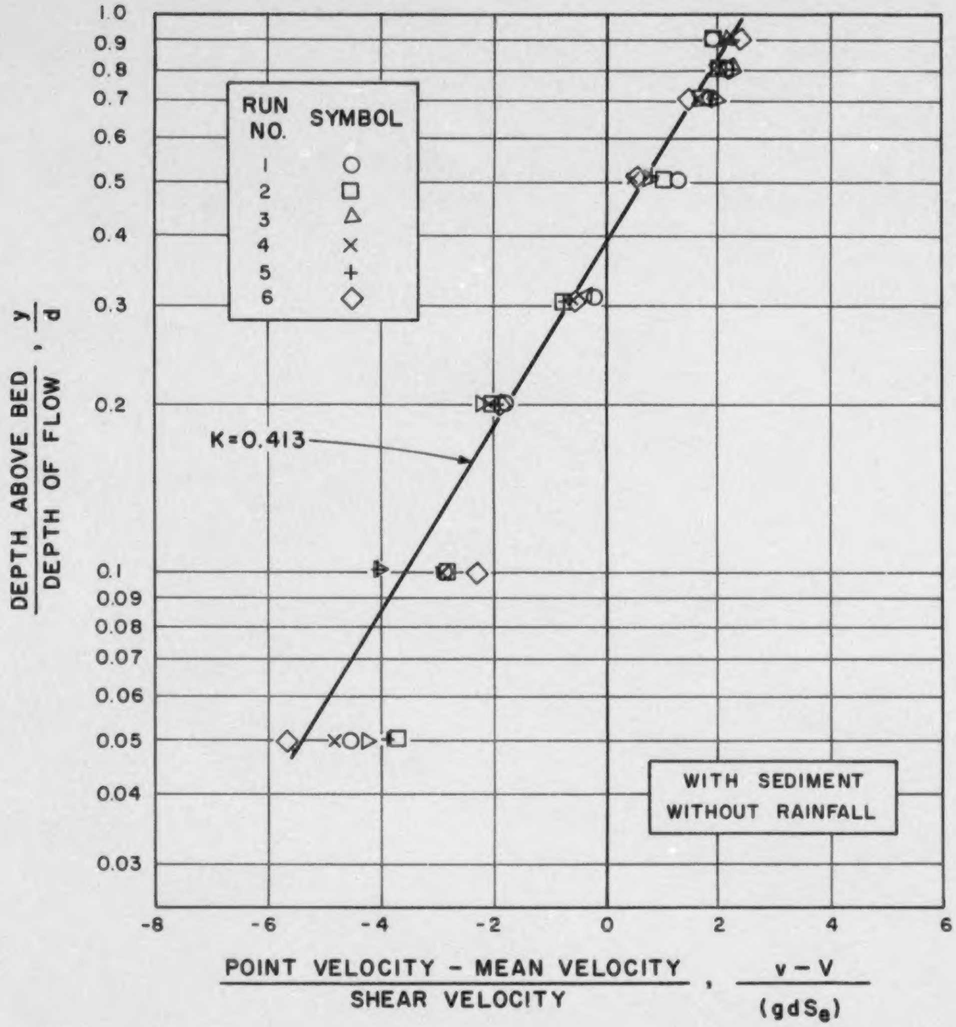

FIGURE 22 VELOCITY DISTRIBUTION REGRESSION CURVE FOR TEST SERIES 3 (0.20 FT. DEPTH OF FLOW) USING PRANDTL TUBE AND MANOMETER.

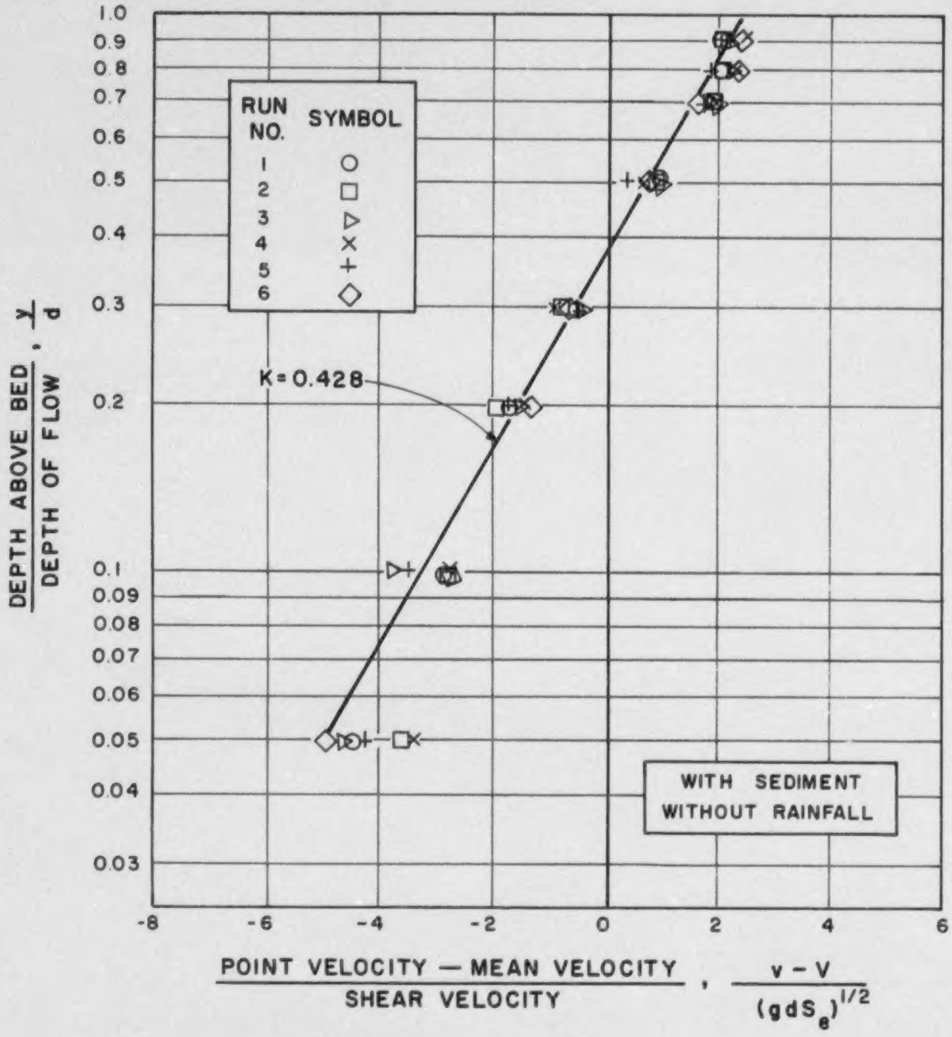

FIGURE 23 VELOCITY DISTRIBUTION REGRESSION CURVE FOR TEST SERIES 3 (0.20 FT. DEPTH OF FLOW) USING PRANDTL TUBE AND TRANSDUCER.

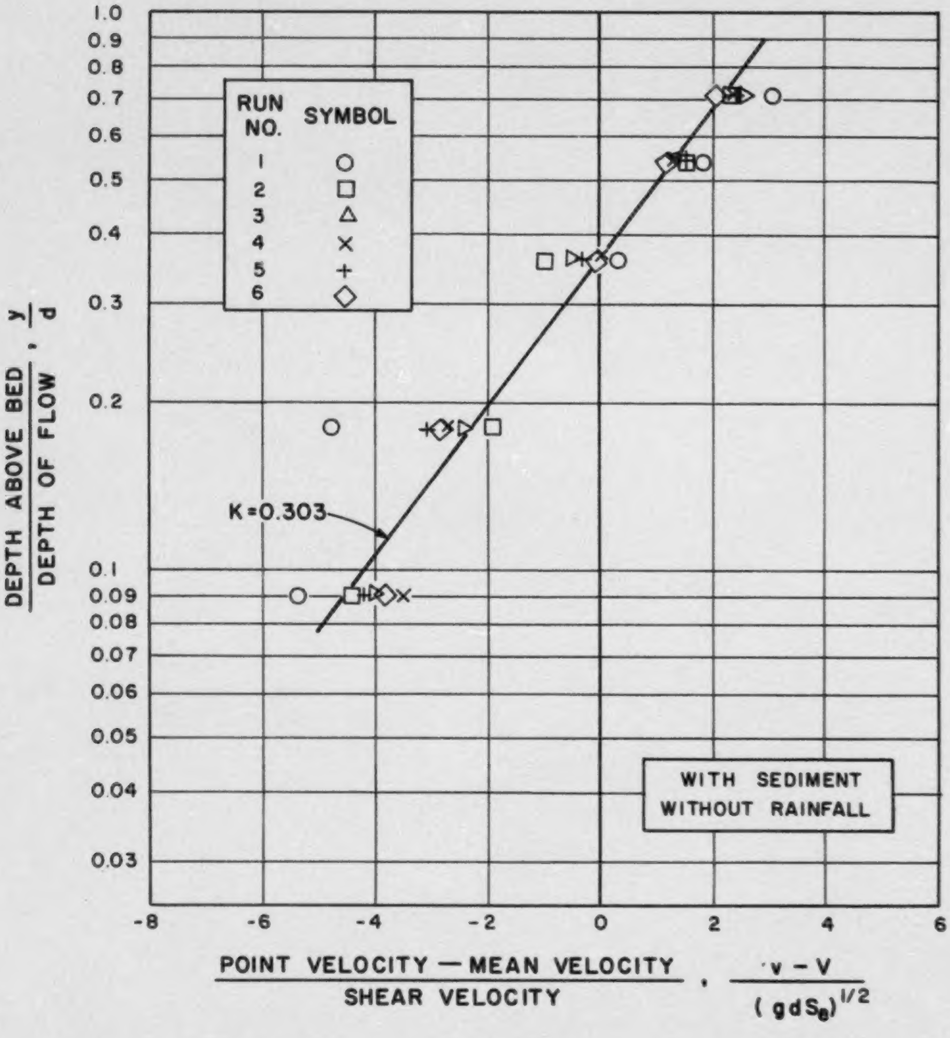

FIGURE 24 VELOCITY DISTRIBUTION REGRESSION CURVE FOR TEST SERIES 4 (0.112 FT. DEPTH OF FLOW) USING PRANDTL TUBE AND MANOMETER.

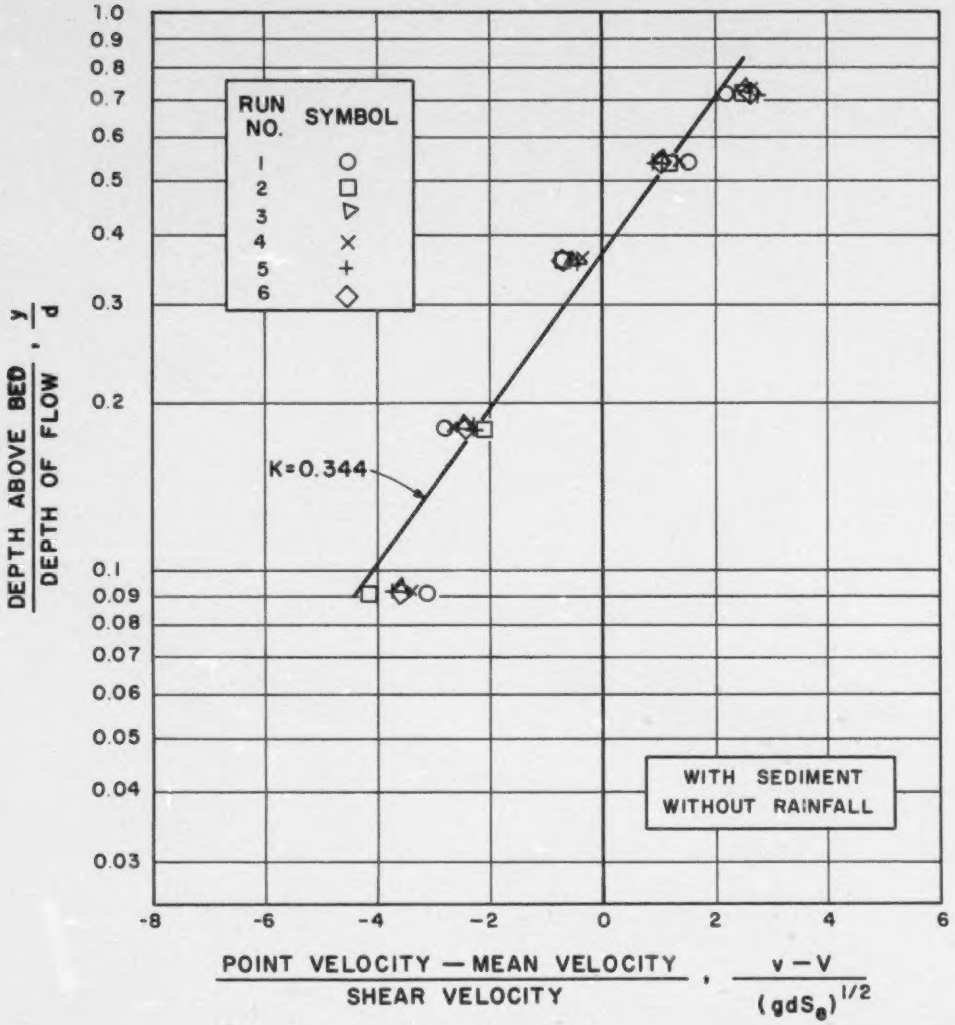

FIGURE 25 VELOCITY DISTRIBUTION REGRESSION CURVE FOR TEST SERIES 4 (0.112 FT. DEPTH OF FLOW) USING PRANDTL TUBE AND TRANSDUCER.

Comparison of these values with the series A, B and C values shows that von Karman's universal constant decreased in the presence of suspended sediment in shallow flow.

Effect of simulated rainfall and suspended sediment. Test series 3 and 4 (Runs 7 through 33), without and with simulated rainfall, were run to determine the effect of simulated rainfall and suspended sediment on von Karman's universal constant. The data were again analyzed by regression analysis for a velocity profile of the form of Equation 32.

In test series 3 the range of von Karman's universal constant was relatively small. Table V and Figures 26 through 31 show the average universal constants for various time periods after rainfall was introducted into the system. In test series 4 the average value of von Karman's constant decreased from 0.413 to 0.326 with the addition of rainfall. Table VI and Figures 32 through 37 show the average universal constants for various time periods after rainfall was introduced into the system. With the addition of simulated rainfall the mixing mechanism was altered. Since von Karman's constant depends upon the mechanism of turbulent mixing, the decrease in κ as shown in Figure 43 indicates a reduction in the turbulent momentum transfer coefficient ε_m. Figure 39 shows very little change in the universal constant thereby indicating no significant change in the turbulent momentum transfer coefficient ε_m for test series 3. The differences between test series 3 and 4

TABLE V

REGRESSION ANALYSIS RESULTS OF VELOCITY DEFECT LAW FOR TEST RUNS CONDUCTED WITH SEDIMENT AND WITHOUT AND WITH SIMULATED RAINFALL

(Series 3 - Runs 7 through 33)

Run No.	Time from Beginning of Rainfall min	Regression Coefficients						
		A^1	E^1	κ^2	N^3	F^4	Significance Level	Velocity Distribution Regression Curve Figure No.
				Test Series No. 3				
7 thru 15	-2:30 to -1:00 †	7.883	3.424	0.292	63	420.38	0.001	26
16 thru 18	+0:15	7.205	3.129	0.319	12	373.91	0.001	27
19 thru 21	+1:00	7.704	3.346	0.299	18	735.62	0.001	28
22 thru 24	+1:45	7.326	3.182	0.314	18	-	-	29
25 thru 27	+2:30	7.622	3.310	0.302	18	-	-	30
28 thru 33	+4:00 to +6:00	8.174	3.550	0.282	36	-	-	31

[1] A = slope of the regression line; E = intercept of the regression line at $\log_{10} = 0$.

[2] κ = von Karman's universal constant.

[3] N = number of readings included in the regression.

[4] F = statistical test for goodness to fit.

† - = time before beginning of rainfall; + = time after beginning of rainfall.

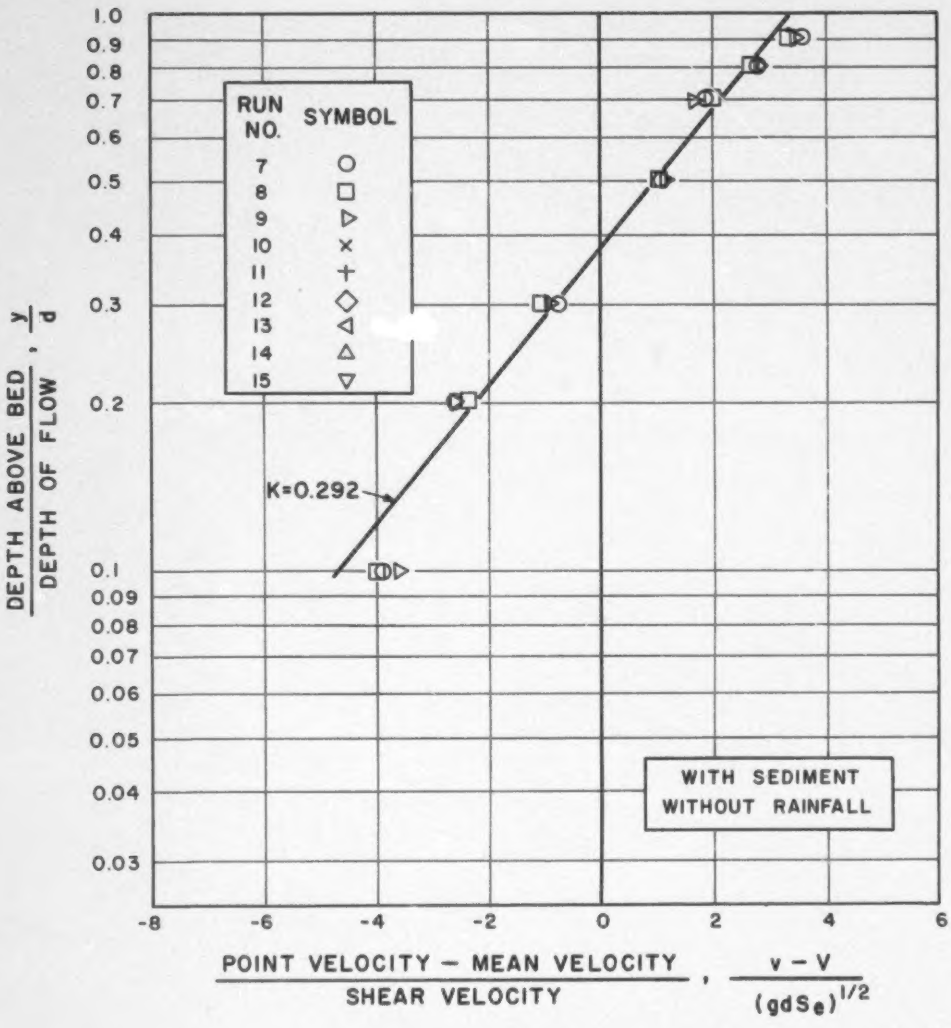

FIGURE 26 VELOCITY DISTRIBUTION REGRESSION CURVE FOR TEST SERIES 3 (0.20 FT. DEPTH OF FLOW) USING PRANDTL TUBE AND TRANSDUCER.

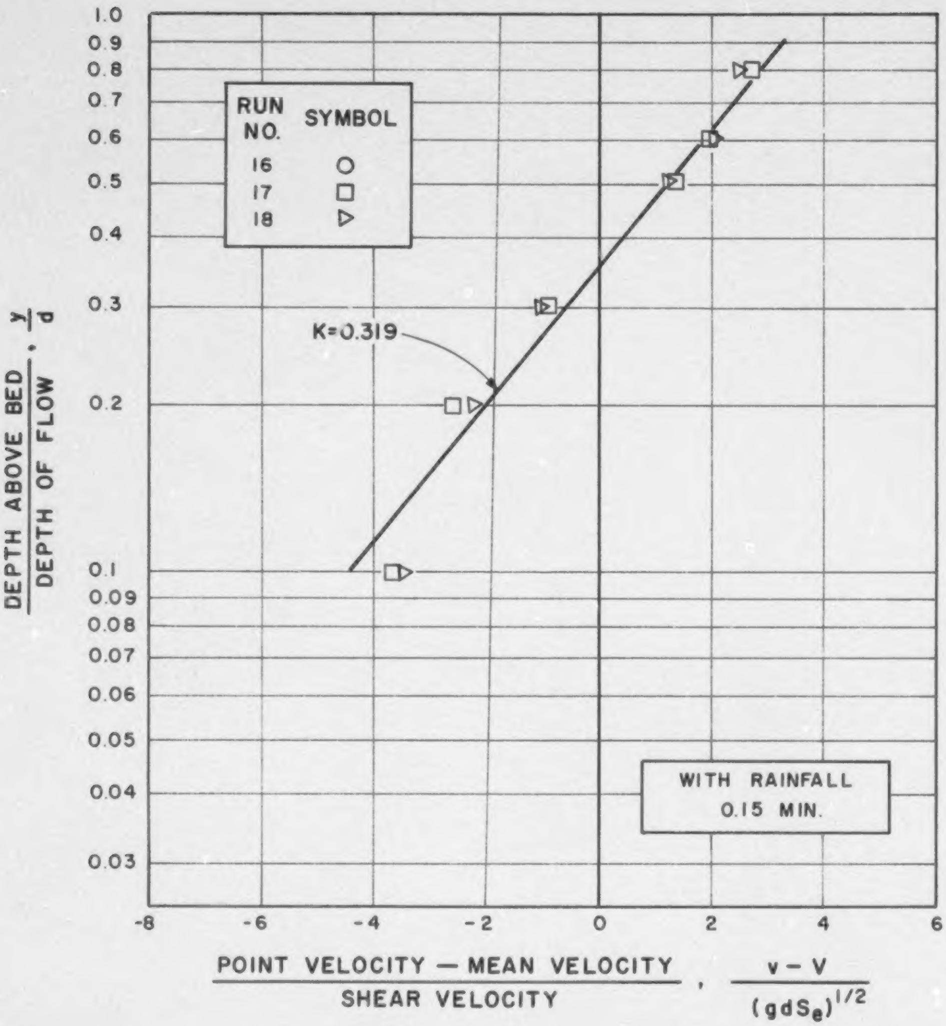

FIGURE 27 VELOCITY DISTRIBUTION REGRESSION CURVE FOR TEST SERIES 3 (0.200 FT DEPTH OF FLOW) USING PRANDTL TUBE AND TRANSDUCER.

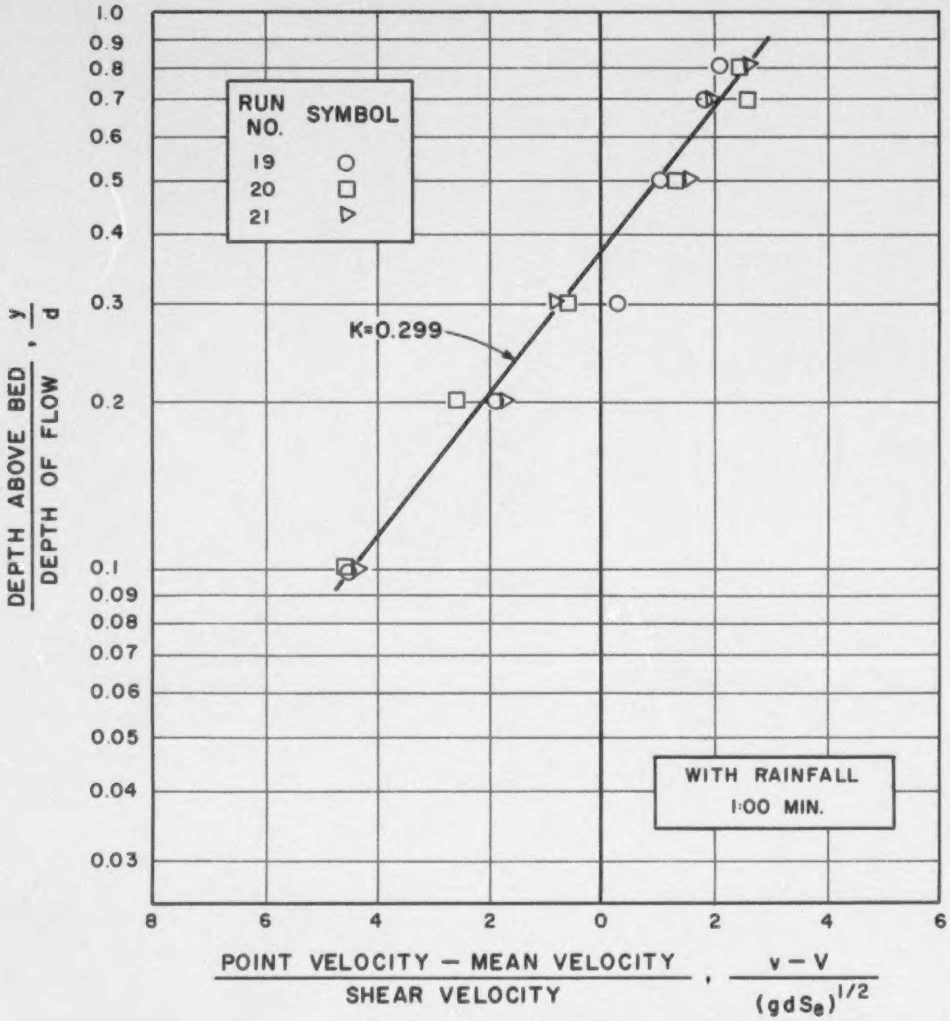

FIGURE 28 VELOCITY DISTRIBUTION REGRESSION CURVE FOR TEST SERIES 3 (0.200 FT. DEPTH OF FLOW) USING PRANDTL TUBE AND TRANSDUCER.

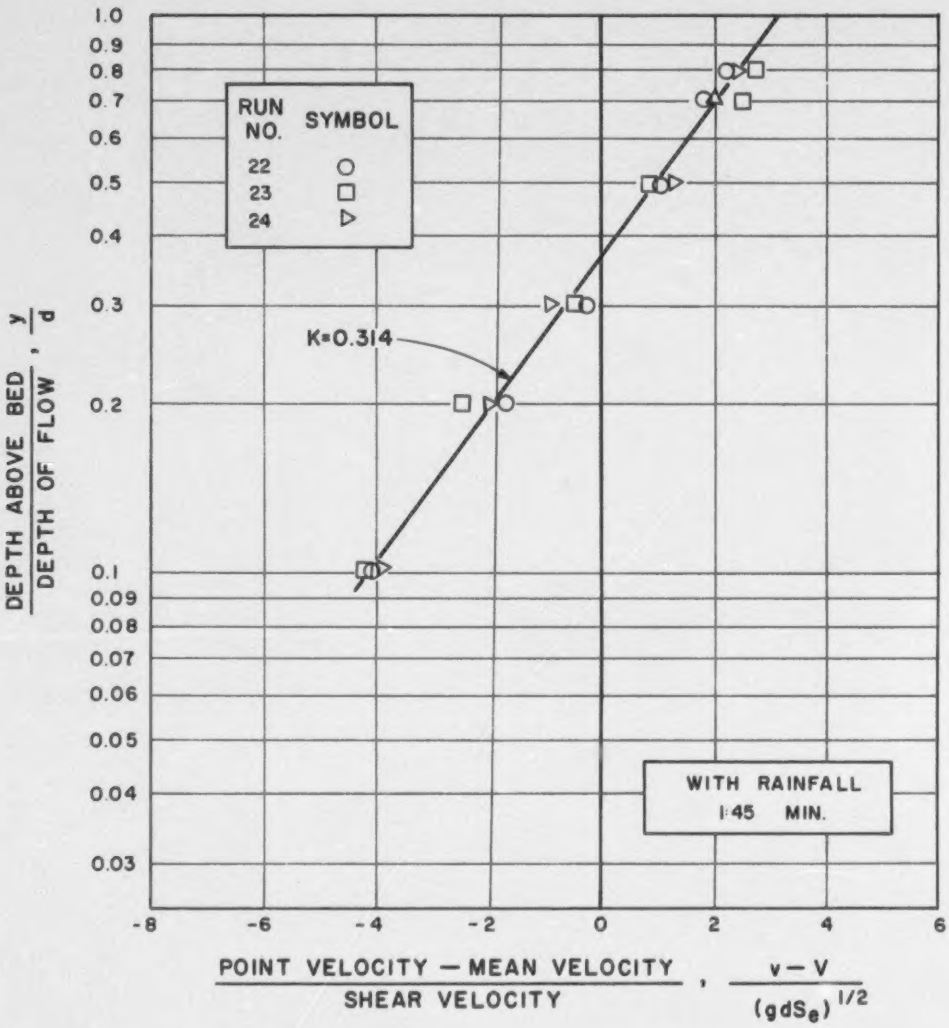

FIGURE 29 VELOCITY DISTRIBUTION REGRESSION CURVE FOR TEST SERIES 3 (0.200 FT. DEPTH OF FLOW) USING PRANDTL TUBE AND TRANSDUCER.

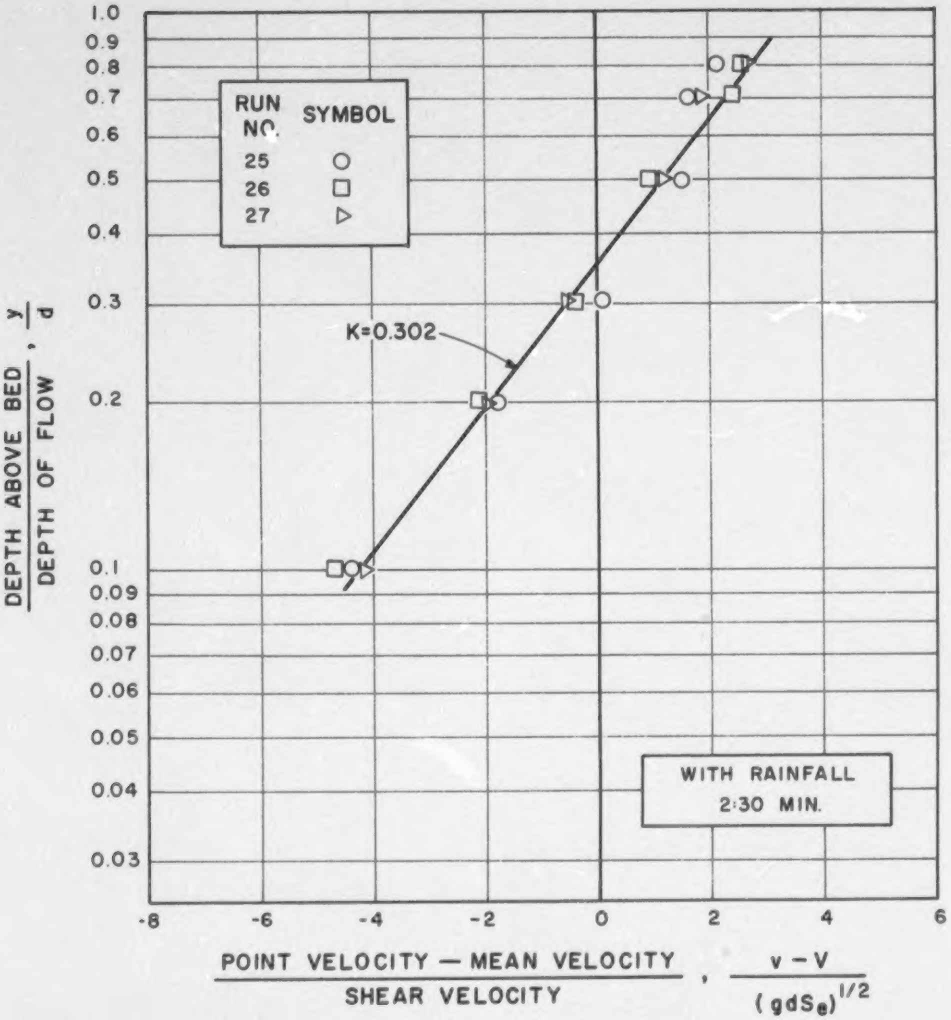

FIGURE 30 VELOCITY DISTRIBUTION REGRESSION CURVE FOR TEST SERIES 3 (0.200 FT. DEPTH OF FLOW) USING PRANDTL TUBE AND TRANSDUCER.

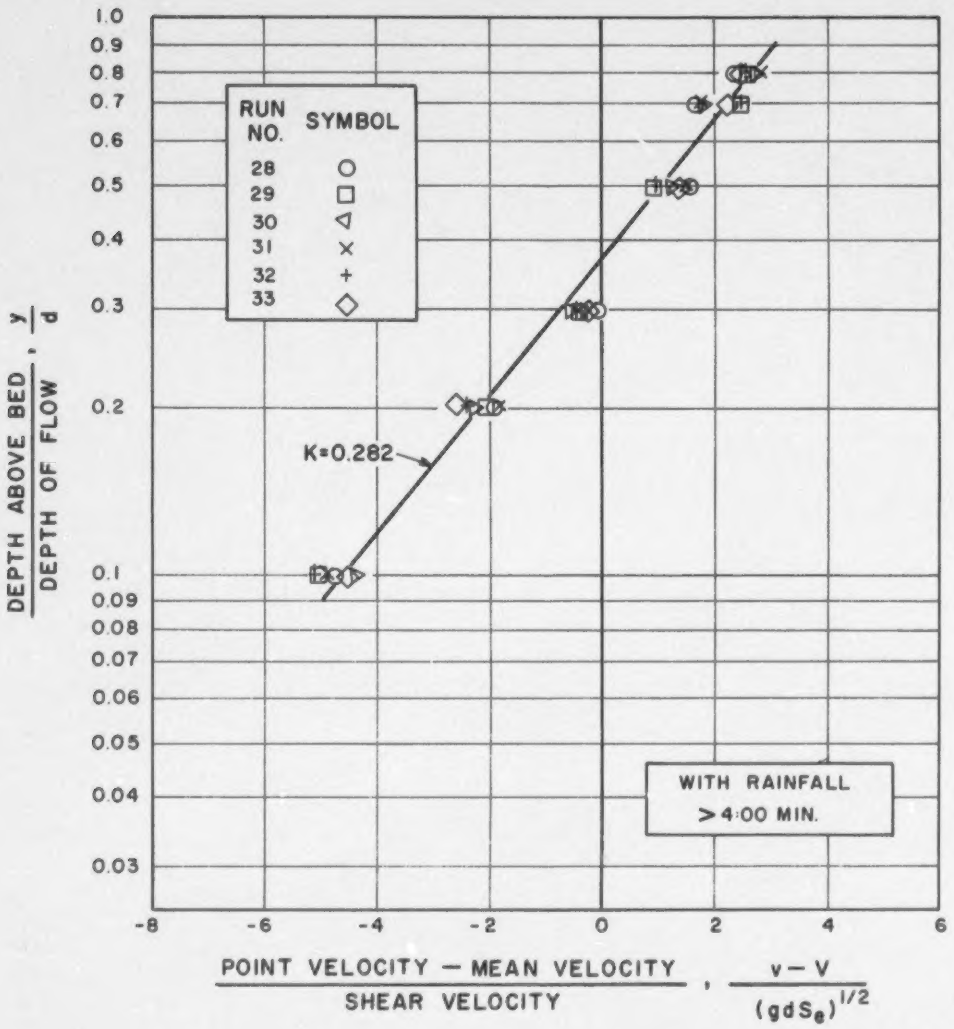

FIGURE 31 VELOCITY DISTRIBUTION REGRESSION CURVE FOR TEST SERIES 3 (0.200 FT. DEPTH OF FLOW) USING PRANDTL TUBE AND TRANSDUCER.

TABLE VI

REGRESSION ANALYSIS RESULTS OF VELOCITY DEFECT LAW FOR TEST RUNS CONDUCTED WITH SEDIMENT AND WITHOUT AND WITH SIMULATED RAINFALL

(Series 4 - Runs 7 through 33)

Run No.	Time from Beginning of Rainfall min	Regression Coefficients A^1	Regression Coefficients E^1	κ^2	N^3	F^4	Significance Level	Velocity Distribution Regression Curve Figure No.
			Test Series No. 4					
7 thru 15	-2:30 to -1:00 †	5.562	2.415	0.413	30	879.80	0.001	32
16 thru 18	+0.15	6.016	2.654	9.382	14	158.08	0.001	33
19 thru 21	+1:00	6.177	2.727	0.373	14	176.32	0.001	34
22 thru 24	+1:45	6.188	2.708	0.372	14	191.50	0.001	35
25 thru 27	+2:30	6.811	2.989	0.338	14	182.05	0.001	36
28 thru 33	+4:00 to +6:00	7.065	3.091	0.326	28	374.32	0.001	37

[1] A = slope of the regression line; E = intercept of the regression line at $\log_{10} = 0$.

[2] κ = von Karman's universal constant.

[3] N = number of readings included in the regression.

[4] F = statistical test for goodness to fit.

† - = time before beginning of rainfall; + = time after beginning of rainfall.

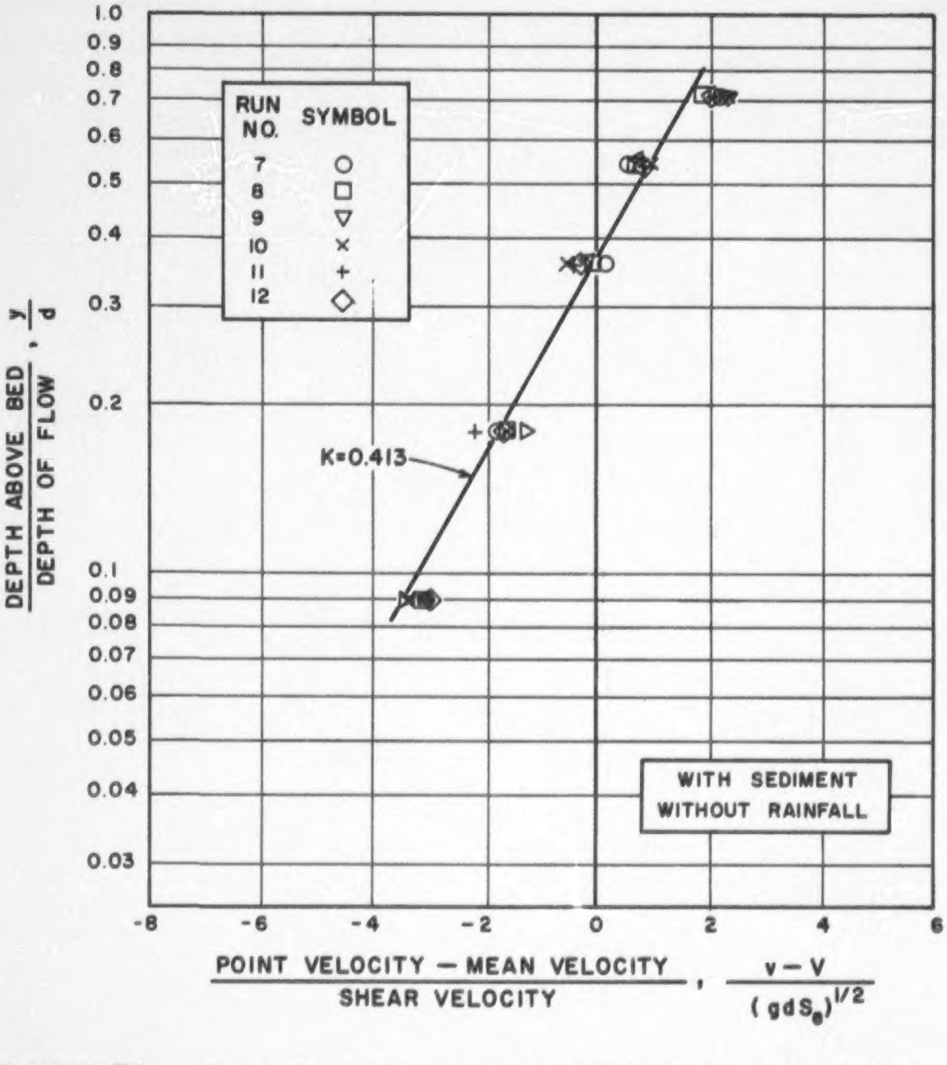

FIGURE 32 VELOCITY DISTRIBUTION REGRESSION CURVE FOR TEST SERIES 4 (0.112 FT. DEPTH OF FLOW) USING PRANDTL TUBE AND TRANSDUCER.

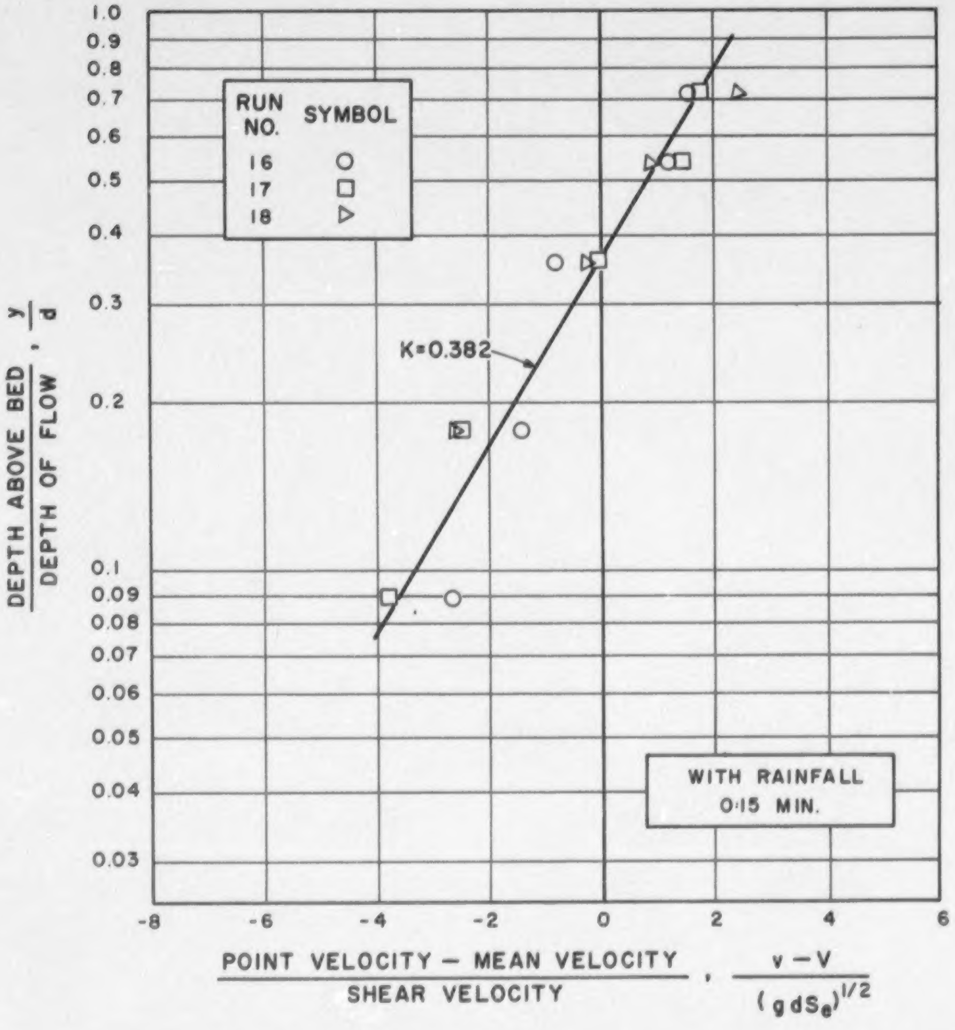

FIGURE 33 VELOCITY DISTRIBUTION REGRESSION CURVE FOR TEST SERIES 4 (0.112 FT. DEPTH OF FLOW) USING PRANDTL TUBE AND TRANSDUCER.

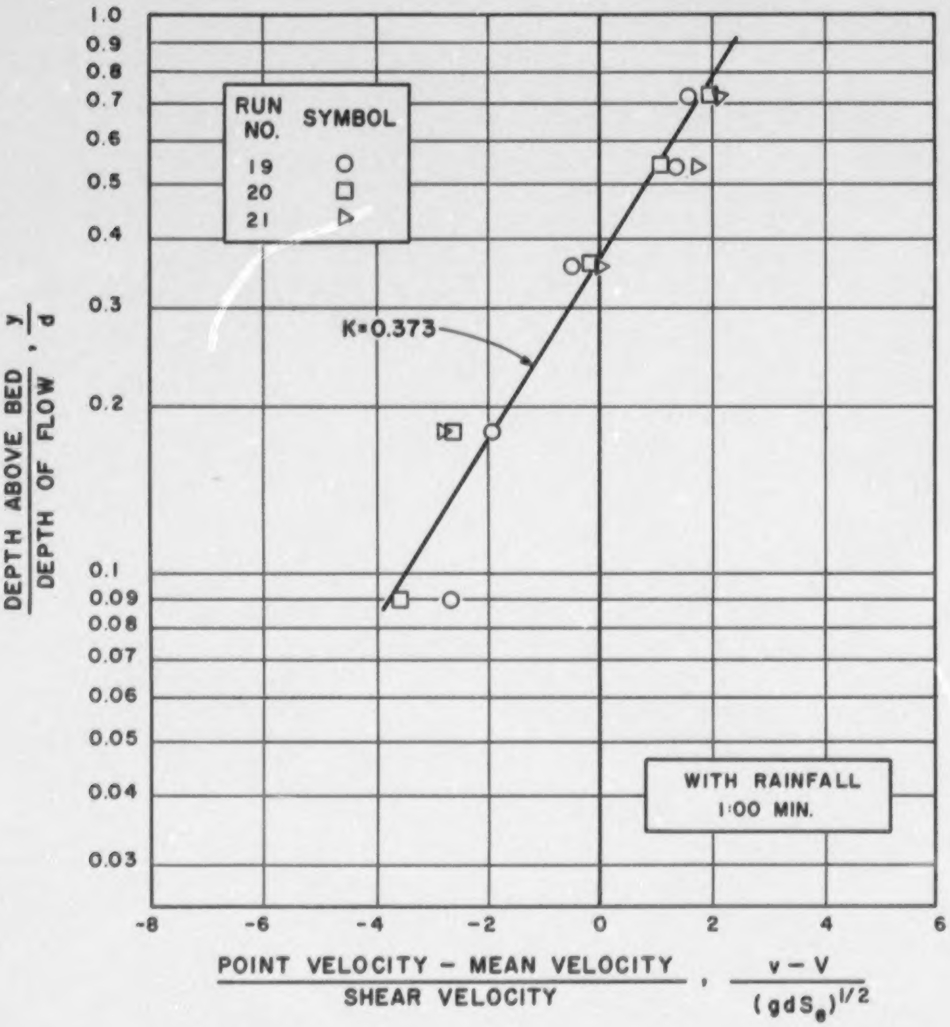

FIGURE 34 VELOCITY DISTRIBUTION REGRESSION CURVE FOR TEST SERIES 4 (0.112 FT. DEPTH OF FLOW) USING PRANDTL TUBE AND TRANSDUCER.

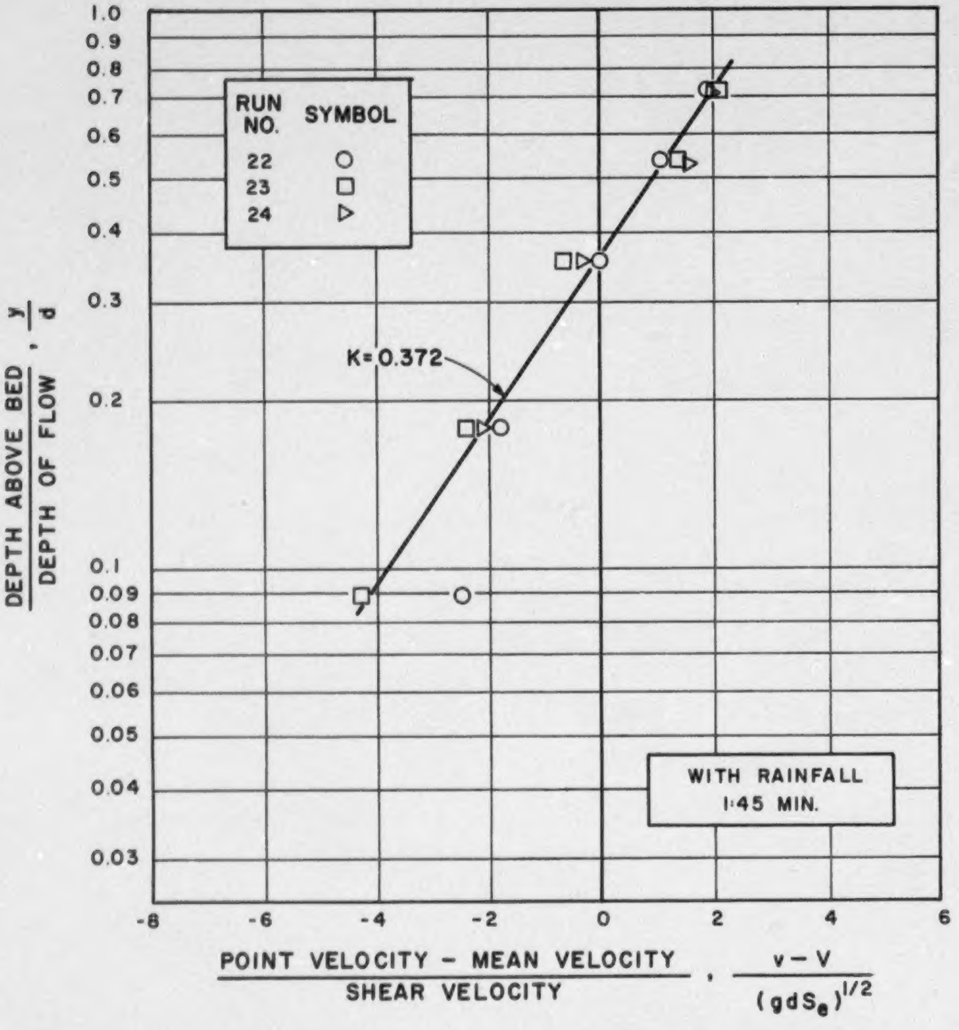

FIGURE 35 VELOCITY DISTRIBUTION REGRESSION CURVE FOR TEST SERIES 4 (0.112 FT. DEPTH OF FLOW) USING PRANDTL TUBE AND TRANSDUCER.

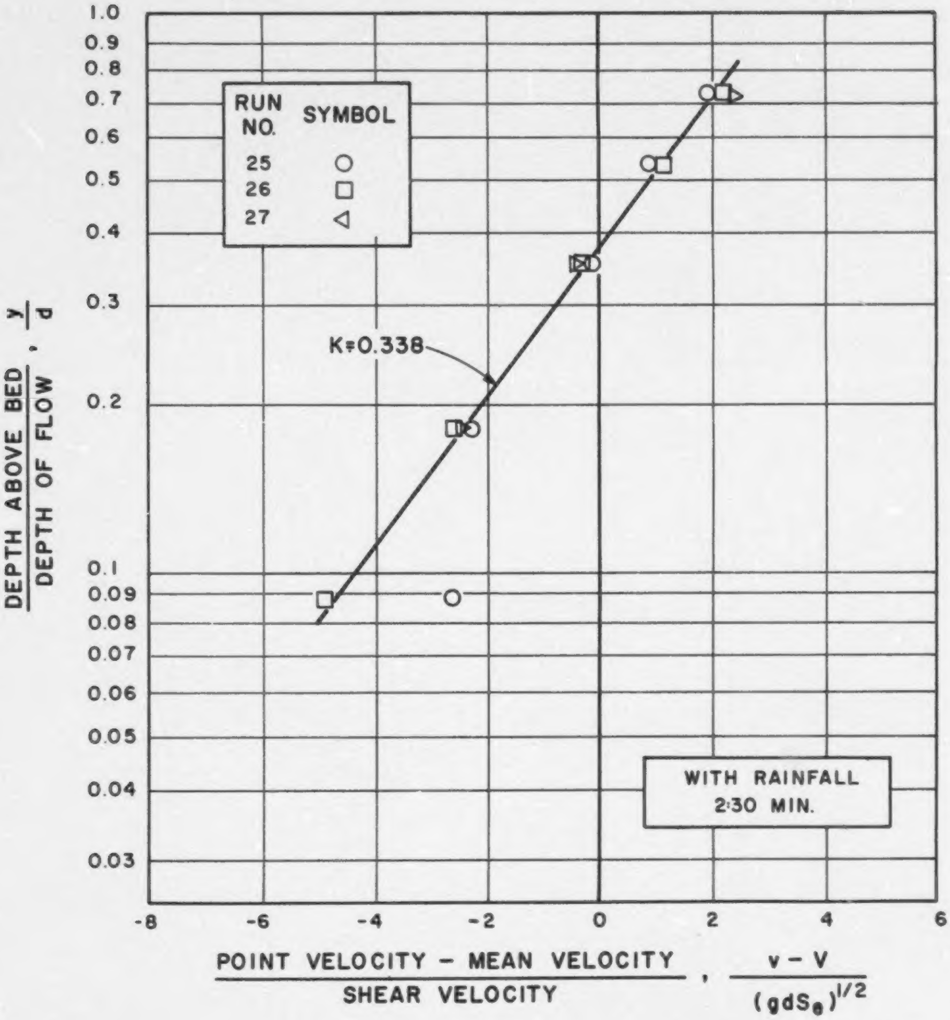

FIGURE 36 VELOCITY DISTRIBUTION REGRESSION CURVE FOR TEST SERIES 4 (0.112 FT. DEPTH OF FLOW) USING PRANDTL TUBE AND TRANSDUCER.

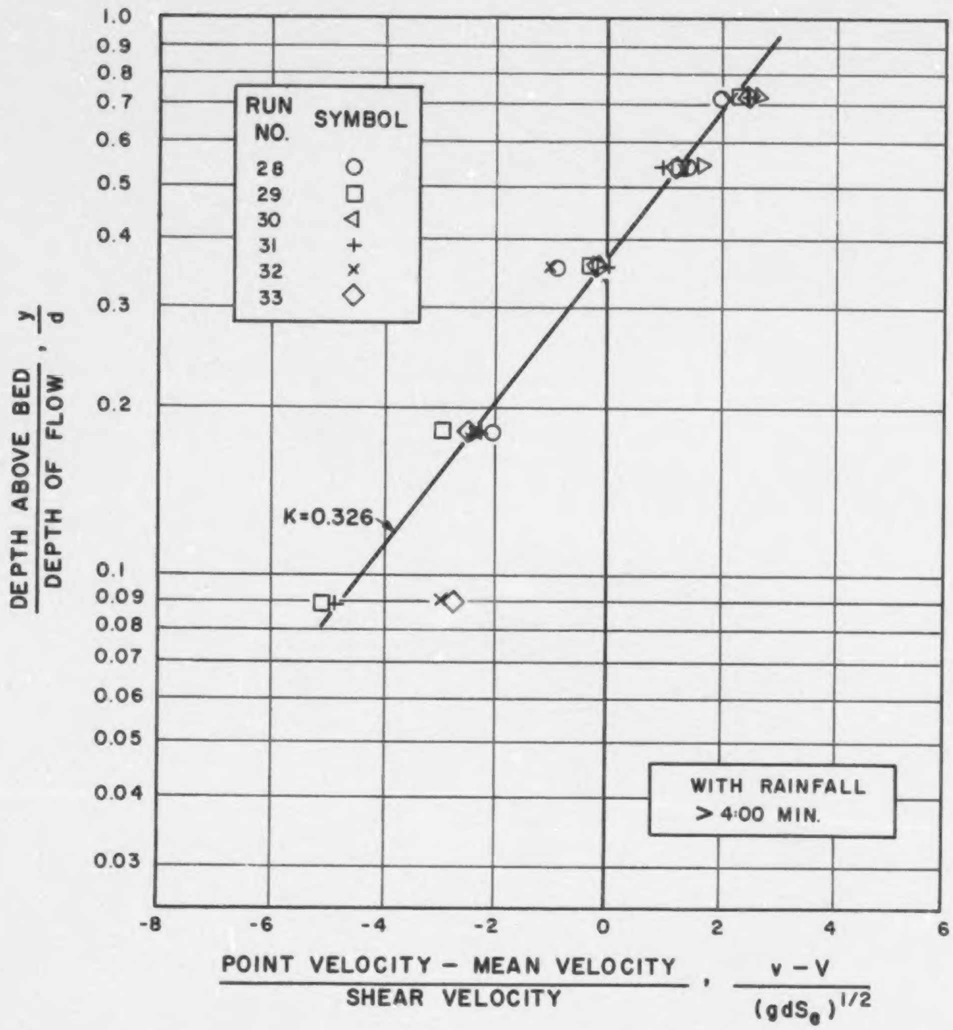

FIGURE 37 VELOCITY DISTRIBUTION REGRESSION CURVE FOR TEST SERIES 4 (0.112 FT. DEPTH OF FLOW) USING PRANDTL TUBE AND TRANSDUCER.

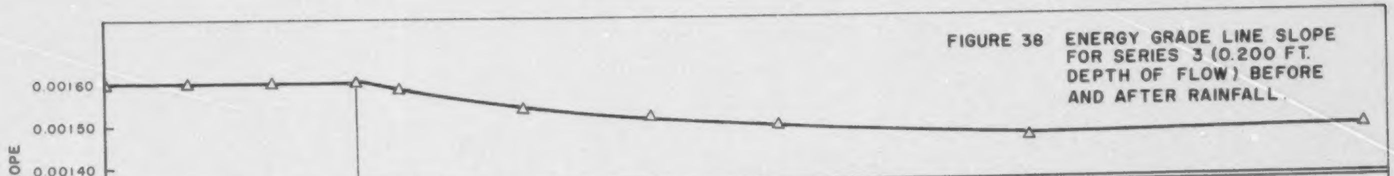

FIGURE 38 ENERGY GRADE LINE SLOPE FOR SERIES 3 (0.200 FT. DEPTH OF FLOW) BEFORE AND AFTER RAINFALL.

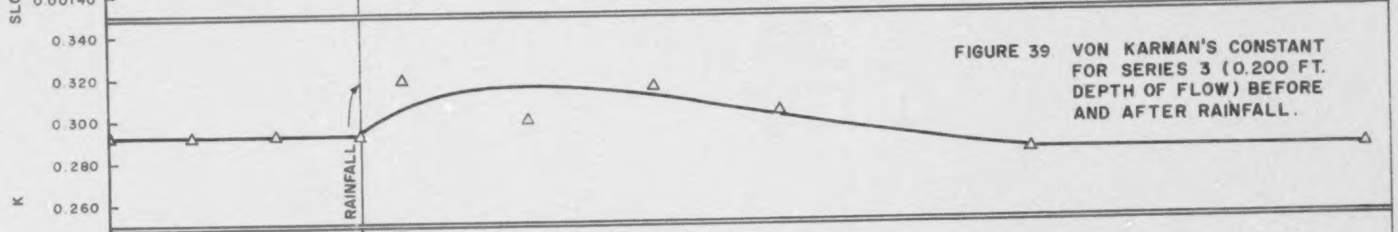

FIGURE 39 VON KARMAN'S CONSTANT FOR SERIES 3 (0.200 FT. DEPTH OF FLOW) BEFORE AND AFTER RAINFALL.

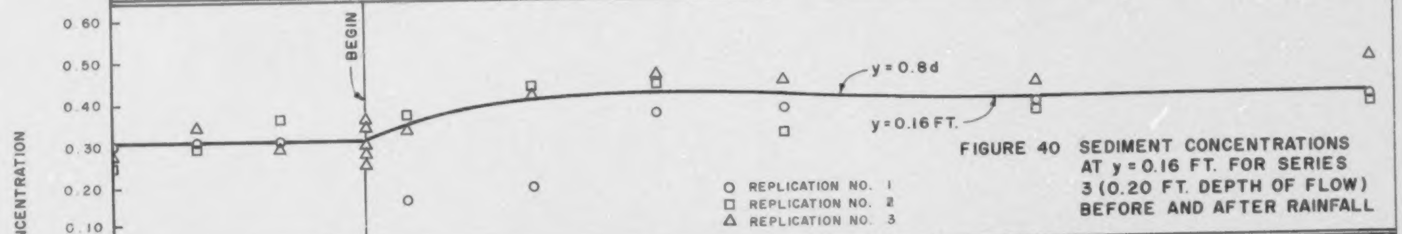

FIGURE 40 SEDIMENT CONCENTRATIONS AT y = 0.16 FT. FOR SERIES 3 (0.20 FT. DEPTH OF FLOW) BEFORE AND AFTER RAINFALL

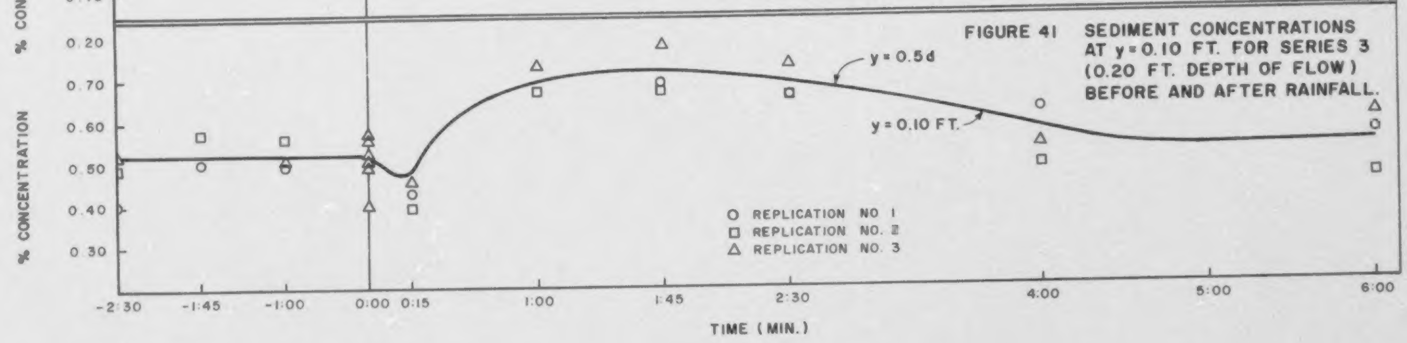

FIGURE 41 SEDIMENT CONCENTRATIONS AT y = 0.10 FT. FOR SERIES 3 (0.20 FT. DEPTH OF FLOW) BEFORE AND AFTER RAINFALL.

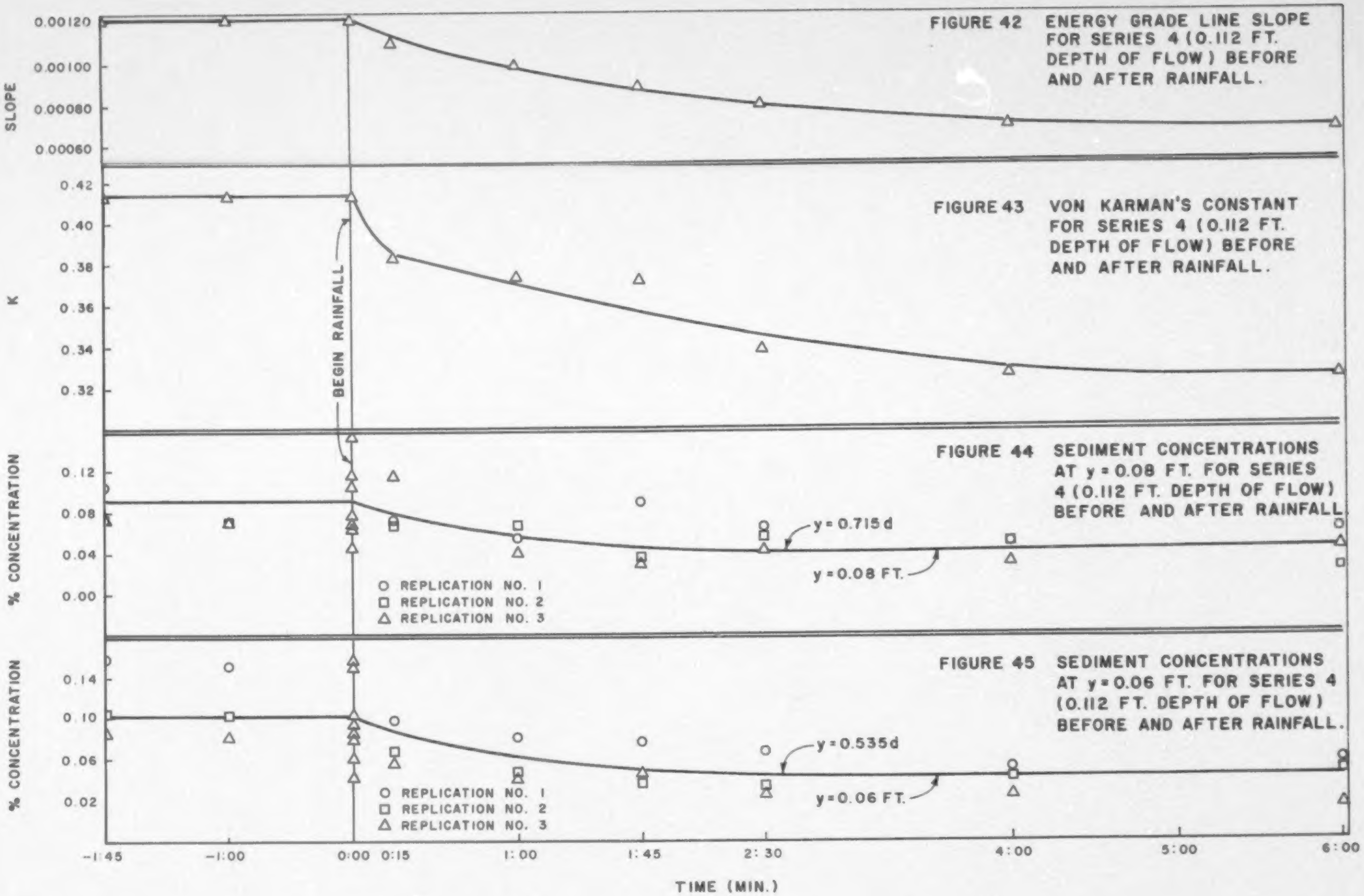

FIGURE 42 ENERGY GRADE LINE SLOPE FOR SERIES 4 (0.112 FT. DEPTH OF FLOW) BEFORE AND AFTER RAINFALL.

FIGURE 43 VON KARMAN'S CONSTANT FOR SERIES 4 (0.112 FT. DEPTH OF FLOW) BEFORE AND AFTER RAINFALL.

FIGURE 44 SEDIMENT CONCENTRATIONS AT y = 0.08 FT. FOR SERIES 4 (0.112 FT. DEPTH OF FLOW) BEFORE AND AFTER RAINFALL.

FIGURE 45 SEDIMENT CONCENTRATIONS AT y = 0.06 FT. FOR SERIES 4 (0.112 FT. DEPTH OF FLOW) BEFORE AND AFTER RAINFALL.

in values of von Karman's constant resulting from simulated rainfall cannot be readily explained. Test series 3, with a depth of flow of 0.20 ft, tended to show a slight increase in von Karman's constant as a result of rainfall, but the increase was not pronounced. Test series 4, with 0.112 ft depth of flow, showed a marked reduction in von Karman's constant after simulated rainfall was introduced into the study.

Effect of Rainfall on Sediment Transport Capacity of Shallow Flow

Test series 3 and 4 (Runs 7 through 33) were conducted to determine the effects of rainfall on the sediment transport capacity of the shallow flow.

In test series 3 (0.20 ft depth of flow) the suspended sediment load concentration at 0.16 ft and 0.10 ft from the bed increased slightly with the addition of rainfall and then decreased until equilibrium conditions were re-established in the flow. Table XI (in the Appendix) and Figures 40 and 41 show the average sediment concentrations in percent for various time periods before and after simulated rainfall was introduced into the system. Turbulence was initially increased by the addition of simulated rainfall in this test (indicated by an increase in the von Karman's constant). The increased turbulence appears to have been capable of transporting more suspended sediment.

In test series 4 (0.112 ft depth of flow) the suspended sediment load concentration at 0.08 ft and 0.06 ft from the bed was decreased with the addition of rainfall. Table XI (in the Appendix) and Figures 44 and 45 show the average sediment concentrations for various time periods before and after simulated rainfall was introduced into the system. Turbulence in the flow decreased (indicated by a decrease in the von Karman's constant) until a lower transport capacity was established.

In test series 4 the transport capacity of suspended load in the flow was decreased by the simulated rainfall and suspended sediment. In test series 3 the transport capacity of the flow was increased slightly with the initiation of rainfall and then decreased after the initial rainfall period. The reason for this apparent anomaly is not known but it may be caused by the fact that the depths of flow were different, or there may have been errors in the experimental procedure. The tests were replicated three times and the replications were relatively consistent. Further tests will be required before general conclusions can be reached concerning the effect of rainfall on the transport of sediment on shallow flow.

Variations Between Test Series

Variations in results between test series and between test runs were assumed to be relative and can possibly be attributed to (1) the assumption of an infinitely wide channel which was not satisfied in test series A, B, 1 and 2, (2) variations in rainfall intensity patterns in test series 3 and 4, (3) nonuniform flow conditions in test series 1, 3 and 3, (4) secondary flow, and (5) instrument error.

Infinitely Wide Channel

Preliminary tests were conducted in the research flume to determine flow conditions at the center. Series B tests (isovels) indicated isovels deviating from the horizontal at the center of the flume as shown in Figures 46 through 49. Since the deviations from the horizontal were small and are within the accuracy of the instrument used, an infinitely wide channel was assumed for the 0.30 ft depth of flow. Series C tests (isovels) indicated horizontal isovels at the center of the flume as shown in Figures 50 and 51. An infinitely wide channel was therefore assumed for all depths of flow of 0.30 ft and less. Bazin, according to Glass (8), stated that rectangular channels can be assumed infinitely wide if the bottom width is five times greater than the depth of flow.

Rainfall Intensity

Preliminary tests were conducted in the research flume to determine the rainfall intensity pattern. The tests were run with nozzle pressures of 6 psi. The rinfall intensity pattern shown in Figure 52 was developed from point volumetric samples collected

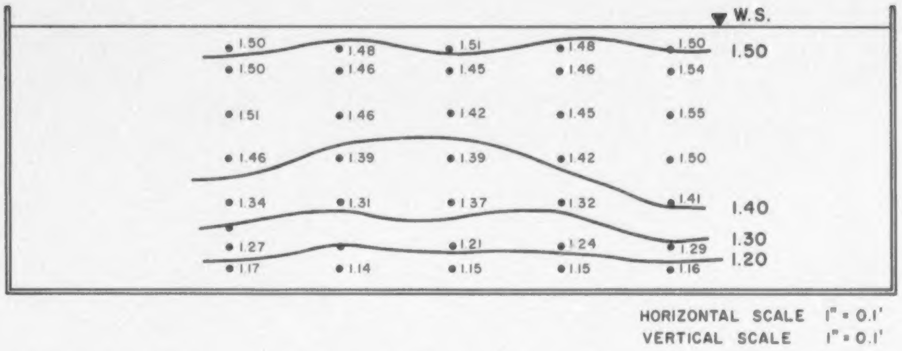

FIGURE 46 CLEAR WATER ISOVELS FOR SERIES B (0.30 FT. DEPTH OF FLOW) WITH SIMULATED RAINFALL USING PRESSURE TRANSDUCER.

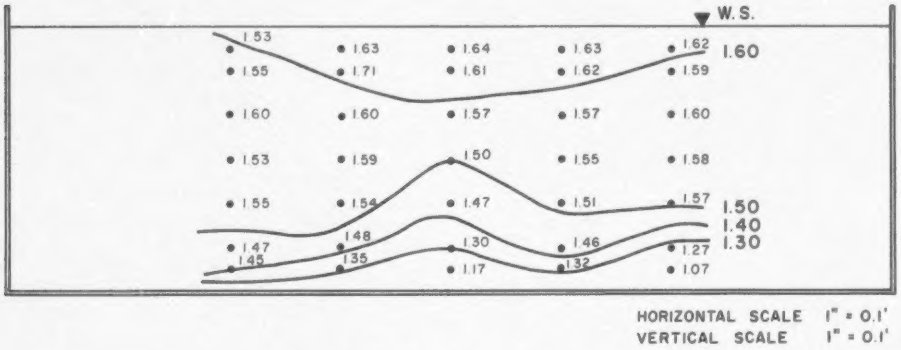

FIGURE 47 CLEAR WATER ISOVELS FOR SERIES B (0.30 FT. DEPTH OF FLOW) WITHOUT SIMULATED RAINFALL USING PRESSURE TRANSDUCER.

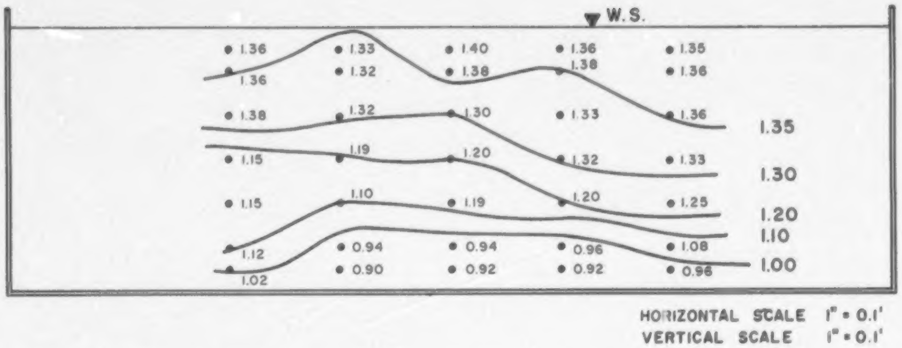

FIGURE 48 CLEAR WATER ISOVELS FOR SERIES B (0.30 FT. DEPTH OF FLOW) WITH SIMULATED RAINFALL USING INCLINED MANOMETER

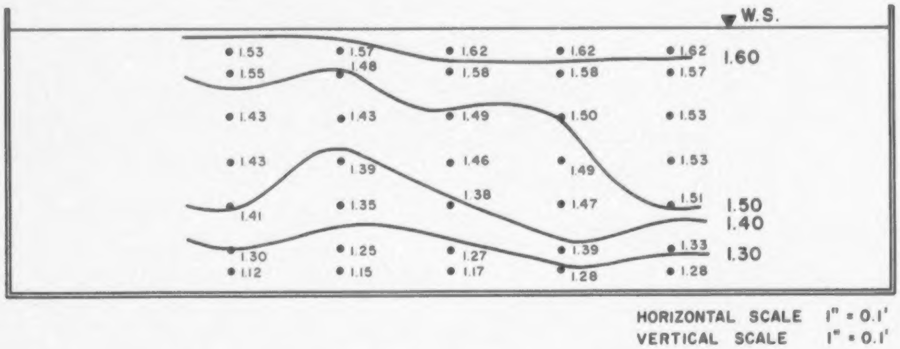

FIGURE 49 CLEAR WATER ISOVELS FOR SERIES B (0.30 FT. DEPTH OF FLOW) WITHOUT SIMULATED RAINFALL USING INCLINED MANOMETER

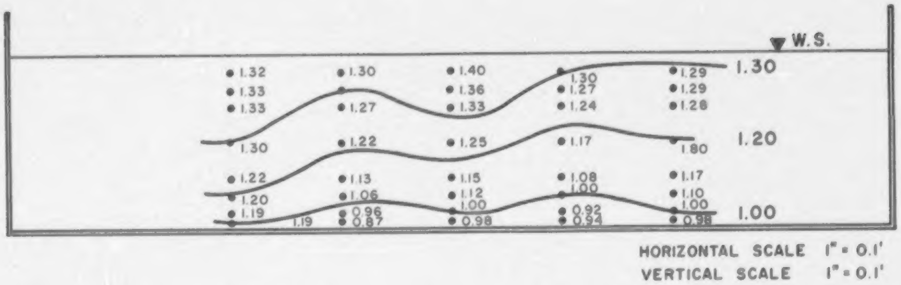

FIGURE 50 CLEAR WATER ISOVELS FOR SERIES C (0.20 FT. DEPTH OF FLOW) WITHOUT SIMULATED RAINFALL USING INCLINED MANOMETER.

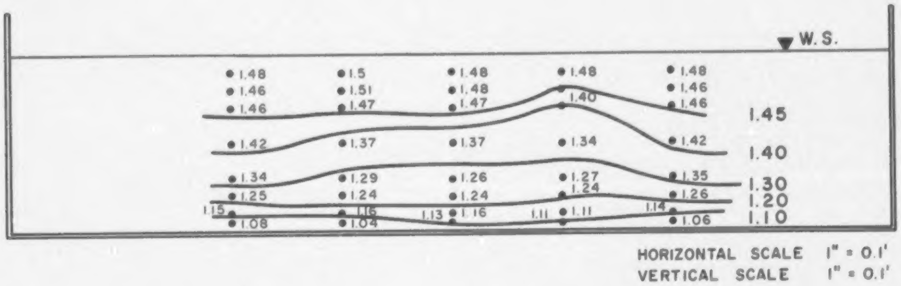

FIGURE 51 CLEAR WATER ISOVELS FOR SERIES C (0.20 FT. DEPTH OF FLOW) WITHOUT SIMULATED RAINFALL USING PRESSURE TRANSDUCER.

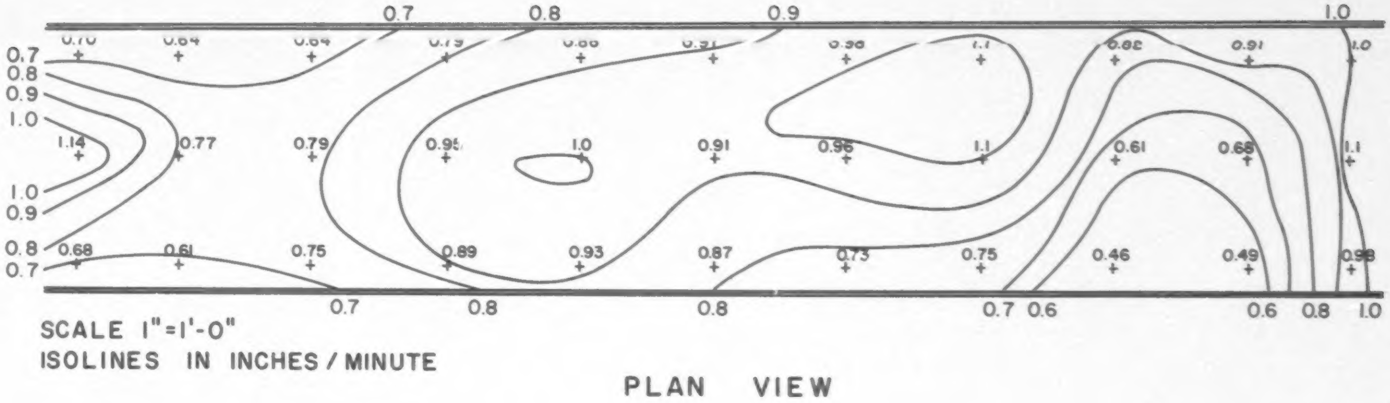

FIGURE 52 RAINFALL INTENSITY DISTRIBUTION IN RESEARCH FLUME.

along the flume bed at nozzle 5. Rainfall intensity patterns developed for other nozzles indicated similar variations in intensity patterns.

Flow Conditions

Approximately uniform flow was attained in test series A, B, C and 2 without rainfall. Gradually varied flow occurred in test series 1, 3 and 4 without rainfall while spatially varied flow occurred in these tests with rainfall.

Uniform flow. In test series with uniform flow the slope of the energy grade line was parallel to the slope of the water surface and the flume bed.

Gradually varied flow. The dynamic equation for gradually varied flow (steady flow with depth varying gradually along the length of the flume) was used to determine the slope of the energy grade line in tests 1, 3 and 4 without rainfall. Using the energy equation, Chow (3) derived the following differential equation for gradually varied flow:

$$S_e = \left(\frac{\alpha Q^2 \, T}{g \, A^3} - 1.0 \right) \frac{dy}{dx} + S \quad \ldots\ldots \quad (33)$$

where $\frac{dy}{dx}$ $\left(\frac{\Delta y}{\Delta x}\right.$ for this study$\left.\right)$ is the change in depth per unit length of channel, α is the energy coefficient, T is the top width and other notations are the same as those previously defined. In the derivation of Equation 33, Chow made the following assumptions:

1. The head loss at a section is the same as for a uniform flow having the velocity and hydraulic radius of the section.
2. The slope of the channel is small.
3. The channel has constant alignment and shape.
4. The velocity-distribution coefficients are constant.
5. The conveyance and section factor are exponential functions of the depth of flow.
6. The roughness coefficient is independent of the depth of flow and constant throughout the channel reach under consideration.

The water surface slopes for nonuniform flow conditions are shown in Figures 53, 55 and 57 (Appendix) for test series 1, 3 and 4. Energy grade line slope values were used to determine the shear velocity used in Equation 33.

Spatially varied flow. The dynamic equation for spatially varied flow (with increasing discharge) was used in this study to determine the slope of the energy grade line in test series 3 and 4 with equilibrium rainfall conditions. Using the momentum equation, Chow (3) derived the following differential equation for spatially varied flow:

$$S_e = \left(\frac{\alpha \, Q^2}{g \, A^2} d - 1.0 \right) \frac{dy}{dx} + S - \frac{2\alpha' Q \, q_*}{g \, A^2} \quad . \; . \; . \; . \qquad (35)$$

where, q_* is $\frac{dQ}{dx} \left(\frac{\Delta Q}{\Delta x} \right.$ for this study $\left. \right)$ or the discharge per unit length of the channel and $\frac{dy}{dx}$ $\left(\frac{\Delta y}{\Delta x}\right.$ for this study$\left.\right)$ is the change in depth and α' is an energy coefficient. Other notations are the same as those previously defined. The following assumptions were used in the derivations:

1. Flow was unidirectional (effects of the cross currents and accompanying turbulence were neglected).
2. Lateral unevenness of the water surface was neglected.
3. The velocity distribution across the research flume was constant and uniform ($\alpha = 1.0$).
4. The pressure in the flow was hydrostatic ($\alpha' = 1.0$).
5. Slope of the research flume was small so that its effects on the pressure head and on the force on channel sections were neglected.
6. The effect of air entrainment was neglected.

The water surface slopes for equilibrium rainfall conditions are shown in Figures 56 and 58 (Appendix) for series 3 and 4. Energy grade line values were used to determine the shear velocity used in appropriate equations.

Secondary Flow

Secondary flow is the movement of water particles on a cross section normal to the longitudinal direction of flow. This secondary circulation conforms to certain laws, not yet fully understood by investigators, which result in several spiral systems of flow in a flume. Gibson, according to Leliavsky (10), concluded that twin spiral currents exist causing upward secondary flow at the walls and a downward cross current at the centerline. The strength of this secondary circulation has been estimated to be 5 percent of the main current. The effect of secondary circulation on the distribution of suspended sediment has not been well established although these secondary currents have apparently caused variations in the velocity and sediment data.

Instrument Error

Two velocity head indicators were used in this study to measure the point velocities in the flow. A Pitot-static tube was connected to a differential inclined manometer and a pressure transducer as shown in Figures 8 and 9. The differential inclined manometer (accuracy ± 0.005 ft) was read to 0.01 ft and estimated to the nearest 0.005 ft. A variation of 0.005 ft in the manometer reading caused an error of approximately ± 0.1 ft per second. The pressure transducer (accuracy ± 0.0002 ft) was read to 0.004 ft. Due to the sensitivity of the pressure transducer, point velocity fluctuations were experienced making accurate readings difficult, therefore average readings were used instead of instantaneous readings. A difference in indicator accuracy was a source of variation between velocity head readings.

A stainless-steel pipette sampler was used in this study to siphon suspended and bed-load sediment samples from the flow. During test series with rainfall air was siphoned through the pipette while operating at 0.9d and above. Samples siphoned from near the bed of the flume showed considerable variations between runs. Variations in these samples near the bed were due to low velocities at the bed and the slow sampling rates.

CHAPTER IV

SUMMARY AND CONCLUSIONS

Summary

Studies were conducted in a closed system recirculating research flume to evaluate the relative effects of rainfall on von Karman's universal constant and the transport capacity of the flow. The tests conducted are outlined in Table II. Two different velocity head indicators were used with the Pitot-static tube to determine point velocities in the flow. A stainless steel-pipette sediment sampler was used to siphon point sediment concentrations from the flow. Regression analyses were performed on the velocity data to determine the best fit dimensionless velocity curve on semilogarithmic paper. Von Karman's universal constant was then evaluated from the slope of the regression line.

Sediment samples were taken at 45 second intervals from the beginning of simulated rainfall to determine the effect of rainfall on sediment transport.

Conclusions

1. Suspended sediment reduces the value of the von Karman's universal constant. A significant reduction in von Karman's universal constant is shown in Table IV where the values of κ obtained

in Test Series A, B and C (clear water) are shown with those obtained in Test Series 1, 2, 3 and 4 (with sediment). The reduction of κ with suspended sediment indicates that the mixing is less effective and that the sediment tends to suppress or dampen out the turbulence.

2. Test Series 4 indicates that simulated rainfall and suspended sediment reduces the value of von Karman's universal constant of turbulent exchange which characterizes the effectiveness of the turbulence in transfering momentum. Reduction of κ means that the mixing is less effective and the simulated rainfall and suspended sediment tend to suppress the turbulence.

3. The velocity distribution at the centerline of the flume for all test series (with and without rainfall) were of the logarithmic form (within the accuracy of the instrumentation) and followed the velocity defect law.

4. The suspended load transport capacity of the flow appears to be reduced under simulated rainfall conditions due to a reduction in von Karman's universal constant.

Future Studies

1. This study indicates that secondary circulation may be a source of error between Test Series 3 and 4; therefore, it is recommended that additional studies be conducted to determine the

the effects of secondary circulation on the suspended load transport in shallow flow.

2. This study indicates that rainfall affects the characteristics of the flow; therefore, it is recommended that additional studies be conducted to determine the effects of rainfall on the secondary circulation.

3. This study also indicates that the slope of the bed and the discharge should be varied to determine their effects on von Karman's universal constant.

LIST OF REFERENCES

LIST OF REFERENCES

1. Brown, C. B., "Sediment Transportation," Engineering Hydraulics, Edited by H. Rouse, John Wiley & Sons, Inc., New York, N. Y., 1950, Chapter 7, p. 795.

2. Chien, M., "The Present Status of Research on Sediment Transport," Trans. ASCE, 122:833-884, 1956.

3. Chow, V. T., Open Channel Hydraulics, McGraw-Hill Book Company, Inc., New York, N. Y., 1959.

4. Colby, B. R. and Hembree, C. H., "Computations of Total Sediment Discharge, Niabrara River Near Cody, Wyoming," U. S. Geol. Survey, WSP #1357, 1955.

5. Culbertson, J. K. and Dawdy, P. R., "A Study of Fluvial Characteristics and Hydraulic Variables Middle Rio Grande New Mexico," U. S. Geol. Survey, WSP #1498 F, 1964.

6. Einstein, H. A., "Formulas for the Transportation of Bed-Load," Trans. ASCE, 107:561-573, 1942.

7. Einstein, H. A., "The Bed-Load Function for Sediment Transportation in Open Channel Flows," Technical Bulletin No. 1026, U. S. Dept. of Agriculture, Washington, D. C., p. 10, 1950.

8. Glass, L. J. and Smerdon, E. T., "The Effect of Rainfall on the Velocity Distribution in Shallow Channel Flow," Trans. ASAE, 10:330-332, 336, 1967.

9. Kalinske, A. A., "Movement of Sediment as Bed-Load in Rivers," Trans. Am. Geophys. Union, 28:615-620, 1947.

10. Leliavsky, S., An Introduction to Fluvial Hydraulics, Constable and Company, Ltd., London, 1959.

11. MacDougall, C. A., "Bed-Sediment Transportation in Open Channels," Trans. Am. Geophys. Union, 14:491-495, 1933.

12. Meyer, L. D. and McCune, D. L., "Development of a Rainfall Simulator for Runoff Plots," Agricultural Engineering, 39: 644-648, October, 1958.

13. Nail, F. M., "Flume Studies of Sediment Transportation in Shallow Flow with Simulated Rainfall," M.S. Thesis, Department of Agricultural Engineering, Texas A&M University, January, 1966.

14. O'Brien, M. P., "Review of the Theory of Turbulent Flow and Its Relation to Sediment Transportation," *Trans. Am. Geophys. Union*, 34:487-491, 1933.

15. Pien, C. L., "Investigation of Turbulence and Suspended Material Transportation in Open Channels," Ph.D. Dissertation, University of Iowa, 1941.

16. Rouse, H., "Modern Conceptions of the Mechanics of Fluid Turbulence," *Trans. ASCE*, 102:534, 1937.

17. Rouse, H., *Engineering Hydraulics*, Edited by H. Rouse, John Wiley and Sons, Inc., New York, N. Y., 1950, pp. 86-90, 794-804.

18. Shulits, S., "The Schoklitsch Bed-Load Formula," *Engineering*, June, 1935.

19. Smerdon, E. T., "Effect of Rainfall on Critical Tractive Forces in Channels with Shallow Flow," *Trans. ASAE*, 7:287-290, 1964.

20. Vanoni, V. A., "Transportation of Suspended Sediment by Water," *Trans. ASCE*, 111:67-133, 1946.

21. *Water, The Yearbook of Agriculture*, U.S. Dept. of Agriculture, Washington, D. C., p. 139, 1955.

RELATED LITERATURE

RELATED LITERATURE

1. Chow, V. T., Handbook of Applied Hydrology, McGraw-Hill Book Co., Inc., New York, N. Y., pp. 17-23, 1964.

2. Dobbins, W. E., "Effect of Turbulence on Sedimentation," Trans. ASCE, 109:629-655, 1944.

3. Johnson, J. W., "The Importance of Considering Side Wall Friction in Bed-Load Investigations," Civil Engineering, 12:329-331, June, 1942.

4. Kalinske, A. A., and Pien, C. L., "Experiments on Eddy-Diffusion and Suspended-Material Transportation in Open Channels," Trans. Am. Geophys. Union, 23:530-536, Part II, 1943.

APPENDIX A

APPENDIX A

LIST OF SYMBOLS

Symbol	Description	Dimensions
A	area	L^2
A_*	constant	
A'	constant or empirical coefficient	
B_*	constant	
B'	constant or empirical coefficient	
B_s	dimensionless part of, ϕ_s	
B_b	dimensionless part of, ϕ_b	
C_s	sediment coefficient	
c_a	sediment concentration at an arbitrary reference level	
c	sediment concentration at a y distance from the bed	
D	diameter of sediment particle	L
d	depth of flow	L
g	acceleration of gravity	LT^{-2}
K	proportionality constant	
$1'$	length	L
m	empirical exponent	
Q	total discharge	L^3T^{-1}
q	discharge per unit width of flow	L^2T^{-1}

Symbol	Description	Dimensions
q_s	sediment discharge per unit width of flow	L^2T^{-1}
q_c	critical discharge per unit width of flow	L^2T^{-1}
q_*	discharge per unit length	L^2T^{-1}
R_b	hydraulic radius of the bed	L
R'_b	hydraulic radius of the sediment particle	L
S	slope of the bed	
S_e	slope of the energy gradient	
S_w	slope of the water surface	
T	top width	L
$\bar{u}$	mean vertical velocity fluctuations	LT^{-1}
V	mean velocity	LT^{-1}
V_r	mean velocity of flow with rainfall	LT^{-1}
V_*	shear velocity, $\sqrt{\tau_o/\rho}$ or $\sqrt{gdS_e}$	LT^{-1}
$\bar{v}$	mean horizontal velocity fluctuations	LT^{-1}
v_f	fall velocity of a sediment particle in still water	LT^{-1}
v	point velocity	LT^{-1}
y	distance from flume bed	L
z	exponent, $v_f/\kappa\sqrt{\tau_o/\rho}$	
α, α'	energy coefficient	
κ	von Karman's universal constant	
γ	unit weight of the water	FL^{-3}

Symbol	Description	Dimensions
γ_s	unit weight of the sediment	FL^{-3}
ε_m	momentum transfer coefficient	
ε_s	sediment transfer coefficient	
δ	thickness of the laminar sublayer	L
η_b	roughness coefficient due to bed	
η'_b	roughness coefficient due to sediment particles	
η_o	constant	
η	Boussinesq kinematic viscosity	L^2T^{-1}
π	3.1416	
μ	micron	L
ρ	mass density of the fluid	$FL^{-4}T^2$
ρ_s	mass density of the sediment	$FL^{-4}T^2$
τ	tractive force	FL^{-2}
τ_c	critical tractive force	FL^{-2}
τ_o	tractive force at the bed	FL^{-2}
ϕ	intensity of bed-load transport	
ϕ_s	suspended-load transport function	
ϕ_b	bed-load transport function	
ϕ_t	total-load transport function	
ψ	intensity of flow	

APPENDIX B

TABLE VII
REGRESSION ANALYSIS RESULTS OF VELOCITY DEFECT LAW FOR TESTS CONDUCTED WITHOUT SIMULATED RAINFALL (Series A through 4 - Runs 1 through 6)

Run No.	Velocity Head Indicator[1]	Regression Coefficients A[2]	Regression Coefficients E[2]	κ[3]	N[4]	F[5]	Significance Level	Velocity Distribution Regression Curve Figure No.
				Test Series A				
1	M	3.640	1.581	0.632	7	54.87	0.001	13
2	M	4.298	1.866	0.535	7	40.66	0.001	13
3	M	3.525	1.531	0.652	7	61.56	0.001	13
4	M	4.601	1.988	0.500	7	106.08	0.001	13
5	M	4.432	1.925	0.519	7	443.24	0.001	13
				Test Series B				
1	M	3.579	1.554	0.633	7	77.60	0.001	14
	T	5.946	2.582	0.387	7	42.82	0.001	15
2	M	3.244	1.409	0.708	7	84.46	0.001	14
	T	3.056	1.327	0.753	7	158.94	0.001	15
3	M	4.763	2.068	0.483	7	166.80	0.001	14
	T	5.059	2.197	0.454	7	658.18	0.001	15
4	M	3.986	1.731	0.576	7	112.51	0.001	14
	T	3.284	1.426	0.700	7	55.40	0.001	15
5	M	4.223	1.835	0.544	7	83.25	0.001	14
	T	- -	- -	- No run	-	- -	- - -	- - -

TABLE VII. Continued

Run No.	Velocity Head Indicator	Regression Coefficients A	Regression Coefficients E	κ	N	F	Significance Level	Velocity Distribution Regression Curve Figure No.
Test Series C								
1	M	2.829	1.229	0.813	7	202.23	0.001	16
	T	3.598	1.563	0.630	7	696.34	0.001	17
2	M	3.247	1.410	0.709	7	67.73	0.001	16
	T	3.195	1.388	0.720	7	92.38	0.001	17
3	M	3.575	1.553	0.644	7	119.75	0.001	16
	T	3.164	1.374	0.727	7	76.29	0.001	17
4	M	3.658	1.589	0.630	7	--	--	16
	T	3.888	1.689	0.592	7	370.65	0.001	17
5	M	- -	- - -	No. run	-	- -	- - -	- - -
	T	3.517	1.528	0.654	7	558.62	0.001	17
Test Series No. 1								
1	M	5.845	2.538	0.394	9	46.17	0.001	18
	T	5.922	2.572	0.388	9	52.03	0.001	19
2	M	5.949	2.584	0.387	9	97.85	0.001	18
	T	6.195	2.690	0.372	9	117.85	0.001	19
3	M	5.870	2.549	0.392	9	61.74	0.001	18
	T	5.812	2.524	0.395	9	62.89	0.001	19
4	M	6.032	2.620	0.382	9	77.46	0.001	18
	T	6.081	2.641	0.378	9	78.93	0.001	19
5	M	6.691	2.906	0.344	9	124.59	0.001	18
	T	6.287	2.731	0.366	9	143.14	0.001	19
6	M	6.463	2.807	0.356	9	85.48	0.001	18
	T	6.470	2.810	0.355	9	123.80	0.001	19

TABLE VII. Continued

Run No.	Velocity Head Indicator	Regression Coefficients A	Regression Coefficients E	κ	N	F	Significance Level	Velocity Distribution Regression Curve Figure No.
			Test Series No. 2					
1	M	6.555	2.847	0.351	8	--	--	20
	T	6.572	2.854	0.350	8	562.43	0.001	21
2	M	5.750	2.497	0.400	8	706.70	0.001	20
	T	6.064	2.633	0.380	8	--	--	21
3	M	5.757	2.500	0.400	8	--	--	20
	T	5.776	2.508	0.399	8	325.02	0.001	21
4	M	6.019	2.614	0.382	8	548.56	0.001	20
	T	6.442	2.798	0.358	8	162.35	0.001	21
5	M	6.257	2.717	0.367	8	626.34	0.001	20
	T	6.582	2.859	0.350	8	106.41	0.001	21
6	M	5.019	2.180	0.459	8	447.85	0.001	20
	T	5.337	2.318	0.432	8	--	--	21
			Test Series 3					
1	M	5.563	2.416	0.413	8	108.77	0.001	22
	T	5.448	2.366	0.423	8	623.23	0.001	23
2	M	4.948	2.149	0.466	8	187.48	0.001	22
	T	4.959	2.154	0.464	8	148.99	0.001	23
3	M	5.840	2.536	0.394	8	164.23	0.001	22
	T	5.957	2.587	0.386	8	504.24	0.001	23
4	M	5.577	2.422	0.413	8	727.34	0.001	22
	T	5.223	2.268	0.441	8	395.88	0.001	23
5	M	5.616	2.439	0.410	8	118.33	0.001	22
	T	4.989	2.167	0.462	8	115.06	0.001	23
6	M	5.902	2.563	0.390	8	207.24	0.001	22
	T	5.703	2.477	0.403	8	--	--	23

TABLE VII. Continued

Run No.	Velocity Head Indicator	Regression Coefficients A	Regression Coefficients E	κ	N	F	Significance Level	Velocity Distribution Regression Curve Figure No.
			Test Series 4					
1	M	10.196	4.428	0.226	5	47.86	0.005	24
	T	6.306	2.739	0.365	4	31.48	0.025	25
2	M	7.229	3.139	0.318	5	75.61	0.001	24
	T	7.147	3.104	0.322	5	123.92	0.001	25
3	M	6.983	3.033	0.329	5	110.40	0.001	24
	T	6.605	2.868	0.348	5	78.82	0.001	25
4	M	6.604	2.868	0.348	5	77.57	0.001	24
	T	6.766	2.938	0.340	5	84.58	0.001	25
5	M	7.550	3.279	0.306	5	103.42	0.001	24
	T	6.750	2.931	0.342	4	93.06	0.005	25
6	M	6.947	3.017	0.332	5	115.79	0.001	24
	T	6.617	2.874	0.348	5	60.92	0.005	25

[1] M = Manometer; T = Transducer.

[2] A = Slope of the regression line; E = Intercept of the regression line at $\log_{10}\frac{y}{d} = 0$.

[3] κ = von Karman's universal constant.

[4] N = Number of readings included in the regression.

[5] F = Statistical test for goodness of fit.

TABLE VIII

REGRESSION ANALYSIS RESULTS OF VELOCITY DEFECT LAW FOR TEST RUNS CONDUCTED WITHOUT AND WITH SIMULATED RAINFALL (Series 3 and 4 - Runs 7 through 33)

Run No.	Time from Beginning of Rainfall min$^{1/}$	Regression Coefficients A^2	Regression Coefficients E^2	κ^3	N^4	F^5	Significance Level	Velocity Distribution Regression Curve Figure No.
				Test Series No. 3				
7	-2:30	7.821	3.397	0.294	7	239.11	0.001	26
8	-2:30	7.888	3.426	0.292	7	275.23	0.001	26
9	-2:30	7.523	3.267	0.306	7	161.97	0.001	26
10	-1:45	7.226	3.138	0.318	7	123.61	0.001	26
11	-1:45	7.996	3.473	0.288	7	260.89	0.001	26
12	-1:45	7.672	3.332	0.300	7	237.37	0.001	26
13	-1:00	8.159	3.544	0.282	7	63.03	0.001	26
14	-1:00	7.986	3.468	0.288	7	87.87	0.001	26
15	-1:00	7.914	3.437	0.290	7	64.67	0.001	26
16	+0:15	- - -	- - -	No run	-	- - -	- - -	- - -
17	+0.15	7.465	3.242	0.308	6	138.95	0.001	27
18	+1:15	6.944	3.016	0.332	6	186.24	0.001	27
19	+1:00	7.226	3.138	0.318	6	107.77	0.001	28
20	+1:00	8.293	3.602	0.278	6	408.83	0.001	28
21	+1:00	7.593	3.298	0.303	6	344.17	0.001	28
22	+1:45	6.817	2.961	0.337	6	668.66	0.001	29
23	+1:45	7.926	3.442	0.290	6	366.96	0.001	29
24	+1:45	7.235	3.142	0.318	6	529.46	0.001	29

TABLE VIII. Continued

Run No.	Time from Beginning of Rainfall min	Regression Coefficients A	Regression Coefficients E	κ	N	F	Significance Level	Velocity Distribution Regression Curve Figure No.
25	+2:30	7.130	3.096	0.323	6	144.66	0.001	30
26	+2:30	8.219	3.569	0.280	6	937.50	0.001	30
27	+2:30	7.518	3.265	0.306	6	--	--	30
28	+4:00	7.721	3.353	0.298	6	130.59	0.001	31
29	+4:00	8.467	3.677	0.272	6	474.95	0.001	31
30	+4:00	7.908	3.435	0.291	6	627.74	0.001	31
31	+6:00	8.043	3.493	0.286	6	178.92	0.001	31
32	+6:00	8.765	3.806	0.262	6	574.63	0.001	31
33	+6:00	8.140	3.535	0.293	6	291.74	0.001	31
				Test Series No. 4				
7	-2:30	5.346	2.332	0.431	5	102.80	0.001	32
8	-2:30	5.157	2.239	0.446	5	105.26	0.001	32
9	-2:30	5.774	2.508	0.399	5	186.74	0.001	32
10	-1:45	5.789	2.514	0.398	5	85.64	0.001	32
11	-1:45	5.689	2.471	0.405	5	55.16	0.005	32
12	-1:45	5.616	2.439	0.406	5	193.26	0.001	32
16	+0:15	4.672	2.029	0.493	5	38.88	0.005	33
17	+0:15	6.641	2.884	0.347	5	169.80	0.001	33
18	+0:15	7.869	7.869	3.417	4	73.49	0.005	33
19	+1:00	5.041	2.189	0.457	5	52.65	0.010	34
20	+1:00	6.541	2.841	0.352	5	94.31	0.001	34
21	+1:00	8.168	3.547	0.282	4	88.87	0.005	34

TABLE VIII. Continued

Run No.	Time from Beginning of Rainfall min	Regression Coefficients		κ	N	F	Significance Level	Velocity Distribution Regression Curve Figure No.
		A	E					
22	+1:45	4.831	2.093	0.477	5	37.95	0.005	35
23	+1:45	7.190	3.123	0.320	5	--	--	35
24	+1:45	7:103	3.085	0.324	4	72.21	0.005	35
25	±2.30	5.317	2.309	0.433	5	32.87	0.005	36
26	+2:30	7.777	3.377	0.296	5	376.04	0.001	36
27	+2:30	8.173	3.550	0.282	4	147.25	0.005	36
28	+4:00	5.349	2.323	0.430	5	32.15	0.005	37
29	+4:00	8.622	3.744	0.267	5	515.02	0.001	37
30	+4:00	8.070	3.505	0.285	4	441.80	0.001	37
31	+6:00	5.724	2.486	0.402	5	22.28	0.010	37
32	+6:00	7.802	3.388	0.295	5	636.29	0.001	37
33	+6:00	8.029	3.487	0.287	4	619.31	0.001	37

[1] - = Time before beginning of rainfall; + = Time after beginning of rainfall.

[2] A = Slope of the regression line; E = Intercept of regression line at $\log_{10}\frac{y}{d} = 0$.

[3] κ = von Karman's universal constants.

[4] N = Number of readings included in the regression.

[5] F = Statistical test for goodness of fit.

TABLE IX
VELOCITY DATA FOR TEST RUNS WITHOUT SIMULATED RAINFALL
(Series A through 4 - Runs 1 through 6)

Run No.[1]	Velocity Head Indicator[2]	Point Velocities[3] (depth above bed) 0.933d	0.800d	0.667d	0.533d	0.333d	0.200d	0.067d	Average Profile Velocity[3]	Velocity Distribution Regression Curve Figure No.
		Test Series A								
1	M	1.33	1.28	1.27	1.22	1.12	1.02	0.98	1.17	13
2	M	1.36	1.32	1.26	1.17	1.10	0.98	0.94	1.16	13
3	M	1.30	1.25	1.19	1.17	1.08	1.00	0.94	1.13	13
4	M	1.39	1.35	1.30	1.25	1.17	1.02	0.94	1.20	13
5	M	1.36	1.32	1.30	1.25	1.15	1.06	0.92	1.19	13
		Test Series B								
1	M	1.62	1.57	1.53	1.53	1.51	1.33	1.28	1.48	14
	T	1.62	1.58	1.60	1.58	1.59	1.27	1.07	1.46	15
2	M	1.62	1.58	1.50	1.49	1.48	1.39	1.28	1.47	14
	T	1.62	1.62	1.57	1.55	1.41	1.46	1.32	1.52	15
3	M	1.62	1.58	1.49	1.46	1.37	1.27	1.17	1.42	14
	T	1.64	1.61	1.57	1.50	1.47	1.30	1.17	1.46	15
4	M	1.56	1.48	1.43	1.39	1.35	1.25	1.15	1.37	14
	T	1.63	1.71	1.60	1.59	1.54	1.48	1.35	1.55	15
5	M	1.56	1.55	1.43	1.43	1.40	1.30	1.12	1.39	14
	T	1.53	1.55	1.59	1.58	1.55	1.47	1.45	1.53	15

TABLE IX. Continued

Run No.	Velocity Head Indicator	Point Velocities (depth above bed) 0.933d	0.800d	0.667d	0.533d	0.333d	0.200d	0.067d	Average Profile Velocity	Velocity Distribution Regression Curve Figure No.
					Test Series C					
1	M	1.29	1.29	1.28	1.20	1.17	1.10	1.00	0.98	16
	T	1.48	1.46	1.46	1.42	1.35	1.26	1.13	1.36	17
2	M	1.30	1.27	1.24	1.17	1.08	1.00	0.92	0.94	16
	T	1.48	1.55	1.40	1.34	1.27	1.21	1.11	1.32	17
3	M	1.40	1.36	1.33	1.25	1.15	1.12	1.00	0.98	16
	T	1.48	1.48	1.47	1.37	1.26	1.24	1.16	1.35	17
4	M	1.30	1.30	1.27	1.22	1.13	1.06	0.96	0.87	16
	T	1.51	1.51	1.47	1.37	1.29	1.24	1.16	1.35	17
5	M	1.32	1.33	1.33	1.30	1.22	1.20	1.19	1.19	16
	T	1.48	1.46	1.46	1.42	1.34	1.25	1.15	1.36	17

TABLE IX. Continued

Run No.	Veloci-ty Head Indi-cator	Point Velocities (depth above bed) 0.933d	0.800d	0.667d	0.533d	0.333d	0.200d	0.133d	0.067d	0.033d	Average Profile Velocity	Velocity Distribution Regression Curve Figure No.
						Test Series No. 1[4]						
1	M	1.74	1.73	1.67	1.63	1.40	1.08	1.04	1.02	1.00	1.46	18
	T	1.91	1.90	1.78	1.72	1.47	1.26	1.19	1.16	1.12	1.59	19
2	M	1.77	1.75	1.68	1.62	1.47	1.17	1.13	1.02	0.98	1.49	18
	T	1.94	1.92	1.84	1.71	1.51	1.34	1.27	1.16	1.07	1.62	19
3	M	1.78	1.71	1.68	1.54	1.38	1.15	1.04	1.02	0.98	1.46	18
	T	1.95	1.86	1.79	1.62	1.44	1.32	1.22	1.18	1.09	1.59	19
4	M	1.78	1.74	1.69	1.64	1.43	1.17	1.08	1.04	0.98	1.49	18
	T	1.95	1.90	1.81	1.72	1.48	1.31	1.24	1.17	1.09	1.61	19
5	M	1.78	1.75	1.69	1.67	1.43	1.15	1.10	0.94	0.90	1.48	18
	T	1.95	1.86	1.80	1.71	1.51	1.34	1.29	1.09	1.06	1.61	19
6	M	1.77	1.73	1.69	1.60	1.40	1.10	1.08	0.94	0.92	1.46	18
	T	1.94	1.89	1.79	1.68	1.53	1.31	1.20	1.09	1.03	1.60	19

TABLE IX. Continued

Run No.	Velocity Head Indicator	Point Velocities (depth above bed)								Average Profile Velocity	Velocity Distribution Regression Curve Figure No.
		0.933d	0.800d	0.667d	0.533d	0.333d	0.200d	0.133d	0.067d		
					Test Series No. 2						
1	M	1.24	1.22	1.17	1.13	1.02	0.85	0.78	0.57	1.02	20
	T	1.30	1.29	1.23	0.21	1.06	0.91	0.78	0.67	1.08	21
2	M	1.24	1.22	1.19	1.12	1.00	0.90	0.85	0.63	1.04	20
	T	1.31	1.28	1.24	1.17	1.08	0.94	0.88	0.67	1.09	21
3	M	1.20	1.19	1.17	1.08	0.98	0.85	0.78	0.63	1.01	20
	T	1.29	1.24	1.22	1.16	1.04	0.88	0.82	0.73	1.07	21
4	M	1.22	1.20	1.13	1.10	1.00	0.85	0.72	0.63	1.01	20
	T	1.29	1.26	1.18	1.08	1.02	0.83	0.71	0.67	1.03	21
5	M	1.25	1.24	1.20	1.18	1.00	0.92	0.75	0.63	1.04	20
	T	1.30	1.26	1.18	1.12	0.91	0.84	0.69	0.67	1.02	21
6	M	1.22	1.19	1.13	1.10	1.02	0.87	0.80	0.72	1.03	20
	T	1.25	1.23	1.19	1.16	1.03	0.92	0.85	0.72	1.06	21

TABLE IX. Continued

Run No.	Velocity Head Indicator	Point Velocities (depth above bed) 0.900d	0.800d	0.700d	0.500d	0.300d	0.200d	0.100d	0.050d	Average Profile Velocity	Velocity Distribution Regression Curve Figure No.
					Test Series No. 3						
1	M	1.67	1.67	1.65	1.60	1.46	1.21	1.20	1.04	1.48	22
	T	1.89	1.89	1.87	1.79	1.63	1.52	1.41	1.26	1.70	23
2	M	1.67	1.67	1.63	1.58	1.40	1.28	1.20	1.12	1.48	22
	T	1.89	1.89	1.88	1.78	1.61	1.51	1.42	1.35	1.70	23
3	M	1.63	1.62	1.60	1.48	1.39	1.20	1.02	1.00	1.42	22
	T	1.83	1.83	1.79	1.71	1.57	1.45	1.24	1.17	1.62	23
4	M	1.67	1.65	1.60	1.49	1.38	1.28	1.17	0.98	1.45	22
	T	1.85	1.85	1.79	1.70	1.55	1.48	1.37	1.23	1.64	23
5	M	1.63	1.63	1.60	1.49	1.33	1.24	1.02	1.04	1.42	22
	T	1.84	1.83	1.79	1.66	1.57	1.46	1.29	1.30	1.63	23
6	M	1.63	1.60	1.54	1.45	1.35	1.22	1.17	0.85	1.40	22
	T	1.83	1.83	1.76	1.68	1.54	1.48	1.33	1.13	1.62	23

TABLE IX. Continued

Run No.	Velocity Head Indicator	Point Velocities (depth above bed)					Average Profile Velocity	Velocity Distribution Regression Curve Figure No.
		0.715d	0.535d	0.355d	0.179d	0.089d		
				Test Series No. 4				
1	M	1.54	1.46	1.36	1.02	0.98	1.34	24
	T	1.55	1.51	1.35	1.22	1.16	1.40	25
2	M	1.58	1.53	1.36	1.30	1.13	1.42	24
	T	1.61	1.52	1.39	1.30	1.16	1.44	25
3	M	1.57	1.46	1.36	1.24	1.13	1.40	24
	T	1.59	1.51	1.39	1.27	1.20	1.44	25
4	M	1.55	1.47	1.39	1.22	1.17	1.40	24
	T	1.59	1.51	1.41	1.26	1.20	1.44	25
5	M	1.57	1.50	1.39	1.20	1.13	1.41	24
	T	1.59	1.51	1.40	1.27	1.19	1.44	25
6	M	1.57	1.50	1.43	1.24	1.17	1.43	24
	T	1.61	1.51	1.39	1.28	1.20	1.44	25

[1] Run No. 1 = 0.250 ft right of centerline looking downstream.
Run No. 2 = 0.125 ft right of centerline looking downstream
Run No. 3 = Centerline.
Run No. 4 = 0.125 ft left of centerline looking downstream.
Run No. 5 = 0.250 ft left of centerline looking downstream.
(Footnote [1] applies only to Series A, B and C).

[2] M = Manometer; T = Transducer.

[3] Ft/sec.

[4] Centerline runs.

TABLE X
VELOCITY DATA FOR TEST RUNS WITHOUT AND WITH SIMULATED RAINFALL
(Series 3 and 4 - Runs 7 through 33)

Run No.	Time from Beginning of Rainfall[1] min	Point Velocities[2] (depth above bed)							Average Profile Velocity[2]	Velocity Distribution Regression Curve Figure No.
		0.9d	0.8d	0.7d	0.5d	0.3d	0.2d	0.1d		
					Test Series No. 3					
7	-2:30	1.89	1.83	1.72	1.63	1.45	1.27	1.14	1.54	26
8	-2:30	1.91	1.81	1.74	1.64	1.43	1.29	1.13	1.54	26
9	-2:30	1.88	1.82	1.70	1.64	1.44	1.27	1.17	1.54	26
10	-1:45	1.86	1.81	1.71	1.62	1.38	1.26	1.11	1.51	26
11	-1:45	1.88	1.82	1.72	1.64	1.39	1.28	1.11	1.52	26
12	-1:45	1.87	1.82	1.72	1.62	1.40	1.29	1.14	1.52	26
13	-1:00	1.88	1.79	1.66	1.60	1.32	1.16	1.12	1.48	26
14	-1:00	1.88	1.76	1.66	1.61	1.34	1.19	1.11	1.48	26
15	-1:00	1.88	1.76	1.66	1.60	1.34	1.16	1.13	1.48	26
16	+0:15	- -	- -	- -	No run	- -	- -	- -	- -	- -
17	+0:15	----	2.08	2.00	1.94	1.71	1.54	1.43	1.80	27
18	+0:15	----	2.04	2.00	1.93	1.71	1.58	1.45	1.80	27
19	+1:00	----	2.04	2.02	1.94	1.86	1.65	1.39	1.84	28
20	+1:00	----	2.12	2.12	2.00	1.80	1.61	1.42	1.87	28
21	+1:00	----	2.15	2.09	2.05	1.82	1.72	1.47	1.90	28
22	+1:45	----	2.03	1.98	1.91	1.78	1.64	1.41	1.81	29
23	+1:45	----	2.10	2.08	1.91	1.78	1.58	1.42	1.83	29
24	+1:45	----	2.08	2.04	1.97	1.75	1.64	1.46	1.84	29

TABLE X. Continued

Run No.	Time from Beginning of Rainfall min	Point Velocities (depth above bed) 0.9d	0.8d	0.7d	0.5d	0.3d	0.2d	0.1d	Average Profile Velocity	Velocity Distribution Regression Curve Figure No.
25	+2:30	----	2.03	1.99	1.94	1.82	1.65	1.39	1.82	30
26	+2:30	----	2.06	2.04	1.88	1.76	1.59	1.34	1.80	30
27	+2:30	----	2.08	2.01	1.94	1.77	1.62	1.42	1.83	30
28	+4:00	----	2.06	2.00	1.99	1.83	1.65	1.38	1.84	31
29	+4:00	----	2.06	2.05	1.90	1.78	1.61	1.32	1.80	31
30	+4:00	----	2.09	2.01	1.95	1.79	1.61	1.39	1.82	31
31	+6:00	----	2.09	2.01	1.99	1.82	1.66	1.36	1.84	31
32	+6:00	----	2.07	2.04	1.90	1.77	1.58	1.30	1.80	31
33	+6:00	----	2.06	2.03	1.95	1.79	1.56	1.38	1.82	31

TABLE X. Continued

Run No.	Time from Beginning of Rainfall min	Point Velocities (depth above bed)					Average Profile Velocity	Velocity Distribution Regression Curve Figure No.
		0.175d	0.535d	0.355d	0.188d	0.093d		
				Test Series No. 4				
7	-2:30	1.44	1.34	1.31	1.18	1.11	1.31	32
8	-2:30	1.44	1.34	1.30	1.22	1.10	1.31	32
9	-2:30	1.44	1.34	1.30	1.19	1.07	1.31	32
10	-1:45	1.48	1.39	1.29	1.22	1.11	1.34	32
11	-1:45	1.48	1.39	1.30	1.19	1.14	1.34	32
12	-1:45	1.47	1.39	1.31	1.22	1.12	1.34	32
16	+0:15	1.35	1.34	1.21	1.17	1.09	1.26	33
17	+0:15	1.39	1.37	1.28	1.12	1.04	1.28	33
18	+0:15	1.48	1.38	1.34	1.17	----	1.33	33
19	+1:00	1.35	1.33	1.22	1.13	1.09	1.26	34
20	+1:00	1.41	1.36	1.30	1.13	1.08	1.29	34
21	+1:00	1.45	1.43	1.33	1.16	----	1.33	34
22	+1:45	1.37	1.32	1.22	1.16	1.12	1.26	35
23	+1:45	1.41	1.37	1.29	1.16	1.05	1.30	35
24	+1:45	1.45	1.43	1.32	1.22	----	1.34	35
25	+2:30	1.37	1.31	1.25	1.13	1.12	1.26	36
26	+2:30	1.41	1.34	1.31	1.16	1.03	1.29	36
27	+2:30	1.47	1.43	1.32	1.21	----	1.34	36

TABLE X. Continued

Run No.	Time from Beginning of Rainfall min	Point Velocities (depth above bed)					Average Profile Velocity	Velocity Distribution Regression Curve Figure No.
		0.175d	0.535d	0.355d	0.188d	0.093d		
28	+4:00	1.36	1.32	1.22	1.16	1.12	1.26	37
29	+4:00	1.41	1.37	1.27	1.13	1.03	1.29	37
30	+4:00	1.46	1.40	1.32	1.21	----	1.34	37
31	+6:00	1.36	1.32	1.20	1.13	1.11	1.25	37
32	+6:00	1.41	1.34	1.29	1.18	1.05	1.29	37
33	+6:00	1.46	1.40	1.32	1.21	----	1.34	37

[1] - = Time before beinning of rainfall.
+ = Time after beginning of rainfall.

[2] Ft/sec.

TABLE XI
SEDIMENT CONCENTRATION DATA FOR TEST RUNS WITHOUT SIMULATED RAINFALL
(Series 3 and 4 - Runs 1 through 6)

Run No.	Point Sediment Concentration[1] (depth above bed)							
	0.9d	0.8d	0.7d	0.5d	0.3d	0.2d	0.1d	0.05d
				Test Series No. 3				
1	0.070	0.099	0.143	0.187	0.183	0.283	0.373	0.396
2	0.098	0.103	0.115	0.159	0.210	0.304	0.831	0.348
3	0.168	0.150	0.166	0.216	0.279	0.299	0.863	0.353
4	0.134	0.179	0.189	0.228	0.267	0.395	0.499	0.464
5	0.163	0.180	0.202	0.228	0.291	0.301	0.868	0.387
6	0.231	0.199	0.203	0.256	0.330	0.406 0.	0.543	0.478

Run No.	Point Sediment Concentration[1] (depth above bed)				
	0.715d	0.535d	0.355d	0.188d	0.089d
			Test Series No. 4		
1	0.077	0.132	0.139	-----	0.293
2	0.117	0.080	0.152	0.465	0.131
3	0.255	0.101	0.175	0.419	0.286
4	0.109	0.124	0.143	0.198	0.483
5	0.103	0.136	0.155	-----	0.321
6	0.022	0.105	0.138	0.314	0.355

---

[1] Percent.

TABLE XII

SEDIMENT CONCENTRATION DATA FOR TEST RUNS WITHOUT AND WITH SIMULATED RAINFALL

(Series 3 and 4 - Runs 7 through 33)

Run No.	Time from Beginning of Rainfall[1] min	Point Sediment Concentration[2] (depth above bed) 0.9d	0.8d	0.7d	0.5d	0.3d	0.2d	0.1d	Total Sediment Load C
				Test Series No. 3					
7	-2:30	0.241	0.303	0.355	0.399	0.486	0.571	0.862	0.279
8	-2:30	0.247	0.252	0.378	0.478	0.573	0.767	-----	0.231
9	-2:30	-----	0.278	0.318	0.515	0.353	0.395	0.493	0.241
10	-1:45	0.290	0.310	-----	0.500	0.616	0.746	0.714	0.207
11	-1:45	0.230	0.344	0.451	0.570	0.700	0.973	1.246	0.247
12	-1:45	-----	0.296	0.445	-----	0.482	0.685	0.754	0.211
13	-1:00	0.291	0.306	0.364	0.496	0.588	0.659	0.809	0.735
14	-1:00	0.266	0.360	0.482	0.559	0.718	0.809	1.359	0.286
15	-1:00	-----	0.292	0.402	0.504	0.479	0.454	1.489	0.240
16	+0:15	-----	0.164	0.283	0.429	0.719	1.161	1.873	-----
17	+0:15	-----	0.367	0.331	0.390	0.509	0.679	1.034	0.667
18	+0:15	-----	0.330	0.372	0.445	0.575	0.601	1.428	-----
19	+1:00	-----	0.192	0.374	0.722	1.014	1.317	1.766	-----
20	+1:00	-----	0.430	0.533	0.666	0.767	0.973	1.290	0.624
21	+1:00	-----	0.414	0.601	0.725	1.039	1.167	1.436	-----
22	+1:45	-----	0.367	0.483	0.685	1.002	1.139	1.399	-----
23	+1:45	-----	0.435	0.498	0.666	0.747	0.848	1.237	0.614
24	+1:45	-----	0.458	0.551	0.775	1.099	1.043	1.202	-----

TABLE XII. Continued

Run No.	Time from Beginning of Rainfall min	Point Sediment Concentration (depth above bed) 0.9d	0.8d	0.7d	0.5d	0.3d	0.2d	0.1d	Total Sediment Load C
25	+2:30	-----	0.371	0.485	0.654	1.042	1.086	1.312	-----
26	+2:30	-----	0.314	0.462	0.649	0.643	0.809	1.154	0.542
27	+2:30	-----	0.435	0.502	0.730	0.933	1.053	1.063	-----
28	+4:00	-----	0.377	0.412	0.616	0.848	1.101	1.293	-----
29	+4:00	-----	0.357	0.364	0.483	0.545	0.629	0.828	0.621
30	+4:00	-----	0.425	0.524	0.536	0.754	0.829	1.164	-----
31	+6:00	-----	0.371	0.293	0.550	0.984	0.804	1.521	-----
32	+6:00	-----	0.361	0.448	0.448	0.558	0.561	0.790	0.606
33	+6:00	-----	0.469	0.526	0.593	0.649	0.726	0.912	-----

TABLE XII. Continued

Run No.	Time from Beginning of Rainfall min	Point Sediment Concentration (depth above bed)					Total Sediment Load C
		0.715d	0.535d	0.355d	0.188d	0.089d	
				Test Series No. 4			
7	-2:30	0.116	0.095	0.163	0.683	0.515	0.094
8	-2:30	0.045	0.061	0.093	-----	0.281	0.197
9	-2:30	0.064	0.042	0.066	0.093	0.273	0.059
10	-1:45	0.105	0.156	0.254	0.726	-----	0.067
11	-1:45	-----	0.104	0.150	0.454	0.548	0.076
12	-1:45	0.077	0.085	0.099	0.139	0.183	0.079
13	-1:00	0.153	0.151	0.259	0.337	0.269	0.068
14	-1:00	0.070	0.102	0.131	0.232	1.831	0.074
15	-1:00	0.070	0.082	0.107	0.492	0.154	0.082
16	+0:15	0.071	0.099	0.144	0.679	0.286	-----
17	+0:15	0.070	0.068	0.097	0.932	0.160	0.031
18	+0:15	0.115	0.058	0.054	0.139	0.479	-----
19	+1:00	0.055	0.082	0.148	0.377	0.725	-----
20	+1:00	0.069	0.046	0.097	0.588	0.156	0.028
21	+1:00	0.041	0.042	0.054	0.091	0.107	-----
22	+1:45	0.091	0.079	0.093	0.418	0.159	-----
23	+1:45	0.034	0.039	0.067	0.125	0.786	0.022
24	+1:45	0.033	0.048	0.035	0.255	0.328	-----

TABLE XII. Continued

Run No.	Time from Beginning of Rainfall min	Point Sediment Concentration (depth above bed)					Total Sediment Load C
		0.715d	0.535d	0.355d	0.188d	0.089d	
25	+2:30	0.066	0.069	0.112	0.190	0.084	-----
26	+2:30	0.056	0.035	0.053	0.087	0.359	0.031
27	+2:30	0.044	01027	0.039	0.442	0.170	-----
28	+4:00	0.051	0.054	0.075	0.134	0.221	-----
29	+4:00	0.051	0.047	0.049	0.089	0.095	0.028
30	+4:00	0.032	0.028	0.038	0.043	0.052	-----
31	+6:00	0.062	0.059	0.099	0.443	1.455	-----
32	+6:00	0.046	0.048	0.059	0.395	0.083	0.035
33	+6:00	0.025	0.015	0.045	0.072	0.090	-----

---

[1] - = Time before beginning of rainfall.
+ = Time after beginning of rainfall.

[2] Percent.

TABLE XIII
RESEARCH FLUME DATA FOR TEST RUNS CONDUCTED WITHOUT SIMULATED RAINFALL
(Series A through 4 - Runs 1 through 6)

Run No.	Velocity Head Indicator[1]	Total Depth d ft	Mean Velocity V fps	Discharge Q cu ft/sec	Shear Velocity $(gdS_e)^{1/2}$ fps	Resistance Coefficient f
Test Series A						
1	M	0.30	1.17	0.351	0.088	0.0451
2	M	0.30	1.15	0.345	0.088	0.0464
3	M	0.30	1.13	0.339	0.088	0.0480
4	M	0.30	1.20	0.360	0.088	0.0430
5	M	0.30	1.19	0.357	0.088	0.0440
Test Series No. 1						
1	M	0.30	1.46	0.438	0.103	0.0398
	T	0.30	1.59	0.477	0.103	0.0334
2	M	0.30	1.49	0.447	0.103	0.0381
	T	0.30	1.62	0.486	0.103	0.0322
3	M	0.30	1.46	0.438	0.103	0.0399
	T	0.30	1.59	0.477	0.103	0.0336
4	M	0.30	1.49	0.447	0.103	0.0382
	T	0.30	1.62	0.486	0.103	0.0325
5	M	0.30	1.48	0.444	0.103	0.0386
	T	0.30	1.61	0.483	0.103	0.0326
6	M	0.30	1.46	0.438	0.103	0.0398
	T	0.30	1.60	0.480	0.103	0.0333

TABLE XIII. Continued

Run No.	Velocity Head Indicator	Total Depth d ft	Mean Velocity V fps	Discharge Q cu ft/sec	Shear Velocity $(gdS_e)^{1/2}$ fps	Resistance Coefficient f
			Test Series No. 2			
1	M	0.30	1.02	0.306	0.090	0.0621
	T	0.30	1.08	0.324	0.090	0.0553
2	M	0.30	1.04	0.312	0.090	0.0600
	T	0.30	1.09	0.327	0.090	0.0543
3	M	0.30	1.01	0.303	0.090	0.0640
	T	0.30	1.07	0.321	0.090	0.0568
4	M	0.30	1.01	0.303	0.090	0.0641
	T	0.30	1.03	0.309	0.090	0.0613
5	M	0.30	1.04	0.312	0.090	0.0602
	T	0.30	1.02	0.306	0.090	0.0623
6	M	0.30	1.03	0.309	0.090	0.0615
	T	0.30	1.06	0.318	0.090	0.0573
			Test Series No. 3			
1	M	0.20	1.48	0.296	0.097	0.0340
	T	0.20	1.70	0.340	0.097	0.0257
2	M	0.20	1.48	0.296	0.097	0.0340
	T	0.20	1.71	0.342	0.097	0.0257
3	M	0.20	1.42	0.284	0.097	0.0372
	T	0.20	1.62	0.324	0.097	0.0284
4	M	0.20	1.45	0.290	0.097	0.0357
	T	0.20	1.64	0.328	0.097	0.0276
5	M	0.20	1.42	0.284	0.097	0.0372
	T	0.20	1.63	0.284	0.097	0.0280
6	M	0.20	1.40	0.280	0.097	0.0382
	T	0.20	1.62	0.324	0.097	0.0285

TABLE XIII. Continued

Run No.	Velocity Head Indicator	Total Depth d ft	Mean Velocity V fps	Discharge Q cu ft/sec	Shear Velocity $(gdS_e)^{\frac{1}{2}}$ fps	Resistance Coefficient f
			Test Series No. 4			
1	M	0.112	1.34	0.150	0.066	0.0196
	T	0.112	1.40	0.157	0.066	0.0178
2	M	0.112	1.43	0.160	0.066	0.0173
	T	0.112	1.44	0.161	0.066	0.0169
3	M	0.112	1.39	0.156	0.066	0.0180
	T	0.112	1.44	0.161	0.066	0.0171
4	M	0.112	1.40	0.157	0.066	0.0177
	T	0.112	1.44	0.161	0.066	0.0170
5	M	0.112	1.41	0.158	0.066	0.0177
	T	0.112	1.44	0.158	0.066	0.0171
6	M	0.112	1.43	0.160	0.066	0.0173
	T	0.112	1.44	0.161	0.066	0.0169

[1] M = Manometer; T = transducer.

TABLE XIV.

RESEARCH FLUME DATA FOR TEST RUNS CONDUCTED WITHOUT AND WITH SIMULATED RAINFALL
(Series 3 and 4 - Runs 7 through 33)

Run No.	Time from Beginning of Rainfall min	Total Depth d ft	Mean Velocity V fps	Discharge Q cu ft/sec	Shear Velocity $(gdS_e)^{1/2}$ fps	Resistance Coefficient f
			Test Series No. 3			
7	-2:30	0.20	1.54	0.308	0.101	0.0348
8	-2:30	0.20	1.54	0.308	0.101	0.0347
9	-2:30	0.20	1.54	0.308	0.101	0.0349
10	-1:45	0.20	1.51	0.302	0.101	0.0361
11	-1:45	0.20	1.52	0.304	0.101	0.0355
12	-1:45	0.20	1.53	0.306	0.101	0.0352
13	-1:00	0.20	1.48	0.296	0.101	0.0376
14	-1:00	0.20	1.48	0.296	0.101	0.0375
15	-1:00	0.20	1.48	0.296	0.101	0.0375
16	- - -	- - -	- - -	No Run	- - -	- - -
17	+0:15	0.20	1.80	0.360	0.102	0.0258
18	+1:15	0.20	1.80	0.360	0.102	0.0258
19	+1:00	0.200	1.84	0.368	0.104	0.0254
20	+1:00	0.200	1.87	0.374	0.104	0.0245
21	+1:00	0.200	1.90	0.380	0.104	0.0235
22	+1:45	0.200	1.81	0.362	0.104	0.0265
23	+1:45	0.200	1.83	0.366	0.104	0.0259
24	+1:45	0.200	1.84	0.368	0.104	0.0255

TABLE XIV. Continued

Run No.	Time from Beginning of Rainfall min	Total Depth d ft	Mean Velocity V fps	Discharge Q cu ft/sec	Shear Velocity $(gdS_e)^{1/2}$ fps	Resistance Coefficient f
25	+2:30	0.200	1.82	0.364	0.105	0.0265
26	+2:30	0.200	1.80	0.360	0.105	0.0271
27	+2:30	0.200	1.83	0.366	0.105	0.0263
28	+4:00	0.200	1.84	0.368	0.106	0.0264
29	+4:00	0.200	1.81	0.362	0.106	0.0272
30	+4:00	0.200	1.83	0.366	0.106	0.0266
31	+6:00	0.200	1.84	0.368	0.106	0.0262
32	+6:00	0.200	1.80	0.360	0.106	0.0275
33	+6:00	0.200	1.82	0.364	0.106	0.0269
			Test Series No. 4			
7	-2:30	0.11	1.31	0.144	0.066	0.0204
8	-2:30	0.11	1.31	0.144	0.066	0.0204
9	-2:30	0.11	1.31	0.144	0.066	0.0206
10	-1:45	0.11	1.36	0.149	0.066	0.0197
11	-1:45	0.11	1.36	0.149	0.066	0.0196
12	-1:45	0.11	1.36	0.149	0.066	0.0196
16	+0:15	0.11	1.26	0.139	0.063	0.0200
17	+0:15	0.11	1.28	0.141	0.063	0.0193
18	+0:15	0.11	1.33	0.146	0.063	0.0180
19	+1:00	0.11	1.26	0.139	0.060	0.0183
20	+1:00	0.11	1.29	0.142	0.060	0.0172
21	+1:00	0.11	1.33	0.146	0.060	0.0164

TABLE XIV. Continued

Run No.	Time from Beginning of Rainfall min	Total Depth d ft	Mean Velocity V fps	Discharge Q cu ft/sec	Shear Velocity $(gdS_e)^{\frac{1}{2}}$ fps	Resistance Coefficient f
22	+1:45	0.11	1.26	0.139	0.057	0.0162
23	+1:45	0.11	1.30	0.143	0.057	0.0154
24	+1:45	0.11	1.34	0.147	0.057	0.0144
25	+2:30	0.11	1.26	0.139	0.054	0.0144
26	+2:30	0.11	1.29	0.142	0.054	0.0138
27	+2:30	0.11	1.34	0.147	0.054	0.0128
28	+4:00	0.11	1.26	0.139	0.050	0.0127
29	+4:00	0.11	1.29	0.142	0.050	0.0122
30	+4:00	0.11	1.34	0.147	0.050	0.0113
31	+6:00	0.11	1.25	0.137	0.050	0.0129
32	+6:00	0.11	1.29	0.142	0.050	0.0121
33	+6:00	0.11	1.34	0.147	0.050	0.0113

[1]
- = time before beginning of rainfall.
+ = time after beginning of rainfall.

TABLE XV
VELOCITY DISTRIBUTION CALCULATIONS FOR TEST RUNS CONDUCTED WITHOUT SIMULATED RAINFALL
(Series A through 4 - Runs 1 through 6)

Run No.	Velocity Head Indicator[1]	$\frac{v - V}{(gdS_e)^{1/2}}$						
		0.933d[2]	0.800d	0.667d	0.533d	0.333d	0.200d	0.067d
				Series A				
1	M	1.826	1.302	1.121	0.571	-0.604	-1.676	-2.133
2	M	2.349	1.836	1.123	0.176	-0.630	-1.951	-2.427
3	M	1.946	1.410	0.659	0.463	-0.512	-1.432	-2.140
4	M	2.191	1.739	0.169	0.632	-0.313	-1.985	-2.917
5	M	1.959	1.447	1.270	0.733	-0.408	-1.444	-3.061

Run No.	Velocity Head Indicator	0.93d	0.80d	0.67d	0.53d	0.33d	0.20d	0.13d	0.07d	0.03d
					Series 1					
1	M	2.691	2.577	2.001	1.646	-0.545	-2.656	-4.053	-4.243	-3.324
	T	3.106	2.958	1.803	1.231	-1.238	-3.281	-3.920	-4.185	-4.596
2	M	2.697	2.475	1.816	1.200	-0.190	-3.145	-3.484	-4.570	-4.959
	T	3.020	2.826	2.077	0.789	-1.156	-2.736	-3.404	-4.531	-5.377
3	M	3.159	2.489	2.143	0.809	-0.797	-2.960	-4.067	-4.219	-4.608
	T	3.525	2.674	1.990	0.307	-1.492	-2.579	-3.561	-4.004	-4.831
4	M	2.828	2.496	1.929	1.460	-0.572	-3.125	-3.991	-4.350	-4.939
	T	3.238	2.751	1.909	1.061	-1.318	-3.600	-3.613	-4.285	-5.085
5	M	2.903	2.571	2.004	1.771	-0.507	-3.216	-3.738	-5.270	-5.695
	T	3.244	2.625	1.828	0.884	-0.999	-2.641	-3.115	-5.080	-5.370
6	M	3.014	2.568	2.225	1.395	-0.550	-3.517	-3.694	-5.059	-5.257
	T	3.347	2.808	1.837	0.809	-0.674	-2.812	-3.808	-4.486	-5.486

TABLE XV. Continued

Run No.	Velocity Head Indicator	$\frac{v - V}{(gdS_e)^{1/2}}$ 0.93d	0.80d	0.67d	0.53d	0.33d	0.20d	0.13d	0.07d
					Series 2				
1	M	2.386	2.203	1.643	1.255	0.012	-1.895	-2.716	-5.046
	T	2.424	2.342	1.633	1.458	-0.238	-1.867	-3.342	-4.572
2	M	2.188	2.007	1.636	0.860	-0.404	-1.582	-2.094	-4.501
	T	2.366	2.090	1.636	0.834	-0.184	-1.672	-2.379	-4.685
3	M	2.186	2.000	1.809	0.817	-0.267	-1.724	-2.574	-4.136
	T	2.501	1.908	1.675	0.983	-0.283	-2.147	-2.737	-3.799
4	M	2.381	2.195	1.430	1.030	-0.031	-1.720	-3.137	-4.127
	T	2.945	2.525	1.643	0.598	-0.151	-2.206	-3.503	-3.968
5	M	2.388	2.207	1.841	0.879	-0.385	-1.315	-3.191	-4.482
	T	3.093	2.617	1.735	1.113	-0.124	-1.985	-3.614	-3.876
6	M	2.152	1.780	1.201	0.801	-0.041	-1.688	-2.490	-3.366
	T	2.051	1.849	1.466	1.040	-0.365	-1.573	-2.381	-3.841

TABLE XV. Continued

Run No.	Velocity Head Indicator	$\frac{v - V}{(gdS_e)^{\frac{1}{2}}}$ 0.90d	0.80d	0.70d	0.60d	0.30d	0.20d	0.10d	0.05d
				Series 3					
1	M	1.912	0.912	1.785	1.274	-0.219	-1.838	-2.879	-4.547
	T	1.942	1.942	1.765	0.947	-0.705	-1.867	-3.002	-4.547
2	M	1.903	1.903	1.522	1.003	0.810	-2.050	-2.888	-3.785
	T	1.918	1.918	1.830	0.736	-0.934	-2.066	-2.908	-3.702
3	M	2.218	2.084	1.960	0.749	-0.265	-2.193	-4.064	-4.268
	T	2.197	2.179	1.793	0.879	-0.567	-1.737	-3.913	-4.687
4	M	2.274	2.147	1.636	0.424	-0.739	-1.679	-2.868	-4.804
	T	2.146	2.110	1.523	0.607	-1.014	-1.652	-2.819	-4.280
5	M	2.204	2.193	1.946	0.735	-0.892	-1.866	-4.079	-3.875
	T	2.108	2.090	1.649	0.336	-0.653	-1.821	-3.495	-3.443
6	M	2.407	2.149	1.488	0.610	-0.532	-1.831	-2.355	-5.654
	T	2.234	2.216	1.474	0.561	-0.827	-1.446	-2.988	-5.016

TABLE XV. Continued

Run No.	Velocity Head Indicator	$\frac{v - V}{(gdS_e)^{1/2}}$ 0.71d	0.54d	0.36d	0.18d	0.09d
				Series 4		
1	M	3.034	1.820	0.312	-4.780	-5.386
	T	2.125	1.521	-0.754	-2.831	-3.153
2	M	2.293	1.511	-0.010	-1.922	-4.415
	T	2.462	1.190	-0.775	-2.146	-4.235
3	M	2.558	0.954	-0.553	-2.423	-3.959
	T	2.406	1.059	-0.615	-2.473	-3.615
4	M	2.253	1.050	-0.221	-2.777	-3.541
	T	2.337	1.117	-0.376	-2.742	-3.653
5	M	2.391	1.400	-0.279	-3.087	-4.126
	T	2.336	1.146	-0.555	-2.559	-3.706
6	M	2.116	1.125	0.092	-2.865	-3.874
	T	2.537	0.980	-0.726	-2.432	-3.604

[1] M = Manometer; T = Transducer.

[2] Depth above bed.

TABLE XVI

VELOCITY DISTRIBUTION CALCULATIONS FOR TEST RUNS CONDUCTED WITHOUT AND WITH SIMULATED RAINFALL

(Series 3 and 4 - Runs 7 through 33)

Run No.	Time from Beginning of Rainfall min[1]	$\frac{v - V}{(gdS_e)^{\frac{1}{2}}}$						
		0.90d[2]	0.80d	0.70d	0.50d	0.30d	0.20d	0.10d
					Series No. 3			
7	-2:30	3.497	2.849	1.774	0.960	-0.827	-2.596	-3.938
8	-2:30	3.615	2.654	1.943	1.025	-1.080	-2.431	-3.999
9	-2:30	3.368	2.819	1.649	1.062	-0.998	-2.591	-3.658
10	-1:45	2.085	3.169	2.122	1.322	-1.089	-2.237	-3.790
11	-1:45	3.469	2.884	1.951	1.197	-1.312	-2.381	-4.052
12	-1:45	3.327	2.879	1.931	0.946	-1.256	-2.315	-3.827
13	-1:00	3.965	3.013	1.817	1.195	-1.539	-3.121	-3.538
14	-1:00	3.936	2.715	1.769	1.245	-1.377	-2.881	-3.653
15	-1:00	3.943	2.740	1.776	1.212	-1.370	-3.144	-3.420
16	+0:15	-	-	-	No Run	-	-	-
17	+0:15		2.742	1.957	1.355	-0.980	-2.618	-3.717
18	+0:15		2.404	1.961	1.277	-1.014	-2.265	-3.535
19	+1:00		2.080	1.825	1.040	0.257	-1.900	-4.524
20	+1:00		2.487	2.563	1.325	-0.649	-2.601	-4.525
21	+1:00		2.494	1.854	1.495	-0.895	-1.827	-4.403
22	+1:45		2.181	1.757	1.020	-0.324	-1.737	-4.048
23	+1:45		2.669	2.481	0.811	-0.533	-2.534	-4.234
24	+1:45		2.436	2.009	1.260	-0.971	-2.030	-3.925

TABLE XVI. Continued

Run No.	Time from Beginning of Rainfall min	$\frac{v - V}{(gdS_e)^{1/2}}$ Depth above Bed 0.90d	0.80d	0.70d	0.50d	0.30d	0.20d	0.10d
25	+2:30		2.151	1.658	1.187	0.031	-1.791	-4.441
26	+2:30		2.671	2.430	0.865	-0.438	-2.173	-4.743
27	+2:30		2.614	1.889	1.173	-0.621	-2.099	-4.225
28	+4:00		2.346	1.657	1.523	-0.084	-1.962	-4.784
29	+4:00		2.650	2.488	0.900	-0.353	-2.067	-5.048
30	+4:00		2.706	1.909	1.253	-0.423	-2.269	-4.518
31	+6:00		2.557	1.744	1.478	-0.276	-1.887	-4.976
32	+6:00		2.811	2.470	0.995	-0.295	-2.306	-5.156
33	+6:00		2.520	2.211	1.357	-0.282	-2.627	-4.553

		Depth above Bed 0.715d	0.535d	0.357d	0.179d	0.089d
				Series No. 4		
7	-2:30	1.933	0.431	0.029	-1.914	-3.101
8	-2:30	1.875	0.442	-0.256	-1.374	-3.214
9	-2:30	1.992	0.524	-0.063	-1.740	-3.544
10	-1:45	2.172	0.748	-0.629	-1.710	-3.418
11	-1:45	2.193	0.809	-0.523	-2.237	-3.030
12	-1:45	1.964	0.775	-0.374	-1.832	-3.286
16	+0:15	1.464	1.236	-0.854	-1.457	-2.679
17	+0:15	1.740	1.332	0.099	-2.574	-3.853
18	+0:15	2.429	0.855	0.254	-2.559	--

TABLE XVI. Continued

Run No.	Time from Beginning of Rainfall min	$\frac{v - V}{(gdS_e)^{1/2}}$ 0.715d	0.535d	0.357d	0.179d	0.089d
19	+1:00	1.501	1.301	-0.546	-2.002	-2.725
20	+1:00	1.965	1.035	0.190	-2.761	-3.636
21	+1:00	1.993	1.657	0.102	-2.734	--
22	+1:45	1.791	0.992	-0.741	-1.882	-2.527
23	+1:45	2.022	1.291	-0.066	-2.465	-4.307
24	+1:45	1.850	1.574	-0.356	-2.183	--
25	+2:30	1.950	0.922	-0.343	-2.514	-2.621
26	+2:30	2.228	0.964	0.285	-2.386	-4.904
27	+2:30	2.347	1.560	-0.449	-2.440	--
28	+4:00	2.025	1.117	-0.905	-2.093	-2.767
29	+4:00	2.541	1.619	-0.327	-2.994	-5.066
30	+4:00	2.412	1.337	-0.309	-2.434	--
31	+6:00	2.215	1.306	-1.093	-2.417	-2.818
32	+6:00	2.418	0.974	-0.049	-2.286	-4.881
33	+6:00	2.410	1.289	-0.263	-2.436	--

[1] Time before the beginning of rainfall; + time after beginning of rainfall.

[2] Depth above bed.

APPENDIX C

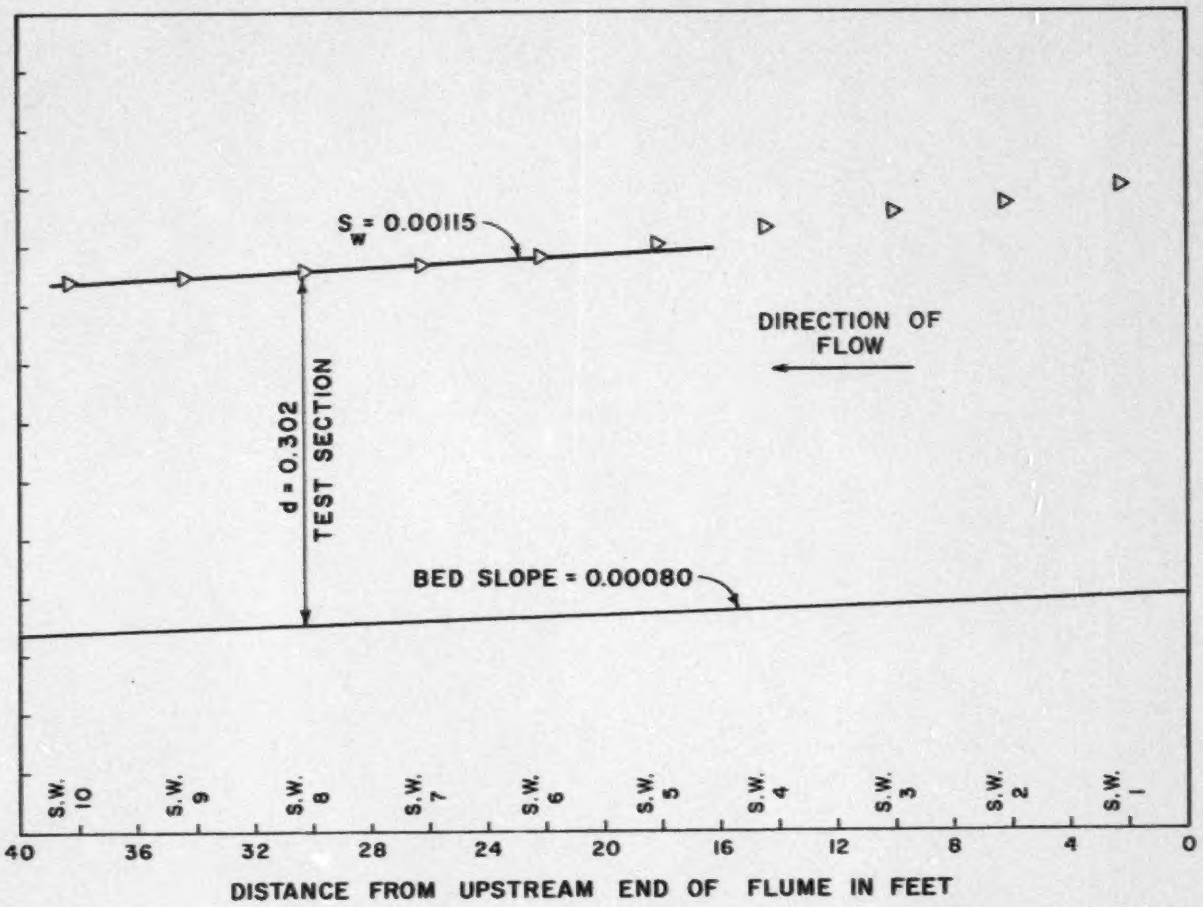

FIGURE 53 WATER SURFACE SLOPES FOR SERIES I WITHOUT RAINFALL

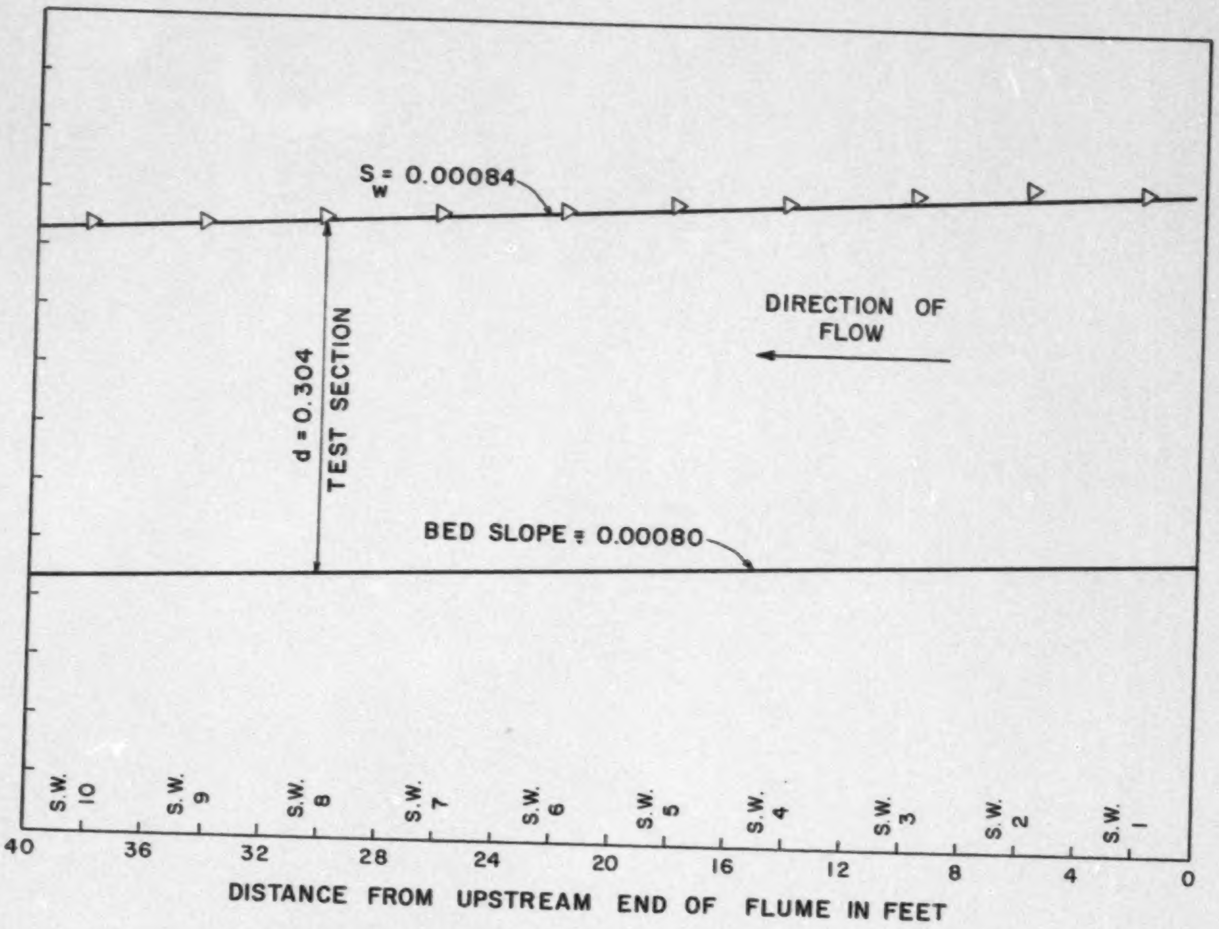

FIGURE 54 WATER SURFACE SLOPES FOR SERIES 2 WITHOUT RAINFALL

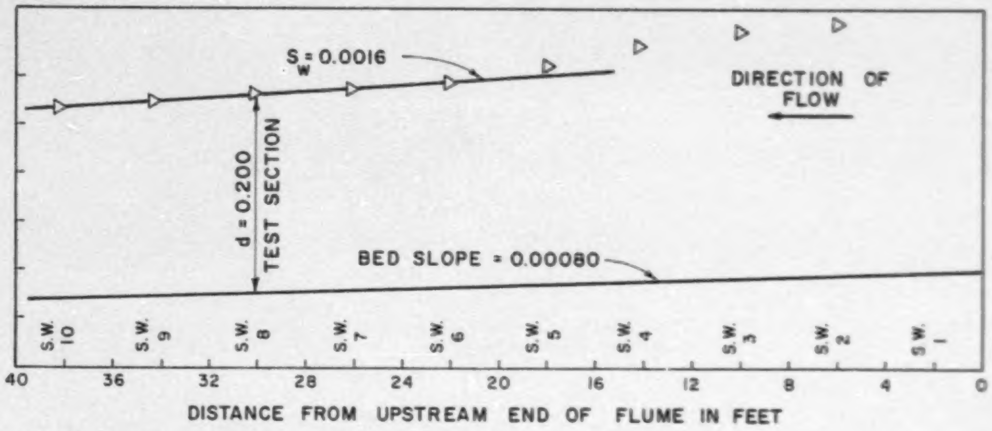

FIGURE 55 WATER SURFACE SLOPES FOR SERIES 3 WITHOUT RAINFALL

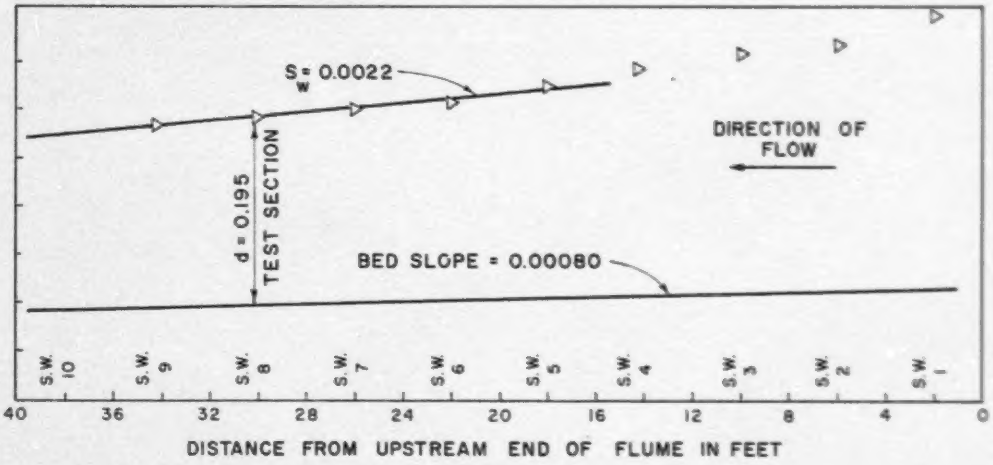

FIGURE 56 WATER SURFACE SLOPES FOR SERIES 3 WITH RAINFALL

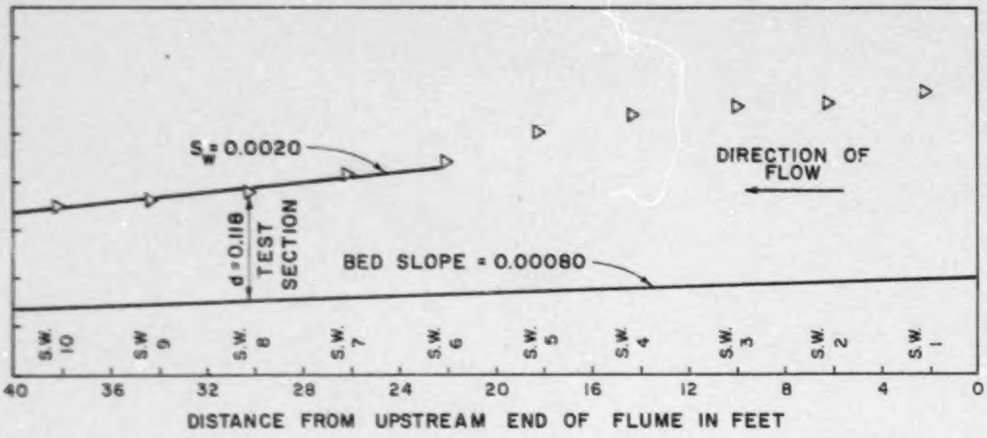

FIGURE 57 WATER SURFACE SLOPES FOR SERIES 4 WITHOUT RAINFALL

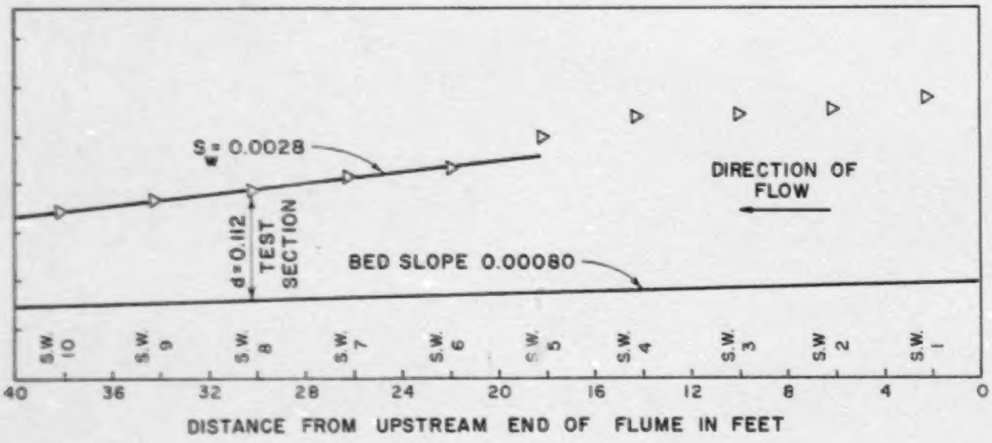

FIGURE 58 WATER SURFACE SLOPES FOR SERIES 4 WITH RAINFALL